


Fall 2013

Influence Of Cholesterol And Bilayer Asymmetry On Membrane Protein Distribution In Polymer-Tethered Raft-Mimicking Lipid Membranes

Noor Fueza Hussain
Purdue University

Follow this and additional works at: https://docs.lib.purdue.edu/open_access_dissertations

 Part of the [Biophysics Commons](#), and the [Polymer Chemistry Commons](#)

Recommended Citation

Hussain, Noor Fueza, "Influence Of Cholesterol And Bilayer Asymmetry On Membrane Protein Distribution In Polymer-Tethered Raft-Mimicking Lipid Membranes" (2013). *Open Access Dissertations*. 119.
https://docs.lib.purdue.edu/open_access_dissertations/119

This document has been made available through Purdue e-Pubs, a service of the Purdue University Libraries. Please contact epubs@purdue.edu for additional information.

PURDUE UNIVERSITY
GRADUATE SCHOOL
Thesis/Dissertation Acceptance

This is to certify that the thesis/dissertation prepared

By Noor Feuza Hussain

Entitled

Influence of Cholesterol and Bilayer Asymmetry on Membrane Protein Distribution in
Polymer-Tethered Raft-Mimicking Lipid Membranes

For the degree of Doctor of Philosophy

Is approved by the final examining committee:

Christoph Naumann

Chair

Steve Wassall

Garth Simpson

Christine Hrycyna

To the best of my knowledge and as understood by the student in the *Research Integrity and Copyright Disclaimer (Graduate School Form 20)*, this thesis/dissertation adheres to the provisions of Purdue University's "Policy on Integrity in Research" and the use of copyrighted material.

Approved by Major Professor(s): Christoph Naumann

Approved by: Eric Long

Head of the Graduate Program

11/21/2013

Date

INFLUENCE OF CHOLESTEROL AND BILAYER ASYMMETRY ON MEMBRANE
PROTEIN DISTRIBUTION IN POLYMER-TETHERED RAFT-MIMICKING LIPID
MEMBRANES

A Dissertation

Submitted to the Faculty

of

Purdue University

by

Noor Feuza Hussain

In Partial Fulfillment of the

Requirements for the Degree

of

Doctor of Philosophy

December 2013

Purdue University

West Lafayette, Indiana

I dedicate my dissertation to my late parents Nizarul Hussain and Asma Hussain

ACKNOWLEDGEMENTS

A tale that can be taken to a sound end should not be left in the half way even if we found a good juncture, and I am happy to conclude my Ph.D. by writing the dissertation and like to thank all those who took me to the winning line.

It is a privilege and great honor to have a perfectionist like Prof. Christoph A. Naumann as my mentor. It is indeed a great achievement to work under him and the support and enthusiasm shown by him towards the research is enormous. I have enjoyed learning from his guidance and dedication to research, and his overall supervision of my work ensured that my training experience is the most productive not only on the research level, but also professionally. I also take this opportunity to thank my committee members, Prof. Garth J. Simpson, Prof. Christine A. Hrycyna and Prof. Stephen R. Wassall for their help and advice. In addition, I would like to express my honor to be a student at Indiana University Purdue University Indianapolis (IUPUI), a prestigious and State of the art Institution. I also express my heartfelt thanks to all the staff members who helped in different ways during my stay at IUPUI.

I sincerely thank Dr. Amanda P. Siegel for all her help, invaluable advices, and her willingness to teach me all techniques I benefited from. She also provided Figure 10 (D, E, I, J) XY scans and helped me in proof reading my dissertation, thank you for

being such a good friend. I wish to express my gratitude to Merrell Johnson for providing me Atomic Force Microscopy images for my research work. I like to extend my appreciation to my fellow colleagues Jiayun Gao (Eric) for providing me the epi-images in Figure 15 and Yifan Ge for providing the epi-image in Figure 9 D. Yifan Ge also assisted me to get the E_{raft} values for 37 mol % cholesterol in Figure 17. Dr. Daniel E. Minner, Vincent Herring, and YuHung Lin (Corey) were always helpful in my research work and gave valuable advice during my stay at IUPUI.

I also take this opportunity to thank my relatives and friends who helped in numerous ways in my difficult periods throughout the Ph.D. I sincerely thank Dr. Azeez Razak, Dr. Gayani C. Kodippili, Dr. Dina A. Moustafa, Christopher K. Wach, Dulanji Kuruppu, Dr. Rafat Siddiqui, and Dr. Aruni de Silva for their various contributions.

I am extremely grateful to my husband Irshad Cassim, for without his endless love, support, encouragement, understanding, and helping in taking care of our daughter, the completion of my doctorate would not have been possible. My sweetheart Manaal Cassim, thank you for being such a nice girl to Mom. I am also very grateful to my sisters Hafsa Imtiaz and Hifaza Azarm, and to my brother Shuaib Hussain who instilled in me determination throughout my Ph.D. program. For without their understanding and calming voice, I would not be who, and where I am today.

It was my late parents who continued belief in me and in my ability to succeed in the carrier path that I have chosen, and not to leave a good story in the half way and to carry it to the end and this was the base for my determination to complete my Ph.D. I duly dedicate my dissertation to my late parents Nizarul Hussain and Asma Hussain.

TABLE OF CONTENTS

	Page
LIST OF TABLES	ix
LIST OF FIGURES	x
LIST OF ABBREVIATIONS	xiii
ABSTRACT	xvi
CHAPTER 1. INTRODUCTION	1
1.1 Rationale and Objectives	1
1.2 Organization	7
CHAPTER 2. BACKGROUND	8
2.1 The Role of Lipid Heterogeneities in Membrane Protein Distribution and Function	8
2.1.1 The Role of Lipid Rafts in Protein Distribution and Function	9
2.1.2 Raft-Mediated Signaling Platforms	9
2.1.3 Leaflet Asymmetry in Biological Membranes and Raft-Mediated Trans bilayer Signaling	10
2.1.4 Significance of Cholesterol for Lipid Rafts	11
2.2 Protein Studies Involving Raft Domains	12
2.3 Raft-Mimicking Model Lipid Mixtures and Protein Sequestration Studies	13
2.3.1 Mixing Thermodynamics of Raft-Mimicking Lipid Mixtures	14
2.3.2 Integrin Sequestration in Raft-Mimicking Model Membranes	15
2.4 Polymer-Tethered Phospholipid Lipid Bilayer	16

	Page
2.4.1 Impact of Lipopolymers on Dynamics	17
2.4.2 Impact of Lipopolymers on Elastic Properties	18
2.4.3 Lipopolymer Induced Buckling Structures in Polymer-Tethered Lipid Monolayers	18
2.4.4 Mean-Field Theory Calculations of Polymer-Tethered Membrane.....	20
2.5 Thin Film Buckling and Buckling Theory of Straight-Sided Blister	21
2.5.1 Significance of Buckles and Membrane Curvature in Biological Systems.....	22
2.6 Methodology	23
2.6.1 Langmuir-Blodgett/Langmuir-Schaefer Deposition	23
2.6.2 Combined Epi-fluorescence Microscopy (EPI) and Confocal Fluorescence Detection System.....	25
2.6.3 Fluorescence Correlation Spectroscopy (FCS)	28
2.6.4 Photon Counting Histogram (PCH) Analysis	30
2.6.5 Atomic Force Microscopy (AFM)	32
CHAPTER 3. MATERIALS AND EXPERIMENTAL SECTION	34
3.1 Materials.....	34
3.2 Experimental Procedures.....	35
3.2.1 Construction of Polymer-Tethered Bilayers using LB/LS Transfer Techniques	35
3.2.1.1 Building Symmetric Bilayers	36
3.2.1.2 Building Asymmetric Bilayers.....	38
3.2.1.3 Elucidating the Stability of Asymmetric Bilayers.....	39
3.2.1.4 Characterization of l_o - l_d Phase Separation in Symmetric/Asymmetric Bilayers.....	39
3.2.1.5 Building Raft-Mimicking Lipid Domains Containing Symmetric Bilayers with Different Cholesterol Concentrations	40

	Page
3.2.1.6 Preparation of Polymer-tethered Monolayers and Bilayers with Different Concentrations of Cholesterol	40
3.2.2 Protein Incorporation into Lipid Bilayers and Detection with Fluorescence Microscope	41
3.2.3 Combined EPI Microscopy, Confocal Fluorescence Correlation Spectroscopy (FCS), and Confocal Fluorescence Intensity Analysis	42
3.2.3.1 Determination of Integrin Brightness and Oligomerization Status from PCH	43
3.2.3.2 Protein Sequestration Analysis (E_{raft}) and Protein Migration Analysis (X_{migrate}).....	44
3.2.4 Image Acquisition and Analysis.....	45
3.2.4.1 Acquisition and Analysis of EPI-Micrograph Images of LB Monolayers with Different Concentration of Cholesterol with 3 mol% DSPE PEG-5000	45
3.2.4.2 Atomic Fluorescence Microscopy and Image Analysis from Nanoscope 6.1 Software	46
3.2.5 Calculating Different Buckling Parameters with Different Cholesterol Containing LB Monolayers.....	47
3.2.5.1 Calculating the Monolayer Film Thickness with Increasing Cholesterol Concentration	48
3.2.6 Investigating the Distribution of Lipopolymer, Cholesterol and the Lipids in LB Monolayers.....	49
CHAPTER 4. RESULTS AND DISCUSSION.....	50
4.1 Influence of Bilayer Asymmetry on Integrin Sequestration	50
4.1.1 Symmetric and Asymmetric l_o - l_d phase Separations in Polymer- Tethered Lipid Bilayers.....	50
4.1.2 Design and Characterization of Asymmetric Bilayers	51

	Page
4.1.3 Elucidating the Stability of Bilayer Asymmetry	53
4.1.4 Characterizing l_o and l_d Domains in the Symmetric and Asymmetric Bilayer	55
4.1.5 Comparison of Integrins ($\alpha_v\beta_3$ and $\alpha_5\beta_1$) Sequestration in Asymmetric and Symmetric Bilayers (in the presence and absence of ECM ligands)	57
4.1.6 Influence of Ligand Addition on Dimerization and Brightness of $\alpha_v\beta_3$ and $\alpha_5\beta_1$ Integrins	61
4.1.7 Potential Mechanisms for the Integrin Sequestration in Symmetric and Asymmetric Systems.....	63
4.2 The Effect of Cholesterol Concentration on Integrin Sequestration in Different Raft Mimicking Lipid Mixtures	66
4.3 Effect of Lipopolymer and Cholesterol Concentration on the Buckling Process in Phospholipid Monolayers	74
4.3.1 Buckling Phenomena in SOPC: DSPE PEG-5000 Monolayers.....	74
4.3.2 Cholesterol Induced Buckling in Polymer-Tethered Monolayers with 3 mol% DSPE-PEG 5000.....	75
4.3.2.1 EPI Micrographs and AFM Images of Polymer-tethered Monolayers with Different CHOL Concentration	76
4.3.2.2 Quantitative Analysis of EPI-micrograph and AFM Images of the Monolayers with Different Cholesterol Concentration.....	79
4.3.2.3 Stress Related Parameters Obtained from EPI-micrograph and AFM Images of the Monolayers with Different Cholesterol Concentration	83
4.3.2.4 Buckling Regions as Diffusion Barriers.....	86
CHAPTER 5. CONCLUSION	89
REFERENCES	92
VITA	104

LIST OF TABLES

Table	Page
Table 1: Different lipid composition to build LB/LS monolayers.....	38
Table 2: Monolayer film thickness with increasing cholesterol concentration	49
Table 3: Characterization of l_o - l_d phase separations in asymmetric and symmetric bilayers	57

LIST OF FIGURES

Figure	Page
Figure 1: Schematic diagram of l_o - l_d phase separations in polymer-tethered lipid bilayers of asymmetric (left) and symmetric (right) bilayers.	6
Figure 2: The phase diagram of DOPC: DPPC: CHOL lipid mixture at 24 °C.	15
Figure 3: Fabrication of phospholipid bilayer using a Langmuir trough showing the LB (A) and LS (B) transfer technique	25
Figure 4: Schematic representation of the EPI microscope and the FCS	26
Figure 5: (A) Fluctuation intensity collected for Alexa 555 labeled $\alpha_v\beta_3$ monoclonal antibody in solution for 10 s intervals through two channels (B) Auto correlation curves (C) Histogram of the photon counts for the same fluctuation analysis.....	29
Figure 6: Schematic diagram of the AFM microscope showing the beam deflection method.....	33
Figure 7: Schematic of l_o - l_d phase separations in polymer-tethered lipid bilayers of asymmetric (left) and symmetric (right) lipid compositions..	51
Figure 8: EPI-micrographs showing the asymmetric and the symmetric lipid bilayers observed through the NBD and DiI channels.	52
Figure 9: Epi-micrograph images showing the stability of the asymmetric bilayer with respect to time, surfactant and the flip flop of the lipid molecules.	54
Figure 10: CS - XY scans of $\alpha_v\beta_3$ integrin distribution in the presence of monolayer spanning (asymmetric bilayer) and bilayer-spanning (symmetric bilayer)	59
Figure 11: Comparison of E_{raft} values for symmetric (Bl_o domains) and asymmetric (Ml_o domains) bilayers for $\alpha_v\beta_3$ and $\alpha_5\beta_1$ integrins.....	60

Figure	Page
Figure 12: PCH curves for $\alpha_v\beta_3$ (A, C) and $\alpha_5\beta_1$ (B, D) before (<i>light markers</i>) and after (<i>dark markers</i>) ligand binding	62
Figure 13: The confirmation change of the $\alpha_v\beta_3$ integrin upon addition of the extracellular matrix ligands.	65
Figure 14: Simplified DOPC: DPPC: CHOL phase diagram showing the phase boundary of the l_o - l_d coexisting phase and the DOPC: DPPC: CHOL mixtures of different CHOL molar concentrations	67
Figure 15: EPI micrographs of LB/LS monolayers and bilayers of raft-mimicking lipid mixtures with different percentage of CHOL (DOPC: DPPC-1:1).....	68
Figure 16: CS-XY scans of $\alpha_v\beta_3$ integrin distribution in DOPC/DPPC/CHOL mixtures with the 20 mol% and 35 mol% CHOL.	69
Figure 17: E_{raft} values for different concentrations of cholesterol for DOPC: DPPC-1:1 raft mimicking mixtures	70
Figure 18: XY scans of the $\alpha_v\beta_3$ integrin distribution in the 20 mol% and 35 mol% CHOL. A, B, C, D box = $10.5 \times 10 \mu\text{m}^2$	71
Figure 19: Dimerization values of the integrins for different CHOL concentration in raft-mimicking lipid domains.	73
Figure 20: EPI micrographs of physisorbed polymer-tethered lipid monolayers comprised of SOPC: 3 mol% DSPE-PEG5000 with 5 mol%, 30 mol% , and 40mol% CHOL	76
Figure 21: EPI micrographs comparing the distribution of TAMRA-DSPE PEG 2000 (A) NBD-DHPE (B), and NBD-6-cholesterol	78
Figure 22: AFM images of the polymer-tethered lipid monolayers containing SOPC: 3mol% DSPE-PEG 5000, and 5 mol%, 30 mol%, and 40 mol% CHOL	79
Figure 23: Section analysis for 0 mol% CHOL with 3 mol% DSPE-PEG 5000 in SOPC monolayers	80
Figure 24: AFM section analysis for the 40 mol% CHOL with 3 mol% DSPE-PEG 5000.....	80
Figure 25: Buckle height vs. CHOL concentration in the monolayers.....	80

Figure	Page
Figure 26: Width of the buckles from the AFM images for different concentration of CHOL.....	81
Figure 27: The buckle roughness vs. CHOL concentration in the monolayer.....	82
Figure 28: Thickness of the bilayer with increasing CHOL concentration	83
Figure 29: Impact of CHOL molar concentration on bearing area and biaxial stress physisorbed polymer-tethered lipid monolayer	84
Figure 30: FRAP images of the bilayers for 0% CHOL, and 40% CHOL in SOPC with 3 mol% DSPE-PEG 5000 and 0.5 mol% TRITC-DHPE	87
Figure 31: EPI micrographs of physisorbed polymer-tethered lipid bilayer with 0 mol % and 40 mol% CHOL in SOPC with 3 mol% DSPE-PEG 5000	88

LIST OF ABBREVIATIONS

AFM	Atomic force microscopy
APD	Avalanche photodiode
BA	Bearing area
Bl_d	Bilayer associated l_d region
Bl_o	Bilayer associated l_o region
CCD	Charged coupled device
CHOL	Cholesterol
CS-XY	Confocal spectroscopy XY
D	Diffusion coefficient
diC ₁₈ M ₅₀	1,2-dioctadecyl- <i>sn</i> -glycero-3-N-poly(2-methyl-2-oxazoline) ₅₀
DiD	1,1 ¹ -Dioctadecyl-3,3,3 ¹ ,3 ¹ -Tertamethylindodicarbocyanine, 4-chlorobenzene sulfonate salt
DiI	1,1 ¹ -dioctadecyl-3,3,3 ¹ ,3 ¹ tetramethylindodicarbocyanine perchlorate
DOPC	1,2-dioleoyl- <i>sn</i> -glycero-3-phosphocholine
DPPC	1,2-dipalmitoyl- <i>sn</i> -glycero-3-phosphocholine
DSPE-PEG 5000	1,2-distearoyl- <i>sn</i> -glycero-3-phosphoethanolamine-N-[methoxy(polyethylene glycol)-5000]
ECM	Extracellular matrix
Epi	Epi-fluorescence
ER	endoplasmic reticulum
E _{raft}	Raftophilic excess
FCS	Fluorescence correlation spectroscopy
FFS	Fluorescence fluctuation spectroscopy

FN	Fibronectin
FRAP	Fluorescence recovery after photobleaching
GPI	Glycophosphatidylinositol
GUV	Giant unilamellar vesicle
K_A	Area elastic modulus of lipid modulus of lipid layer with the lipopolymer
K_A^0	Area elastic modulus of the bare lipid layer without lipopolymer
k_B	Boltzmann's constant
K_c	Curvature elastic modulus or bending modulus of the film
LB	Langmuir Blodgett
l_d	Liquid disordered
l_o	Liquid ordered
LS	Langmuir Schaefer
MAbs	Monoclonal antibodies
Ml_d	Monolayer associated l_d region
Ml_o	Monolayer associated l_o region
NBD-PE	Triethylammonium Salt of N-(7-nitrobenz-2-oxa-1, 3-dazol-4-yl)-1,2-dihexadecanoyl- <i>sn</i> -glycero-3-phosphoethanolamine
OG	n-Octyl- β -D-glucopyranoside
PBS	Phosphate buffered solution
PC	Phosphatidylcholine
PCH	Photon counting histogram
PE	Phosphatidylethanolamine
PI	Phosphatidylinositol
PS	Phosphatidylserine
PSF	Point spread function
R6G	Rhodamin 6G
SL	Sphingolipids
SOPC	1-stearoyl-2-oleoyl- <i>sn</i> -glycero-3-phosphocholine

SUV	Small unilamellar vesicle
SM	Sphingomyelin
TM	Transmembrane
TRITC-DHPE	Triethylammonium salt of N-(6-tetramethylrhodamine thio-carbamoyl)-1,2-dihexadecanoyl-sn-glycero-3-phosphoethanolamine
VN	Vitronectin
X_p	Mole fraction of the polymer

ABSTRACT

Hussain, Noor F. Ph.D., Purdue University, December 2013. Influence of Cholesterol and Bilayer Asymmetry on Membrane Protein Distribution in Polymer-Tethered Raft-mimicking Lipid Membranes. Major Professor: Christoph A. Naumann.

It is now widely recognized that lipid rafts, which are membrane domains enriched in cholesterol (CHOL) and sphingolipids (SL), play a significant functional role in the plasma membrane. Raft domains particularly affect membrane functionality by causing sequestering of membrane proteins. Underlying mechanisms of raft-associated membrane protein sequestration remain elusive, due to the complexity, transient nature, and small size of raft domains in cellular membranes. To address these challenges, this dissertation unveils the relationship between lipid raft composition and membrane protein sequestration and function using raft-mimicking model membrane mixtures comprised of coexisting liquid-ordered (l_o) and liquid-disordered (l_d) domains with reconstituted membrane proteins. In particular, we address the potentially important, but poorly understood role of membrane asymmetry in membrane protein sequestration and function. A sensitive experimental method comprised of confocal fluctuation spectroscopy and photon counting histogram (PCH) analysis is utilized to analyze the sequestration and oligomerization state of $\alpha_v\beta_3$ and $\alpha_5\beta_1$ integrins in raft-mimicking lipid mixtures. In

asymmetric bilayers, coexisting l_o - l_d phase separations are located in the top leaflet, while the bottom leaflet exhibits a homogeneous l_d phase. The comparison of symmetric bilayers with bilayer-spanning l_o - l_d phase separations results revealed that $\alpha_5\beta_3$ and $\alpha_5\beta_1$ show l_o phase preference in asymmetric bilayers, but l_d phase affinity in symmetric bilayers. Previously it has been shown that integrins translocate from the l_d to l_o phase upon addition of their respective ligands in symmetric bilayers, while there was no notable translocation of integrins in response to addition of native ligands in asymmetric bilayers. These interesting results indicate that integrin sequestration is dependent on l_o and l_d differences in lipid packing density, hydrophobic mismatch of integrin transmembrane and lipid bilayer regions, as well as the interaction between bilayer and integrin extracellular region. Next we investigated the influence of CHOL content on integrin sequestration because CHOL concentration influences lipid packing density, bilayer thickness, and line tension between l_o and l_d domains. Importantly, our data show that CHOL plays a substantial role in integrin sequestration in raft-mimicking lipid mixtures. These findings highlight the important role of bilayer asymmetry, distinct lipid densities and bilayer thicknesses in l_o and l_d regions of the bilayer for the regulation of membrane protein sequestration.

Changes in lipid packing density may also impact membrane elastic properties and lateral stress within the bilayer. Previously it has been shown that phospholipid monolayers with elevated concentration of lipopolymers are able to respond to increasing lateral stress by inducing membrane buckling, a stress relaxation phenomena. As part of the current dissertation, we established that membrane buckling can also be induced by gradually increasing CHOL concentration in polymer-tethered membranes of low

lipopolymer content. Further analysis using quantitative epifluorescence and atomic force microscopy, combined with buckling theory for a thin elastic sheet confirmed that CHOL causes buckling due to the increase in biaxial stress within the membrane. These findings are intriguing in light of the important role of CHOL in membrane functionality.

CHAPTER 1. INTRODUCTION

1.1 Rationale and Objectives

Lipid rafts are regions in biological membranes that are enriched in CHOL, SL and Glycophosphatidylinositol (GPI)-anchored proteins. These functional membrane heterogeneities play a significant role in many membrane-related cellular processes, such as raft-mediated transmembrane signaling, membrane protein sorting, cell adhesion, morphology, and angiogenesis (1-3). Lipid rafts have also been linked with the pathogenesis of several diseases (4). Investigating raft-associated membrane protein functionality remains challenging, due to the small size of raft domains in cellular membranes. Another complication is that lipid raft associations are dynamic and have a short life span in living cells (5, 6).

Consequently, model membranes have emerged as alternative experimental platforms to investigate raft-associated protein processes (7-9). A particular strength of model membrane studies is that sequestering and functionality of membrane proteins can be explored in well-defined, raft-mimicking membrane environments. In combination with single molecule detection techniques, model membranes allow the study of raft-associated protein processes with high sensitivity. Previously our group developed such a model membrane platform, in which the sequestering and

oligomerization status of $\alpha_v\beta_3$ and $\alpha_5\beta_1$ integrins was investigated in tertiary phase separated polymer-tethered lipid bilayers comprised of raft-mimicking liquid-ordered (l_o) and liquid-disordered (l_d) lipid-lipid phase separations (3). Integrins were chosen because of their involvement in many raft-associated activities, such as cell adhesion, morphology, motility, and angiogenesis (10-12). This previous study was performed on symmetric bilayers, where the phase separated l_o - l_d domains were present in both leaflets of the bilayer. Furthermore, the effect of native extra-cellular matrix (ECM) ligands was investigated on the sequestering and oligomerization status of integrins. The obtained results showed that $\alpha_v\beta_3$ and $\alpha_5\beta_1$ in polymer-tethered lipid bilayers favorably separate into l_d domains. Furthermore, the addition of ligands caused significant translocations of both integrins from l_d to l_o regions. These translocations are remarkable because, the addition of ligands did not affect the integrin oligomerization state (3).

Although our previous experiments provided valuable insight of raft-associated sequestration behavior, they did not address the fact of the asymmetric bilayer composition in eukaryotic membranes. The outer (exoplasmic) leaflet of such membranes is rich in SL and phosphatidylcholine (PC) lipids and the inner (cytoplasmic) leaflet contains PC, phosphatidylethanolamine (PE), phosphatidylserine (PS), and phosphatidylinositol (PI) lipids. Similar amounts of CHOL are present in both leaflets (13-16). Asymmetrically distributed lipid-anchored membrane proteins are also observed in the membrane. For example, GPI-anchored proteins are mostly present in the outer leaflet of the membrane; on the other hand, prenylated proteins are found in the inner leaflet. This protein asymmetry exists as a result of different biosynthetic pathways in the biological system (13-15). Interestingly, the clustering of GPI-anchored proteins in

the exoplasmic leaflet of the plasma membrane is associated with the co-clustering of Src kinase in the cytoplasmic leaflet (17). Since both lipid anchored proteins show an affinity for lipid rafts, they have been postulated to form raft-mediated trans-bilayer signaling platforms. Yet, the potentially important role of bilayer asymmetry as such is a process that remains poorly understood.

CHOL levels in the membrane represent another potentially important, but not fully understood process that may influence raft-associated membrane protein processes.

CHOL, a major component in many the cell membranes, affects the functionality of a variety of membrane proteins, including ion channel proteins, transporter proteins, and receptor proteins. Some membrane proteins are selectively enriched in CHOL rich domains (e.g., acetylcholine receptor), while others are predominantly formed in CHOL poor domains (e.g., sarcoplasmic reticulum Ca^{2+} -ATPase) (18). CHOL also plays a significant role in the sorting and rearrangement of transmembrane (TM) proteins. Yet, the specific molecular mechanism of CHOL function on membrane protein sequestration and function remain unclear. For example, it has been shown that CHOL can alter the tilting angle of TM peptides according to the hydrophobic mismatch hypothesis (19). At the same time, CHOL is also known to influence protein sequestration by affecting lipid packing density (19). Again, model membrane studies in well-defined lipid composition are well-suited to shed more light into this fascinating topic.

CHOL not only plays a specific role in protein-membrane interactions that is not well understood, but also influences crucial material properties of biological membranes, such as membranes stiffness. Therefore, my next project was focused on studying the

fascinating mechanical properties and stress relaxation phenomena of cell membranes and the impact of CHOL therein.

Buckling phenomena in biological systems are well documented (20-23). Most, prominently, the human lung shows membrane buckling in response to applied stress. The lung is covered by a monolayer composed of phospholipids and lung proteins that help to reduce the surface tension and allow reversible membrane wrinkling and folding during normal breathing (20). Cytoskeleton-mediated formation of highly curved structures, as found in lamellipodia, filopodia, pseudopodia, phagocytic cups, and axonal growth cones, represent another prominent examples (21-23).

Yet, the underlying mechanisms of membrane buckling remain a topic of open debate. Therefore, efforts have been made to investigate such processes using model membrane systems. Simple lipid monolayer and bilayer systems are not well suited for such studies because they are softer than typical biological membranes. Previously, membrane buckling was successfully investigated on lipid monolayers with lung surfactants (24). Membrane buckling has also been reported on giant vesicles, with actin shells, in which buckles were induced by actin polymerization (25).

More recently, our group reported formation of membrane buckles in physisorbed polymer-tethered membranes (20), (26). Specifically, we were able to induce buckles in such model membrane systems by altering lipopolymer concentrations. Here buckle formation was observed in polymer-tethered monolayers of higher (15-30 mol%) concentrations of poly (2-ethyl-2-oxazoline) lipopolymers, which could be attributed to lateral stress relaxation of the monolayer in response to elevated concentrations of conically shaped lipopolymers in the membrane (20). In addition, a

metric could be derived between membrane elasticity and quantifiable buckling parameters such as, maximum height of buckles (w_{max}) and buckle half width (b), by combining mean-field calculations of polymer-tethered membranes and buckling theory for a straight-sided blister (26). It is well known that CHOL substantially contributes to bending elasticity in model and biological membranes. As a consequence, we hypothesized that membrane buckling in a polymer-tethered membrane could also be induced by CHOL addition.

My research study had two major objectives, namely investigating the role of asymmetric distributions of lipids on protein sequestration and oligomerization, and developing a metric for associating membrane stiffness and membrane buckling by building membranes of different stiffness and observing their buckling behavior. Based on the described rationale, the first objective of my work was to investigate protein recruitment studies in raft-mimicking model membranes of asymmetric compositions and different CHOL content. Here we wanted to investigate the protein recruitment and the resulting molecular process for raft-mimicking lipid mixtures of asymmetric compositions, where phase separated l_o - l_d domains are exclusively present in the top leaflet (monolayer-spanning domains) of the bilayer. In the bottom leaflet, there is a continuous l_d phase. A schematic representation of the symmetric and the asymmetric bilayer system is depicted in Figure 1. To distinguish bilayer-spanning and monolayer-spanning phase separations, the following abbreviations are introduced: ML_o , monolayer associated l_o region; ML_d , monolayer associated l_d region; Bl_o , bilayer-spanning l_o region; Bl_d , bilayer-spanning l_d region. According to these definitions, the symmetric bilayer

contains coexisting Bl_o and Bl_d regions. The asymmetric bilayer has Ml_o/ Bl_d regions and Bl_d regions.

Specifically, we planned to explore the impact of monolayer vs. bilayer-spanning bilayers l_o-l_d domains on sequestering and oligomerization status of integrins. To achieve this objective, we constructed model membranes of asymmetric compositions with l_o-l_d phase separations exclusively located in the top leaflet of the bilayer (bottom leaflet shows l_d phase) and analyzed the integrins sequestration behavior in such membrane systems. The second part of my first objective is to investigate the effect of lipid packing density and hydrophobic thickness on integrin sequestration and oligomerization. In order to achieve this goal, we constructed lipid bilayers with raft-mimicking lipid mixtures of different CHOL content and studied integrin sequestration properties.

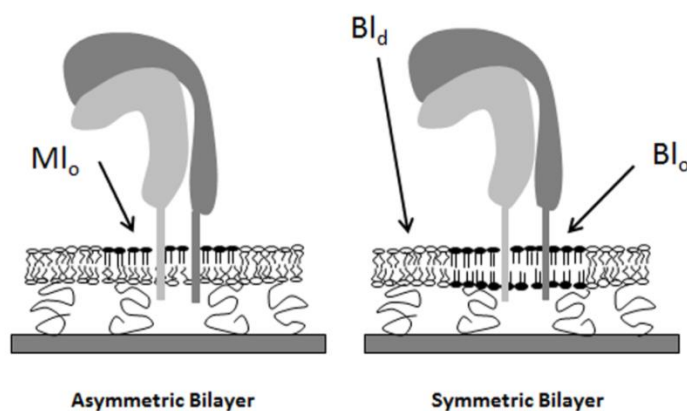


Figure 1: Schematic diagram of l_o-l_d phase separations in polymer-tethered lipid bilayers of asymmetric (left) and symmetric (right) bilayers. In the asymmetric bilayer, l_o-l_d phase separations are totally positioned in the top leaflet (LS monolayer) of the bilayer while the bottom leaflet (LB monolayer) is characterized by a homogenous l_d phase (coexistence between Ml_o and Bl_d regions). In contrast, the symmetric bilayer exhibits bilayer-spanning l_o-l_d regions (coexistence of Bl_o and Bl_d)

My second major objective was to explore the influence of CHOL on lateral stress relaxation phenomena, such as buckling in the membrane. Membrane buckling is

achieved by gradually increasing the CHOL concentration in polymer-tethered membranes containing a low concentration of the lipopolymer 1,2-distearoyl-*sn*-glycero-3-phosphoethanol amine-*n*-[methoxy(polyethylene glycol)-5000] (DSPE-PEG 5000). Both objectives of my thesis are linked in that a thorough characterization of both structural and dynamical properties of polymer-tethered membranes in response to compositional changes is crucial for their application in biophysical studies on membrane proteins.

1.2 Organization

There are five chapters in this dissertation. The first chapter delivers the rationale and the objectives along with the organization of this dissertation. The second chapter gives the background of my dissertation work. It provides information about existing studies on lipid rafts and raft-associated protein processes and the significance of buckling structures in the biological membranes, as well as an introduction into the design and characterization of relevant model membrane systems. Chapter 3 lists the materials and methods of the research work. It describes the procedures on how to make specific model membrane systems and how to analyze them using epifluorescence (EPI) microscopy, atomic force microscopy (AFM) and fluorescence fluctuation spectroscopy (FFS). It also provides the key equations necessary to analyze the buckling processes in polymer-tethered membranes. In addition, this section describes the analytical approach utilized in protein sequestration studies. Chapter four contains the results and the discussion. Here all significant results are provided and discussed in the context of the current knowledge in the field. The fifth chapter presents the conclusion.

CHAPTER 2. BACKGROUND

2.1 The Role of Lipid Heterogeneities in Membrane Protein Distribution and Function

The major component of all cellular membranes is the lipid bilayer, which acts as a structural barrier with a semipermeable character. Cell membranes are highly diversified in terms of their composition and organization. The underlying reason for such a diverse composition and organization and the associated molecular mechanisms for this diversity, remain largely unknown. (27, 28). A hallmark of cellular membranes is the heterogeneous distribution of lipids and membrane proteins into small, dynamic patches. While it has been challenging to characterize such patches at the cellular level, it has been shown that membrane lipid heterogeneity influences membrane protein distribution and function in the cellular membrane (27, 29, 30). Lipid rafts represent one prominent example of functional lipid/protein heterogeneities in cellular membranes (1, 28, 29, 31).

2.1.1 The Role of Lipid Rafts in Protein Distribution and Function

Lipid rafts in the plasma membrane are small (20 nm-200 nm) in size and often represent highly dynamic structures (32, 33). Importantly, these nanodomains are associated with many biologically significant membrane processes, including intracellular membrane trafficking of lipids, TM signaling, pathogenesis, cell adhesion, cell morphology, neural development and angiogenesis (1, 34, 35). Lipid rafts significantly alter protein-protein interactions by incorporating specific proteins, while excluding others. Some raftophilic proteins include GPI-anchored proteins, double acylated proteins (eg., Src-family kinases), α -subunit heterotrimeric G proteins, palmitoylated proteins (HedgeHog), and some TM proteins (36). Raft affinity may also be influenced by molecular processes, such as receptor clustering, which may include TM proteins and lipid-anchored proteins (1, 37). It has also been reported that clustering of rafts by crosslinking agents will expose raft proteins to different membrane environments (1). Importantly, translocation of proteins into rafts can initiate some signaling cascades (38). Caveolae are a subset of rafts found in cell surface invaginations. They are formed by rafts through the polymerization of caveolins (hairpin-like palmitoylated integral membrane proteins). Caveolae are involved in endocytosis, mechano-sensing, lipid, CHOL regulation, and signaling pathways (38, 39).

2.1.2 Raft-Mediated Signaling Platforms

One of the important functions of rafts is their involvement in signal transduction processes. In this case, ligand binding triggers the translocation of specific receptors to lipid rafts, forming concentrated platforms that recruit other proteins into the newly-

formed microenvironment (1, 15). The recruited proteins are then phosphorylated, leading to downstream signaling processes. For example, lipid rafts are believed to play a role in T-cell antigen receptor (TCR) signaling processes (40, 41). TCR signaling abolishes when rafts are disrupted. By contrast TCR cross-linking causes clustering of proteins in rafts, thus triggering immune cell signaling (40). Another example of raft-mediated signaling has been reported in Glial cells (42). Glial-cell derived neurotrophic factor (GDNF) ligands are important in the growth and preservation of the nervous system. They are also involved in the differentiation of kidney cells and spermatogonia (1). These ligands bind to a multicomponent receptor, which is composed of GDNF receptor- α (GFR α) and the RET receptor tyrosine kinase. The receptor- α (GFR α) is localized in rafts through GPI-anchored proteins. When ligands bind to GFR α co-receptors, they recruit RET to lipid raft regions and initiate the phosphorylation of Src, which results in downstream signaling (1),(36).

2.1.3 Leaflet Asymmetry in Biological Membranes and Raft-Mediated Trans bilayer Signaling

The plasma membrane is characterized by an asymmetric composition. The exoplasmic leaflet is rich in SL and PC, whereas the cytoplasmic leaflet is rich in PC, PE, PS, and PI lipids. Similar amounts of CHOL are present in both leaflets (13-16). Importantly, the membrane also contains asymmetrically distributed lipid-anchored membrane proteins. For example, GPI-anchored proteins are mostly present in the exoplasmic leaflet of the membrane. On the other hand, prenylated proteins are only present in the inner leaflet. This protein asymmetry exists as a result of different biosynthetic pathways in the biological system (13-15). It has been established that

clustering of GPI-anchored proteins in the exoplasmic leaflet of the plasma membrane is associated with the co-clustering of Src kinase in the proximal leaflet (17). Both types of raftophilic proteins do not span the bilayer of such a raft-mediated trans-bilayer signaling platform. However the role of bilayer asymmetry in the assembly of bilayer-spanning raft signaling platforms is not well known. Previously asymmetric GUVs have been prepared by Richmond et al (2011) and Chiantia et al. (2011) (43, 44). Richmond and coworkers were able to incorporate SNARE proteins into asymmetric GUVs through incorporating small unilamellar vesicles (SUVs) into GUVs (43). To add to this challenging, but potentially important topic, one objectives of this thesis is to investigate the poorly understood relationship between the inter-monolayer couplings of lipids in raft-mimicking lipid heterogeneities of asymmetric compositions. The resulting molecular process of protein recruitment to and from these heterogeneities is also investigated. Specifically, the first project describes protein recruitment and the resulting molecular processes in raft-mimicking lipid mixtures of asymmetric compositions (monolayer-spanning domains), where the phase-separated l_o - l_d domains are only present in the top leaflet. Also described is a comparison to corresponding data obtained on bilayer-spanning l_o - l_d domains reported previously (3).

2.1.4 Significance of Cholesterol for Lipid Rafts

CHOL, a significant component of the mammalian cell membrane, impacts several key properties of the bilayer. It causes lipid molecules to become more ordered and tightly packed. As another consequence of CHOL addition, the membrane permeability will be reduced and the thickness of the bilayer will increase (45, 46). CHOL is

functionally important because it is a contributing factor for many membrane-associated processes, such as ion transport, membrane enzyme activities, and conformational changes of membrane proteins (18, 47). CHOL has a significant influence on the sorting and rearrangement of TM proteins. Some like the acetylcholine receptors are selectively distributed in CHOL-rich domains, whereas others, such as Sarcoplasmic reticulum Ca^{2+} -aTPase, are located in CHOL-poor domains. (18). It has been postulated that CHOL may influence membrane protein sequestration by altering the hydrophobic thickness of the bilayer (19, 48). For example, it has been shown that CHOL can alter the tilting angle of the TM peptide by rearranging the acyl chain needed for TM mismatch (19). However, the topic remains elusive due to the lack of appropriate data on full TM proteins. To address this important topic the effects of lipid packing density and hydrophobic thickness on integrin sequestration and oligomerization are investigated in the second part of this primary objective. This is achieved through the construction of lipid bilayers with raft-mimicking lipid mixtures of different CHOL content, followed by the study of the integrin sequestration properties.

2.2 Protein Studies Involving Raft Domains

Membrane protein functionality in rafts remains elusive due to their complexity small size and transient nature in plasma membranes. The fact that lipid raft association in cellular membranes is dynamic and short lived represents another major challenging factor in studying these systems (5, 6). Traditionally, common lipid raft analysis procedures in the plasma membrane have included detergent resistant membrane flotation assays, CHOL depletion assays, and the utilization of cross-linking agents (49, 50).

Detergent extraction assay has been utilized to investigate raft associated activities of membrane proteins (51, 52). For example, this method allows the identification of raft proteins involved in signaling cascades (1). The disadvantage of the detergent extraction method is that it is prone to artifacts. This method also influences the physical and thermodynamic properties of the membrane (1, 53). Cross linking assays were employed to detect the formation of microdomains of GPI- anchor proteins (54). Other cross-linking assay include antibody cross-linking, GM1 cholera toxin B (CTxB) cross-linking, and ligand cross-linking (3). CHOL depletion and sequestration assay have been used to disrupt rafts, followed by raft isolation through raft markers and centrifugation (55). This method is also not free of artifacts.

2.3 Raft-Mimicking Model Lipid Mixtures and Protein Sequestration Studies

Model membranes have emerged as an attractive alternative to overcome the challenges of raft characterization in cellular membranes, which complicates the investigation of raft-associated molecular processes. Micron sized coexisting l_o and l_d domains can be easily prepared in lipid vesicles and supported lipid bilayers by using ternary mixtures comprised of a high melting temperature lipid with saturated acyl chains, a low melting temperature lipid with mono-unsaturated acyl chains, and CHOL (56-58). A model mixture of 1,2-dioleoyl-*sn*-glycero-3-phosphocholine (DOPC), 1,2-dipalmitoyl-*sn*-glycero-3-phosphocholine (DPPC), and CHOL, has been used to map the phase boundaries of the two-phase (l_o and l_d) coexistence region of the ternary mixture. (56, 59). Here l_o phase regions are considered as mimetics of lipid rafts. Importantly, depending on their composition and temperature, raft-mimicking domains can change

their sizes from nanoscale to micro scale (60-62). Fluorescence microscopy has been used to observe raft domains using head group labeled fluorescent phospholipids in planar bilayers (58). On the basis of lipid packing and dynamics, coexisting l_o - l_d domains are considered to be promising experimental platforms for investigating raft-mediated protein sequestration processes using sensitive detection techniques (8).

2.3.1 Mixing Thermodynamics of Raft-Mimicking Lipid Mixtures

Giant unilamellar vesicles (GUV) have been used to study properties of raft-mimicking lipid mixtures. Phase diagrams of ternary mixtures of saturated lipids, unsaturated lipids, and CHOL at different temperatures have been determined (56, 57). Fluorescence microscopy has been used to detect liquid domains in GUVs and planar lipid bilayers (56, 63). One phase, the l_d phase, primarily is enriched in unsaturated lipids, while the other phase, the l_o phase primarily contains saturated lipids and CHOL. It was also found that sphingomyelin (SM)-CHOL do not form domains at high temperatures but exhibited domain formation at low temperatures (lower than the melting temperature of SM). This finding affirms that the saturated lipid tail of SM facilitates the formation of raft domains. Domain formation was also observed when SM was substituted with saturated PC (distearyl-PC). This indicates that lipids with saturated acyl chains can pack well with CHOL to form l_o domains. It was also found that CHOL depletion induced the disappearance of raft domains. These domains were able to collide and coalesce and to form stripes (56, 63). A simplified phase diagram with the two-phase coexistence region for DOPC /DPPC/CHOL lipid mixtures at 24°C is depicted in Figure 2. A phase separation of l_o and l_d regions is observed inside the dotted circular region (56). More

recently, experiments have shown that the phase diagram is more complex and it also includes solid-liquid coexistence and a solid phase in the DPPC high percentage area.

(56).

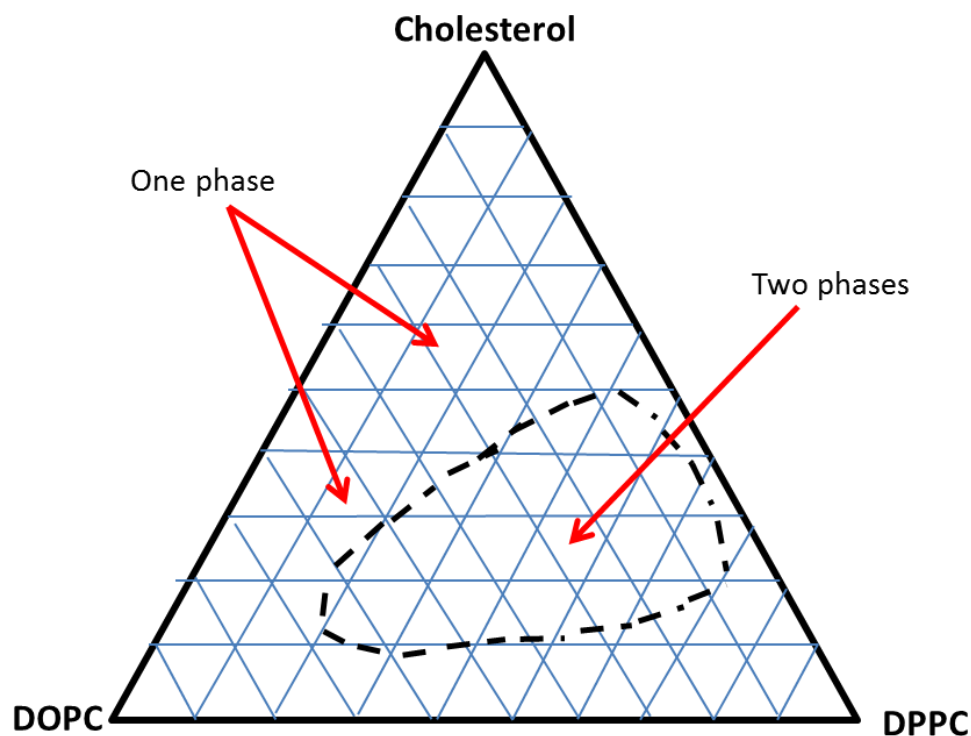


Figure 2: The phase diagram of DOPC: DPPC: CHOL lipid mixture at 24 °C. (adapted from (59))

2.3.2 Integrin Sequestration in Raft-Mimicking Model Membranes

Recently our group investigated the integrin sequestration behavior in raft-mimicking lipid mixtures. Integrins are TM proteins that plays a major role in signaling , cell adhesion, morphology, motility, and angiogenesis (64, 65). Importantly, integrin function can also be regulated by several different factors such as ligand and protein binding, cation activation, and micro-clustering (66-69). Previous studies in our group have analyzed integrins sequestration in l_o - l_d phase separated raft-mimicking membranes

using single molecule sensitive optical methods (3). This study was done on symmetric bilayers, where the phase separated l_o - l_d domains were spanning both leaflets of the bilayer. Furthermore, the effect of ligand addition on the sequestering and oligomerization of integrins was investigated (3). These studies showed that $\alpha_v\beta_3$ and $\alpha_5\beta_1$ in polymer-tethered lipid bilayers favorably separate into l_d domains, and the addition of ligands causes significant integrin translocation to l_o regions. Importantly, ligand addition did not affect the oligomerization status of both integrins. This implies that the translocation of integrins from l_d to l_o upon addition of ligands is not caused by ligand-induced receptor clustering (3).

2.4 Polymer-Tethered Phospholipid Lipid Bilayer

The phospholipid bilayer, as found in lipid vesicles, can be considered as the simplest mimetic of a biological membranes. Similar to cellular membranes, this model system shows bilayer fluidity and allows the incorporation of membrane proteins (70). Solid-supported lipid bilayers have been pursued because they allow membrane characterization using a wide range of highly sensitive biophysical detection techniques (71). However, the close vicinity between bilayer and underlying solid substrate may impair membrane proteins, such as lipid lateral diffusion (72, 73). Moreover, such membrane designs are not well suited to study properties of TM proteins. To overcome these limitations, polymer-supported lipid bilayers have been introduced, in which a hydrophilic polymer layer lifts up the bilayer from the solid substrate (74). Traditionally, polymer-supported bilayers have been stabilized at the polymer-bilayer interface via attractive electrostatic forces or covalent linkages (74). Polymer-tethered tethered lipid

bilayer systems represent the latter case. Previously, polymer-tethered lipid bilayers have been frequently utilized, which are comprised of phospholipids and lipopolymers (73). Here lipopolymers not only lift up the bilayer, but also provide stability between the lipid bilayer and polymer layer. Therefore, such polymer-tethered lipid bilayers are well suited for studies of TM proteins (72, 73). Polymer-tethered lipid bilayers also show fascinating material properties. In particular, varying lipopolymer concentrations in the model membrane will result changing dynamic and mechanical properties in the membrane. Polymer-tethered lipid bilayers can be constructed using Langmuir-Blodgett (LB) and Langmuir-Schaefer (LS) transfer techniques, which allow for control of lipopolymer concentration in the bilayer (74). These film transfer techniques are also attractive because polymer-tethered lipid bilayers of elevated lipopolymer concentrations can be built.

2.4.1 Impact of Lipopolymers on Dynamics

Increasing lipopolymer concentration in polymer-tethered membranes result fascinating membrane dynamics, organization, and elastic properties. Wide-field single microscopy experiments have shown that polymer-tethered membranes are a fascinating model platform for studying obstacle-induced obstructed diffusion (74). Here the degree of the lateral diffusion of lipids and membrane proteins can be controlled by lipopolymer concentration. These systems also show remarkable inter-monolayer coupling phenomena, which include registration of inner and outer monolayer raft mimicking domains and transbilayer coupling of obstructed diffusion (13, 75, 76). Lipopolymers

have also been shown to induce stress in a physisorbed phospholipid bilayer. This influences membrane organization and dynamics (20).

2.4.2 Impact of Lipopolymers on Elastic Properties

Incorporating lipopolymers into model membranes or liposomes will significantly alter the biophysical properties of the system (26). For example, mean field calculations have predicted that addition of lipopolymers in the membrane enhances membrane compressibility and bending stiffness (77). Here polymer type, molecular weight, and concentration are considered to be crucial parameters (77, 78). Previous work in our group has shown that high concentrations of lipopolymer induce lateral stress in physisorbed phospholipid monolayers. This led to buckle-driven delamination of the monolayer, deposited on a glass substrate via LB transfer technique, without causing phase separations between phospholipid and lipopolymers (20, 26). Intriguingly, buckling regions were found to act as diffusion barriers in polymer-tethered lipid bilayers containing poly (2-ethyl-2-oxazoline lipopolymers), thus causing compartmentalization with remarkable parallels to the compartment formation and associated hop diffusion processes of lipids and membrane proteins in plasma membranes(20). Similar results were found in polymer-tethered membranes with increasing concentrations the poly (ethylene oxide) lipopolymer DSPE-PEG 5000. Again elevated lipopolymer concentrations resulted in membrane buckling (26).

2.4.3 Lipopolymer-Induced Buckling Structures in Polymer-Tethered Lipid Monolayers

Alternative mimetic models are attractive to study buckling phenomena in biological systems. Therefore, efforts have been made to investigate buckling processes

using various types of model membrane systems. For example, actin-induced membrane buckling has been investigated by Hackl et al (1998) (25). In this study, actin was used to induce buckles in lipid vesicles by reconstituting thin actin shells in giant vesicles and inducing buckles by actin polymerization. Actin polymerization was carried out by influxing Mg^{2+} into vesicles. Membrane buckling was also investigated on lipid monolayers with lung surfactants (18). Despite these activities, the underlying mechanisms of membrane buckling remained a topic of open debate. Therefore, Siegel et al (2010 and 2012) explored membrane buckling using polymer-tethered membranes comprised of phospholipids and lipopolymers (20, 26). The rationale for this experimental design was that lipopolymers cause membrane buckling by inducing lateral stress in the membrane. In this case, the lateral stress is caused by the conical shape of lipopolymers. In these buckling experiments in polymer-tethered membranes, buckle formation was induced by enhancing lipopolymer molar concentration in the membrane (20, 26). Specifically, widespread membrane buckling was observed in polymer-tethered monolayer systems at high (15-30 mol%) concentrations of poly (2-ethyl-2-oxazoline) lipopolymers (20). In contrast, at low (0-10 mol%) concentrations of lipopolymer, a buckle-free membrane formed. Interestingly, in the case polymer-tethered lipid bilayers with these lipopolymers, membrane buckling in the bottom monolayer prevented formation of the top monolayer at buckling regions, thus resulting in μm -sized bilayer compartments. Notably, membrane buckling was found to be not associated with phospholipid-lipopolymer phase separations (20).

2.4.4 Mean-Field Theory Calculations of Polymer-Tethered Membrane

Depending on the density of grafted polymers on a substrate, two regimes of polymers conformations are distinguished, “mushroom” and “brush” regimes. At low grafting concentrations, polymers are in the “mushroom” conformation and at high concentrations, they are in the “brush” conformation (77, 79). Grafted polymers in the mushroom regime interact with each other and the segment density distribution is described by a Gaussian coil. The dimension of the Gaussian coil is defined by the Flory radius (R_f), a parameter that depends on polymer molecular weight and the specific length of monomer units. (77). At elevated grafting concentrations, where polymer moieties of lipopolymers tend to overlap, polymer conformations are described by a “polymer brush”. In this case, the increased repulsive polymer-polymer interactions cause the stretching of the polymer chains. The dimensions of the polymer brush are defined by scaling laws of polymer physics (80). In an aqueous environment, 3 mol% DSPE-PEG 5000 or higher, fall under the brush regime. In this situation, all the polymer head groups interact with each other and become stretched out (79). Mean field theory calculations can be used to find the approximate length of the polymer brush (L_p), as follows,

$$L_p = n_p a_m^{5/3} (X_p/A_l)^{1/3} \quad \text{Eq. 1}$$

where n_p is the number of monomers, a_m is the length of each monomer, X_p is the mole fraction of lipopolymers, and A_l is the area per lipid (77). An equation has been obtained for the area elastic modulus, which is induced by grafting polymers (77). This has been depicted in Eq. 2. The change in area elastic modulus for varying lipopolymer type and concentrations (X_p) can be calculated from Eq.2.

$$K_A = K_A^0 - \frac{2m_F(1-m_F)k_B T a_p^{2m_F} \left(\frac{A_1^{1-m_F}}{A_{1,0}^2}\right) n_p X_p^{m_F+1}}{1+4m_F \left(\frac{k_B T a_p^{2m_F}}{K_A^0}\right) \left(\frac{A_1^{1-m_F}}{A_{1,0}^2}\right) n_p X_p^{m_F+1}} \quad \text{Eq. 2}$$

K_A = elastic area expansion modulus of a single lipid layer, K_A^0 = elastic area-expansion modulus of a single, bare lipid layer, without polymer, m_F = exponent in dependence of polymer free energy on grafting density ($m_F = 5/6$ for scaling theory and $m_F = 2/3$ for mean field theory). T = absolute temperature, a_p = size of the monomer unit (0.39 nm for DSPE- PEG 5000 (77)), n_p = number of monomer unit per polymer, $A_{1,0}$ = equilibrium area per lipid molecule in the absence of polymer, A_1 = equilibrium area per molecule in the presence of polymer (81), X_p = mole fraction of polymer lipid.

2.5 Thin Film Buckling and Buckling Theory of Straight-Sided Blister

When a thin film is adsorbed to a rigid substrate and sufficient strain is applied, it partially delaminates from the substrate to relieve the compressive stress in the film, causing buckle delamination (25). When lateral stress is applied, the thin film wrinkles or buckles. The buckling behavior not only depends on the magnitude of the compressive forces, but also on the relative rigidity of the proximate substrate. In compliant substrates, the film responds to lateral stress through the wrinkling process. Here, corresponding deformation of the substrate occurs with film relaxation process. When the substrate is stiff, buckle delamination occurs (82).

There are three types of commonly formed buckle delamination patterns. Euler mode, varicose mode, and telephone code mode (83). The buckling process used in this experiment is well suited for the Euler column of buckling mode. In the Euler mode, the plain modulus of the substrate should be much higher than the plain strain modulus of the

film, and the half width of the buckle should be much higher than the thickness of the film (84). Previously it has been shown that these Euler mode requirements are fulfilled to describe the buckling process in polymer-tethered membranes comprised of DSPE-PEG 5000 and phospholipids. (26).

The critical compressive biaxial stress, σ_c at the onset of buckling for an Euler mode is given by the Eq.3, where “b” is the half width of the buckle, “h” is the thickness of the film, “ E_f ” is the plain strain modulus of the film, and “ ν_f ” is the poisons ratio of the film (83).

$$\sigma_c = \frac{\pi^2 E_f}{12 (1-\nu_f^2)} \left(\frac{h}{b}\right)^2 \quad \text{Eq.3}$$

The dimensionless buckling amplitude (ξ) for a given buckle depends on the ratio between the biaxial compressive stress in the unbuckled state (σ_0), and the biaxial compressive stress at the onset of buckling (σ_c). This is represented by the Eq.4 where “ w_{max} ” is the maximum normal displacement for the buckle (83).

$$\xi \equiv \left(\frac{w_{max}}{h}\right) = \sqrt{\frac{4}{3} \left(\frac{\sigma_0}{\sigma_c} - 1\right)} \quad \text{Eq.4}$$

2.5.1 Significance of Buckles and Membrane Curvature in Biological Systems

Curved membranes can be caused by two distinct properties of the film. These are lateral stress in the membranes and the compositional change in the film. Buckling phenomena are well documented in biological systems. The human lung is a good example. The lung is covered by a monolayer composed of phospholipids and lung proteins, which helps reduce surface tension in the lungs. This monolayer undergoes reversible wrinkling and folding during normal breathing (20). Cytoskeleton-induced

membrane structure represents another example. Such a buckling process leads to extensions and highly curved structures in the membranes, such as lamellipodia, filopodia, pseudopodia, phagocytic cups, and axonal growth cones (21-23).

Curved membranes, which are similar to buckles, are also seen in Golgi fenestrations, endoplasm reticulum tubules, and viral budding. They are positively or negatively curved and limited to certain areas. These curvatures are a result of lipid composition, membrane proteins, and helix insertion (22).

2.6 Methodology

2.6.1 Langmuir-Blodgett/Langmuir-Schaefer Deposition

Langmuir-Blodgett (LB)/Langmuir-Schaefer (LS) transfers represent a well-known method for fabricating model lipid bilayers. This method has many advantages over planar lipid bilayer formation via vesicle fusion, in which small unilamellar vesicles (SUVs) are formed in an aqueous solution and then spontaneously settle and burst to form a lipid bilayer on a substrate (85). The LB/LS technique employs a two-step method of assembly to form a planar solid-supported lipid bilayer (74, 86-88). Figure 3 provides a schematic diagram of the LB/LS bilayer formation. The first monolayer (LB layer) spreads at the air-water interface of the film balance system. Next, the monolayer is compressed to a fluid film pressure of 30 mN/m. The system is allowed to equilibrate for about half an hour. Then, the dipper is slowly moved upwards at a speed of 5 mm/s while the Teflon barrier moves inwards, thereby maintaining the area per lipid (Figure 3 A). During the process, a lipid monolayer will be transferred (LB transfer) from the air-water interface to the glass substrate (Figure 3 A).

The LS transfer technique is used to complete the bilayer (Figure 3 B). Here, a thick glass slide is placed at the bottom of the trough, which is then filled with Millipore water. Next the desired lipids are at the air-water interface of the trough. Then, the barrier is compressed in order to attain a certain surface pressure (30 mN/m). Finally, the glass slide with the LB monolayer is pressed through the LS layer and the LB/LS layer system lay under water. This bilayer assembly can be used for imaging purpose.

There are a number of advantages of the LB/LS method over planar bilayer formation from vesicle fusion. First, the dipping procedure enables a very homogeneous bilayer with few defects. Second, due to the layer-by-layer assembly, the fabrication of bilayers of asymmetric composition can be achieved. Third, it is possible to construct polymer-tethered lipid bilayers of elevated lipopolymer concentration, which cannot be obtained using vesicle fusion. It has been shown previously that stable lamellar bilayer structures can only be formed from vesicles containing a low lipopolymer concentration (less than 10 mol %) (78). Finally, the LB/LS method requires only small quantities of lipids (75 μg of lipids per spread).

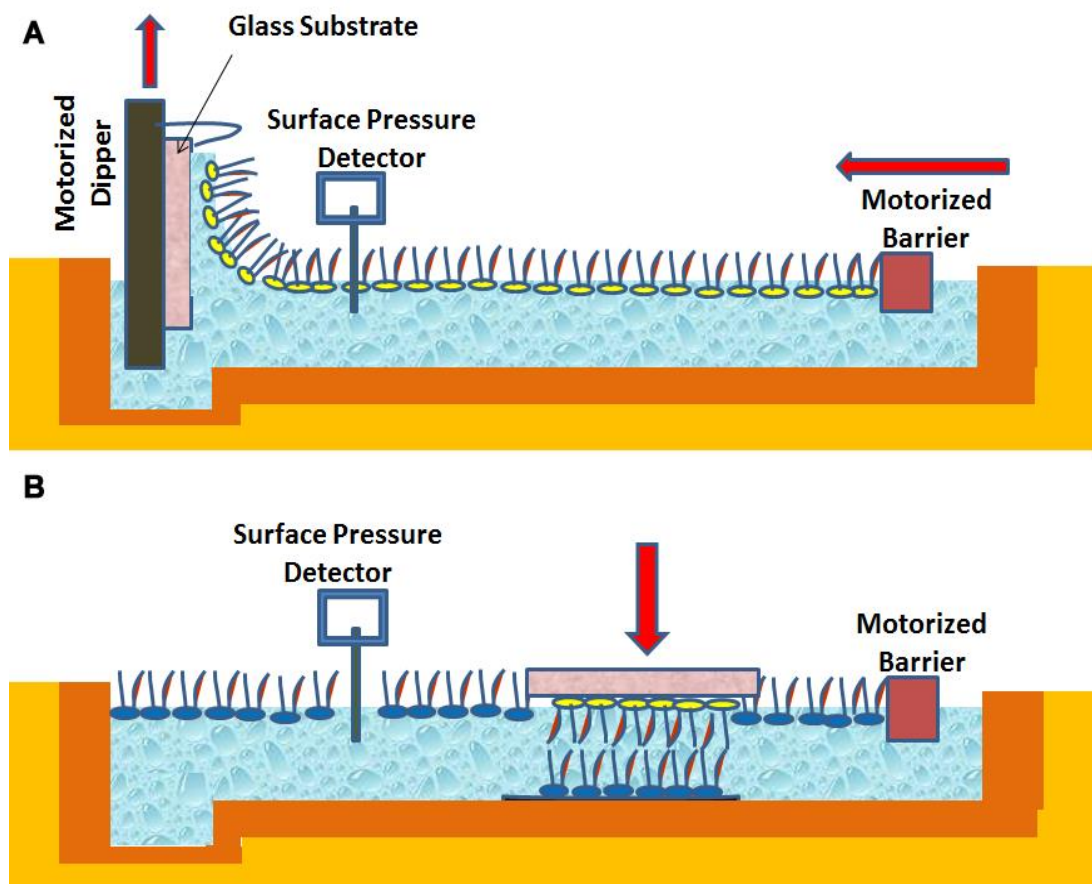


Figure 3: Fabrication of phospholipid bilayer using a Langmuir trough showing the LB (A) and LS (B) transfer technique

2.6.2 Combined Epi-fluorescence Microscopy (EPI) and Confocal Fluorescence Detection System

Characterization of lipid/protein distribution and the oligomerization status of membrane proteins in the polymer-tethered lipid bilayer are performed using a combined EPI and confocal detection system. A schematic diagram of the combined EPI/confocal fluorescence system is depicted in Figure 4. In EPI mode, a sample containing fluorophores is excited by a mercury lamp, which causes the sample to fluoresce. The light from the lamp is first passed through a filter that absorbs all but a specific range of wavelengths that are optimized for the fluorophore under investigation. The beam then

passes through the objective and excites the sample. The emitted fluorescence at a longer wavelength passes through a dichroic mirror and is guided to an eyepiece and/or to charge-coupled device (CCD) camera for recording purposes. A workstation enables the control of the camera and acquisition of fluorescence micrograph.

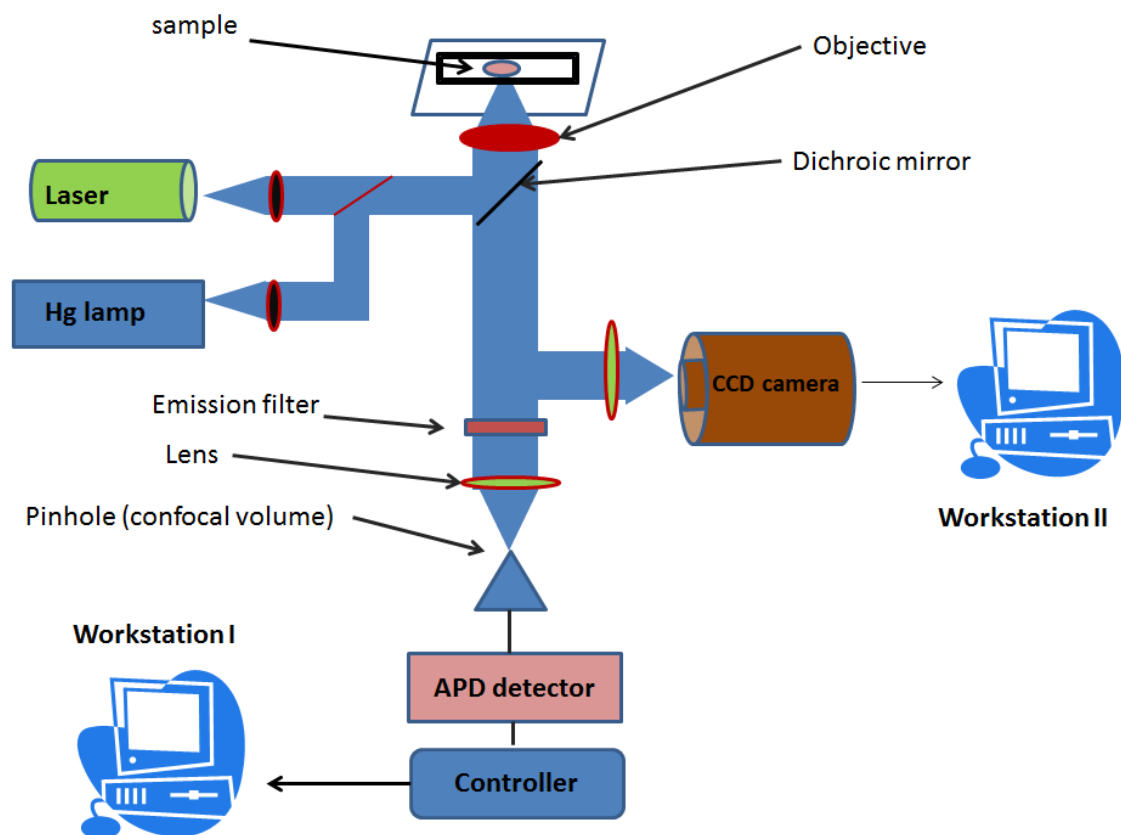


Figure 4: Schematic representation of the combined EPI microscope/confocal fluorescence detection system

Figure 4 also shows a set up for the FFS, which is utilized to analyze probe molecules using FCS and brightness analysis method. Brightness analysis is accomplished using photon counting histogram (PCH) method.

In the FFS setup a laser line is passed through a beam splitter and then focused to a confocal volume, where the sample is placed. The focusing is done by using a higher numerical aperture objective. The sample consists of freely moving fluorescence particles. The emitted fluorescence from the sample is directed back to a beam splitter. Stray fluorescence is avoided by using a pinhole in the confocal volume. This method can be used to detect probe fluorescence with submicron second time resolution. The FCS method allows detection of the intensity fluctuations of fluorescent particles, which enables attainment of the complete kinetic description of the system. Lateral distribution of lipids and proteins in planar model membranes are obtained using an X-Y scanning stage. The avalanche photodiode (APD) detector of the confocal system allows detection of membrane proteins ($\sim 10^{-3}$ mol%) with a single molecule sensitivity. The l_o - l_d phase separation can also be visualized simultaneously using EPI. About 0.5 mol% of dye-labeled lipids typically utilized to image lipid domains using EPI. Unfortunately, this elevated concentration of dye-labeled lipids may cause a higher background signal in the protein detection channel through the APD detector. Therefore, in most experiments, concentrations of dye-labeled proteins and lipids were comparable ($\sim 10^{-3}$ mol%) and detection of protein and lipid distribution was achieved using different channels of the APD detector without a need for EPI. Colocalization studies of membrane proteins in coexisting l_o - l_d domains are feasible because the size of raft domains (around 10 μm) is notably larger than the length scale probed by the confocal spot (the size of the confocal spot is 0.25 fl)

2.6.3 Fluorescence Correlation Spectroscopy (FCS)

Figure 4 illustrates the set up for FFS, which collects data for both FCS and PCH analysis. The laser beam is focused to the focal volume where the sample is placed. This is done by using a higher numerical aperture objective. The sample is excited by the laser and fluorescence is emitted by fluorescence molecules. This emitted fluorescence is directed back through the beam splitter and focused to the confocal volume. A pinhole is introduced in the confocal plane and adjusted to avoid stray fluorescence. The APD detector will acquire emitted fluorescence and the signal is obtained at submicron level intervals. FCS provides complete description of the kinetics of the fluorescence molecules with time (89). This is achieved through analyzing the rate of change in fluorescence with time. In FCS, this fluorescence over time is analyzed using FCS autocorrelation analysis. A schematic diagram of raw data and fluorescence fluctuation analysis of Alexa 555 labeled $\alpha_v\beta_3$ monoclonal antibodies in solution is depicted in Figure 5. It includes the detected fluorescence fluctuation trace over time (A), the corresponding FCS auto correlation curve (B), and the photon counting histogram (PCH) of the different detected fluorescence intensities(C). Here the data analysis is based on 5 different 10 s data acquisition sets. The autocorrelation curve provides information on the change in fluorescence with time in the confocal volume.

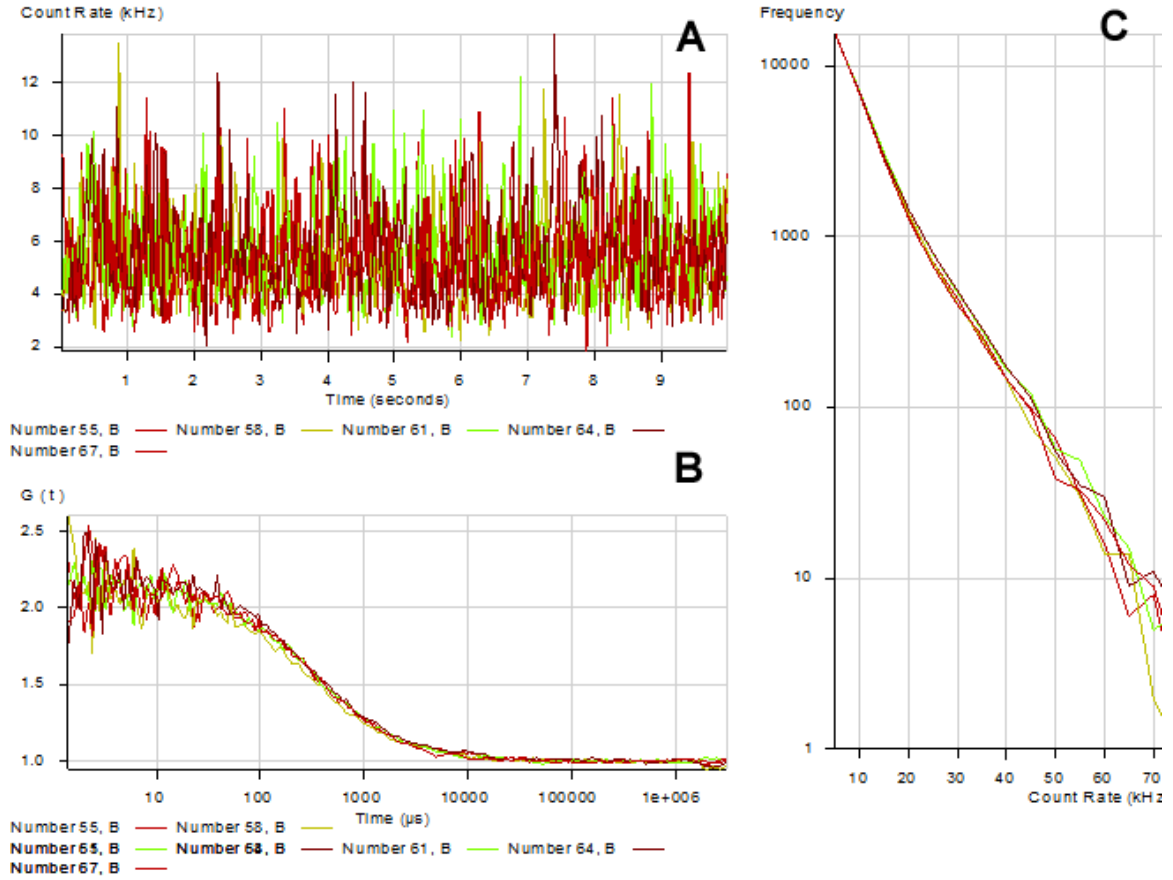


Figure 5: (A) Fluctuation intensity collected for Alexa 555 labeled $\alpha_v\beta_3$ monoclonal antibody in solution for 10s intervals through two channels ; (B) FCS auto correlation curves (C) Histogram of the photon counts for the same fluctuation analysis.

The intensity fluctuation of a typical fluorescence sample is given in Figure 5 A.

The mean value of the photon flux is given by “ $\langle I \rangle$ ”. The deviation of the fluorescence intensity from the average intensity is expressed by:

$$\delta I(t) = I(t) - \langle I \rangle \quad \text{Eq.5}$$

The autocorrelation function $G(\tau)$, compares the value of the signal at any random time “ t ” with the intensity value after a specific time interval (τ).

The normalized autocorrelation function ($G(\tau)$) is given by the following Eq.6 (90, 91):

$$G(\tau) = \frac{\langle \delta I(t) \cdot \delta I(t+\tau) \rangle}{\langle I \rangle^2} \quad \text{Eq. 6}$$

Representative FCS autocorrelation curves of Alexa-555 labeled $\alpha_v\beta_3$ monoclonal antibodies in solution are shown in Figure 5 B. The amount of time the molecule stays in the confocal volume depends on the diffusion coefficient of the molecule. For a planar sample, the normalized autocorrelation function is given in Eq. 7 (92).

$$G(\tau) = 1 + \frac{1}{N} \frac{1}{1+(\tau+\tau_D)} \quad \text{Eq. 7}$$

Where τ_D = the characteristic time a molecule spends in the detection area (detection time) and N = the average number of fluorescence molecules within the detection volume. . The absolute lateral mobility is given by the lateral diffusion coefficient (D). The following Eq. 8 can be used to find D by using the τ_D and the characteristic ω (confocal volume element) value. The ω can be obtained by performing an FCS measurement with molecules of known diffusion coefficient. The FCS method is quite powerful because it provides information about rate constants, probe concentrations, and diffusion coefficients of species (92)

$$D = \frac{\omega^2}{4\tau_D} \quad \text{Eq. 8}$$

2.6.4 Photon Counting Histogram (PCH) Analysis

The PCH method investigates the amplitude of fluorescence fluctuations obtained from the diffusing fluorophores in the confocal volume. PCH can be used to distinguish different molecules with the same diffusion coefficients by finding differences in their brightness. This method is particularly useful because it can differentiate the aggregation status of molecules based on their brightness. PCH analysis is used to determine the average photon concentration $\langle k \rangle$ of defined species with respect to the monomer or

oligomer. We also can calculate the molecular brightness of a certain species (ϵ -average number of photons per sampling time per molecule). The PCH analysis method is built on the following framework. A constant source of light is described by Poisson statistics (89):

$$p(N) = \frac{\langle N \rangle^N \cdot e^{-\langle N \rangle}}{N!} \quad \text{Eq. 9}$$

$p(N)$ = probability of events

N = number of events

The average photon count $\langle k \rangle$ of the PCH is given by the following Eq.10 (89):

$$\langle k \rangle = \frac{\epsilon}{V_0} \int_{V_0} \overline{PSF}(\vec{r}) \bar{d}r = \epsilon \frac{V_{PSF}}{V_0} \quad \text{Eq.10}$$

$\langle k \rangle$ = average photon counts

ϵ = the molecular brightness

V_{PSF} = the illumination volume

V_0 = total sample volume

PSF = point spread function

The molecular brightness is defined as:

$$\epsilon = I_0^N \beta \eta_w T \quad \text{Eq. 11}$$

T = the integration time increment

η_w = the detection efficiency

I_0 = maximum excitation when the fluorophore at center of V_{PSF}

$$I_0 = I_0 \cdot \beta \cdot PSF(r_0) \quad \text{Eq. 12}$$

$N=2$, for 2-photon, and 1, for single photon excitation

β = excitation probability; quantum yield, and instrument bias

The histogram for finding a particle of average brightness ε in V_o is described by the Poisson distribution of ε times the PSF integrated over the volume (given by Eq. 13):

$$p^{(1)}(k; V_o \varepsilon) = \frac{1}{V_o} \int Poisson(k; \varepsilon \cdot PSF(\vec{r})) \overline{d\vec{r}} \quad \text{Eq.13}$$

For “N” number of particles is given as:

$$p^{(N)}(k; V_o, \varepsilon) = (p^{(1)} \otimes p^{(1)} \otimes p^{(1)} \dots \otimes p^{(1)})(k; V_o, \varepsilon) N \text{ times} \quad \text{Eq. 14}$$

$p(N)$Probability distribution of N particles in the confocal volume

$p(1)$ Probability distribution of one particle in the confocal volume

In PCH, we collect photon counts over time inside a volume (V_o) to generate a histogram of photon counts. The shape of this histogram, $P(k; N_{avg}, \varepsilon)$, provides information about the average number, N_{avg} and brightness, ε , of molecules diffusing within the confocal volume:

$$P(k; N_{avg}, \varepsilon) = \sum_0^{\infty} p^{(N)}(k; V_o, \varepsilon) \cdot Poisson(N, N_{avg}, \frac{V_o}{V}) \quad \text{Eq. 15}$$

PCH for 2 species with different brightness is given by the convolution of the two species:

$$P(k; N_1, \varepsilon_1, N_2, \varepsilon_2) = P(k; N_1, \varepsilon_1) \otimes P(k; N_2, \varepsilon_2) \quad \text{Eq.16}$$

2.6.5 Atomic Force Microscopy (AFM)

AFM is a high resolution microscopy that achieves sub nanometer resolution (93).

This powerful scanning probe microscopy method provides accurate information on small height changes. This is accompanied by using a 40 nm probe attached to the cantilever. A schematic representation of an AFM set up is illustrated in Figure 6. AFM can be operated in contact and tapping mode. AFM tapping mode is more suitable for lipid monolayers and bilayers. In tapping mode, the AFM tip during scanning oscillates at a certain frequency. To detect tip deflections caused by the sample, a laser beam is

focused on the backside of the oscillating cantilever with the attracted AFM tip and the reflected laser beam is guided to a position-sensitive photodiode detectors. Consequently, changes in sample height and stiffness are detected AFM photodiodes detectors (94). . Analysis of the sample is achieved by scanning of the sample using a scanning stage` (79).

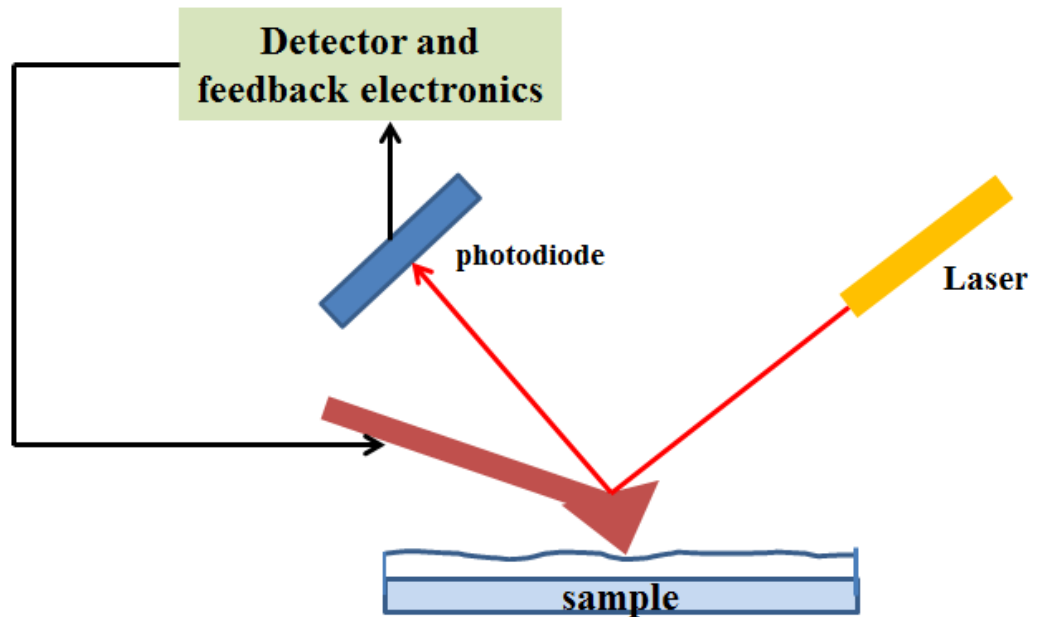


Figure 6: Schematic diagram of the AFM microscope showing the beam deflection method

CHAPTER 3. MATERIALS AND EXPERIMENTAL SECTION

3.1 Materials

The phospholipids 1-stearoyl-2-oleoyl-*sn*-glycero-3-phosphocholine (SOPC), DOPC, DPPC, and CHOL were purchased from Avanti Polar Lipids (Alabaster, AL). The procedure for synthesizing the lipopolymer 1,2-dioctadecyl-*sn*-glycero-3-N-poly(2-methyl-2-oxazoline)₅₀ (diC₁₈M₅₀) has been described previously (95). The dye-labeled lipids N-(7-nitrobenz-2-oxa-1,3-diazol-4-yl)-1,2-dihexadecanoyl-*sn*-glycero-3-phosphoethanolamine, triethylammonium salt (NBD-DHPE), N-(6-tetramethylrhodamine-thiocarbamoyl)-1,2-dihexadecanoyl-*sn*-glycero-3-phosphoethanolamine, triethylammonium salt (TRITC-DHPE), 1,1'-Dioctadecyl-3,3,3',3'-Tetramethylindodicarbocyanine, 4-Chlorobenzenesulfonate Salt (DiD), 1,1'-Dioctadecyl-3,3,3',3'-Tetramethylindodicarbocyanine Perchlorate (DiI), as well as the kits for fluorescently labeling antibodies with Alexa Fluor-555 were obtained from Invitrogen (Carlsbad, CA). The dye-labeled lipopolymer 1,2-dipalmitoyl-*sn*-glycero-3-phosphatidylethanolamine-N-[amino(polyethylene glycol)2000]-TAMRA (DPPE-PEG2000-TAMRA) was synthesized from the sodium salt of the amino-functionalized lipopolymer (Avanti Polar Lipids, Alabaster, AL) and TAMRA (Invitrogen, Eugene, OR), as described before (76). Chloroform (HPLC grade, Fisher Scientific, Pittsburgh, PA) was used as the spreading solvent for the formation of lipid monolayers at the air-water

interface. Milli-Q water (pH =5.5, 18 M Ω -cm resistivity; Milli-Q, Millipore, Billerica, MA) was employed as the subphase material in the film balance trough. Glass coverslips were prepared by first baking them for 3 h at 515°C in a kiln followed by subsequent sonication steps in a bath sonicator using solutions of 1% SDS for 45 min, MeOH saturated with NaOH, and 0.1% HCl (Fisher Scientific) . The slides were rinsed with Milli-pore water in between sonication steps for 10 min. Human integrin $\alpha_v\beta_3$ and $\alpha_5\beta_1$, octyl- β -D-glucopyranoside formulation, the monoclonal antibodies (MAbs) anti-integrin $\alpha_v\beta_3$, and anti-integrin $\alpha_5\beta_1$, human purified vitronectin (VN), and human purified fibronectin (FN) were purchased from Millipore (Billerica, MA). Rhodamin6G (R6G) was obtained from Sigma-Aldrich (St. Louis, MO). The surfactant n-Octyl- β -D-glucopyranoside (OG) Fisher Bio Reagents (Fairlawn, NJ) was used for incorporation of proteins into bilayers. SM-2 biobeads (Bio-Rad, Hercules, CA) were used to remove excess surfactant.

3.2 Experimental Procedures

3.2.1 Construction of Polymer-Tethered Bilayers using LB/LS Transfer Techniques

Polymer-tethered phospholipid bilayers with bilayer-spanning domains were prepared using subsequent LB/LS monolayer transfers. This technique has been described in detail elsewhere (75). The procedure for the preparation of symmetric and asymmetric bilayers only differs in terms of LB and LS monolayer compositions. Here we explain the method briefly. A freshly prepared glass coverslip on a dipper is immersed into the water subphase of the film balance trough (Labcon, Darlington, UK). Next, a chloroform solution of the LB monolayer is spread at the air-water interface. The

monolayer formed at the air-water interface is compressed to a film pressure of 30 mN/m and kept for 40 min. for equilibration. Then, the monolayer is transferred from the air-water interface to the glass slide on the dipper by synchronically moving the film balance barrier inward and the dipper upward. The trough is cleaned before making the next monolayer transfer (LS transfer). To build an LS monolayer, the lipid composition of the LS layer is spread at the air-water interface. Next, the coverslip containing the LB monolayer is carefully pressed through the LS monolayer at the air-water interface and placed at a depression slide at the bottom of the trough (Figure 3). Following the LB/LS transfers, the bilayer was observed under the EPI microscope to confirm the presence and quality of the bilayer. When integrity and cared composition (symmetric vs. asymmetry) were confirmed, the bilayer was transferred to a petri-dish filled with phosphate buffered saline (PBS) for further imaging experiments. Alternatively, in the case of low concentrations of dye-labeled lipids, bilayer integrity was analyzed using confocal APD detection without utilizing EPI.

3.2.1.1 Building Symmetric Bilayers

The same lipid composition in the top and the bottom leaflet is used to build symmetric bilayers, except the bottom leaflet also contains 5 mol% lipopolymer (typically: diC₁₈M₅₀). Lipopolymers are added to uplift the bilayer from underlying glass substrate, thus enhancing lateral fluidity of incorporated proteins and promoting inter leaflet domain registration (75). The presence of domains in the top and bottom leaflet of the bilayer was confirmed by EPI microscopy through NBD-DHPE dye labeled lipids. Table 1 summarizes different LB and LS lipid compositions used throughout this Ph.D.

thesis work. Type I lipid composition in Table 1 was used to make the LB/LS monolayers of the symmetric bilayer. 0.2 mol% NBD-DHPE dye labeled lipid is added to in both leaflets of the bilayer, and 5 mol% diC₁₈M₅₀ is added to the bottom leaflet.

Table 1: Different types of lipid composition to build LB and/ or LS monolayers

Type	Lipid Composition
I	DOPC: DPPC: CHOL (1:1:1)
II	DOPC: DPPC: CHOL (2.1:1.2:1)
III	DOPC: DPPC: CHOL (1.5: 0.5: 1.0)
IV	DOPC:DPPC: CHOL (2.9: 0.32: 1)
V	DOPC: CHOL (2:1)
VI	DOPC: CHOL (4:1)

3.2.1.2 Building Asymmetric Bilayers

In asymmetric bilayers, the composition of the top and the bottom leaflet are different. The top LS monolayer is formed with a Type I lipid composition and the bottom LB layer lipid composition was formed with a Type V lipid composition (Table 1). Here, apart from the major lipid composition, 0.4 mol% NBD-DHPE dye label lipids were added to the LS layer and the LB monolayer contained 5 mol% diC₁₈M₅₀ lipopolymer and 0.1 mol% DiD. Note that the same mol% of CHOL is utilized in each leaflet. In this asymmetric bilayer, we should observe l_o/l_d phase separation in the top leaflet and a homogenous l_d phase in the bottom leaflet. This can be confirmed by fluorescence detection methods (EPI or APD confocal analysis). The phase separation in the top leaflet is visualized by the phase separation of NBD-DHPE dye labeled lipids. The homogenous non-phase separated bottom layer was confirmed by DiD labeled lipids in the bottom layer. As confirmed in control experiments, DiD phase separates in the presence of coexisting l_o-l_d domains. Alternatively, asymmetric bilayers were built using LS and LB compositions of Type II and V, respectively. The LS compositions contained 0.4 mol% NBD-DHPE to confirm the l_o-l_d phase separations in the top leaflet and the LB composition included 0.1 mol% DiD to assure bilayer asymmetry.

3.2.1.3 Elucidating the Stability of Asymmetric Bilayers

To test the stability of asymmetric lipid compositions over time, we conducted a set of control experiments, in which the effects of lipid flip flop surfactant addition on the bilayer asymmetry were tested. In order to test the effect of lipid flip flop on the stability of bilayer asymmetry, a bilayer is prepared with Type III lipid composition in both LS/LB monolayers. Apart from the lipid composition 0.4 mol% NBD-DHPE is added to the top LS leaflet and 0.1 mol% DiD is added to the LB bottom leaflet. This symmetric bilayer composition is the equilibrium composition, which will be attained by the flipping of lipid molecules in an originally asymmetric bilayer with LS and LB lipid composition of Types I and V, respectively. We compare the phase separation of this bilayer with the phase separation of the asymmetric lipid bilayer in order to elucidate the flipping of the lipid molecules from one leaflet to the other. This will be explicitly described in section 3.2.1.2.

Next the stability of membrane asymmetry with respect to surfactant was investigated. It was done by investigating the membrane asymmetry stability in the presence of the required amount of surfactant necessary for integrin incorporation.

3.2.1.4 Characterization of l_o - l_d Phase Separation in Symmetric/Asymmetric Bilayers

We characterize the l_o / l_d phase separated regions in symmetric and asymmetric bilayers through confocal XY scan and FCS in order to determine the brightness, concentration and lateral mobility of dye-labeled lipids. To conduct such experiments, 0.002 mol% TRITC-DHPE dye lipids were added to each leaflet of the symmetric and asymmetric bilayer systems. Then FCS analysis is conducted on these bilayers and the

brightness is analyzed using the PCH method (explained in part 3.2.3.1). The excitation of TRITC-DHPE is done using a 543 nm “HeNe laser”. The diffusion time was obtained from the FCS raw data and this value was used to calculate the diffusion coefficient of the molecule in the different phase regions. Fluorescent intensity analysis was done by using the CS-XY method by using lipid bilayers having 0.02 mol% TRITC-DHPE dye labeled lipids in each leaflet. The concentration of the dye in each phase or the raftophilic excess (E_{raft}) value was calculated as described in the method section 3.2.3.2. Control experiments are done in order to compare the values with binary mixtures of DOPC: CHOL (4:1) and DOPC: CHOL (2:1) containing lipid bilayers.

3.2.1.5 Building Raft-Mimicking Lipid Domains Containing Symmetric Bilayers with Different Cholesterol Concentrations

Symmetric bilayers with raft-mimicking l_o - l_d phase separated lipid mixtures of different CHOL (15 mol%, 20 mol%, 28 mol%, 35 mol%, and 37 mol%) compositions were prepared as well. In this case DOPC and DPPC are maintained at a 1:1 ratio in all bilayers and the CHOL content is systematically varied. Polymer-tethered phospholipid bilayers of symmetric lipid composition were prepared using the LB/LS transfer technique, thereby adapting procedures reported recently for corresponding membrane systems with B_l domains (9; 12). This is also described in this thesis in section 3.2.1.

3.2.1.6 Preparation of Polymer-tethered Monolayers and Bilayers with Different Concentrations of Cholesterol

The standard protocol for preparation of polymer-tethered phospholipid monolayers using LB transfer and bilayers using LB/LS transfers is explained in the thesis section 3.2.1 (3, 75). In the case of polymer-tethered membranes comprised of

phospholipids, CHOL, and DSPE-PEG 5000, the LB monolayer was first prepared by spreading a mixture of lipids with 3 mol % DSPE -PEG 5000, 5-40 mol % CHOL, 0.5 mol% TRITC-DHPE, and the rest with SOPC phospholipids. This monolayer was characterized within 24 hours using EPI and AFM. Next, the bilayer was formed using this same LS monolayer composition as employed in the LB layer, however, without DSPE-PEG 5000.

3.2.2 Protein Incorporation into Lipid Bilayers and Detection with Fluorescence Microscope

Protein incorporation into the polymer-tethered lipid bilayer has been described previously (1). Briefly, micelle-stabilized membrane proteins (1.3×10^{-11} mol) were added to the bilayer sample with 2 ml of 0.08 mg/ml of surfactant (OG). This amount leads to a protein concentration in the bilayer of 10^{-3} mol%. Protein incubation was done for 1.5-2 hrs. Next, a single layer of SM-2 bio-beads (Bio-Rad, Hercules, CA) is added on top of the bilayer for 15 min. to remove the surfactants from the bilayer. The bio-beads were removed by washing with PBS. Finally, fluorescently labeled antibodies were added for 3-4 hrs at room temperature followed by washing with PBS to remove unbound antibodies. Fluorescence detection methods (EPI and confocal XY scan) are used to confirm the incorporation of proteins into the bilayers by detecting Alexa Fluor-555 labeled antibodies. Fluorescence microscopy images, confocal fluorescence intensity, and FCS were obtained for this system. Next, appropriate ligands (VN for $\alpha_v\beta_3$ and FN for $\alpha_5\beta_1$) for integrins were added and incubated for 2-4 hrs at room temperature (molar ratio of integrin: ligand is 1:1). Then the bilayer was rinsed with PBS to remove excess (unbound) ligands and the sample was analyzed using the same fluorescence detection

methods again. A control experiment was done, in which MAbs are added in the absence of membrane proteins, thus obtaining insight into the non-specific binding of MAbs on the bilayer surface.

3.2.3 Combined EPI Microscopy, Confocal Fluorescence Correlation Spectroscopy (FCS), and Confocal Fluorescence Intensity Analysis

EPI microscopy and FFS is performed using confocal Confocor 2 system (Zeiss, Jena, Germany) equipped with an inverted optical microscope (Axiovert 200M, Zeiss, Oberkochen, Germany) with a specific microscope objective (Zeiss C-Apochromat, water immersion, 40 x NA = 1.2) . A Zeiss AxioCam MRm monochrome digital camera and Axiovision 4.8 software is utilized to conduct the EPI studies, which provide information about the presence of l_o and l_d domains in lipid bilayer.

The Confocor 2 system is equipped with several lasers, which include 1.0 mW HeNe1 laser (543 nm) with a 560-615 nm emission filter, 5.0 mW HeNe2 (633 nm) laser with a 650 nm long pass filter, and 30 mW Argon laser (488 nm) 505-530 nm emission filter. Confocal fluorescence intensity analysis was performed confocal spectroscopy XY (CS-XY) scans. These scans were performed in 10 x 10 μm size areas with the step size of 0.5 μm . Three laser lines were used sequentially to perform three separate scans of the bilayer. The HeNe1 laser (543 nm) is used to detect the integrin distribution. The HeNe2 (633 nm) laser is utilized to detect DiD in the bottom leaflet, and the Argon (488nm) laser is employed to detect NBD-DHPE distribution in the top leaflet of the bilayer. Control experiments in the presence of DiD and NBD-DHPE, with no proteins, were conducted to enable accurate background correction for this analysis. The maximum count rate position was selected as the marker for the correct Z-position of the confocal

plane. Fluorescence fluctuation spectroscopy collects data for FCS and brightness analysis method (PCH). Instrumentation set up for this system has been explained in sections 2.6.2 and 2.6.3. FCS data analyzed in terms of autocorrelation analysis (89). The auto correlation curve provides information about the diffusivity of probe molecules in solution and in the bilayer. Specifically, FCS autocorrelation curve provides information on the characteristic diffusion time (τ_2) of the molecules in the detection volume. The obtained diffusion time values are used to calculate the diffusion coefficient of the molecule. This has been explicitly described in section 2.6.3. The data acquisition/analysis of PCH data is described in the next section.

3.2.3.1 Determination of Integrin Brightness and Oligomerization Status from PCH

The brightness and number of particles within the confocal volume are each described by a point spread function. The probability that a particle will have a particular brightness within the volume V_0 can be described by a histogram of the photon counts for a single particle given in Eq. 13, which has been described in section 2.6.4. We assume that particles are independent and the probability distribution of “N” particles in the volume is given by the Eq.14 in section 2.6.4 (the probability of seeing 1 particle “N” times). The average concentration of the number of particles in the V_0 is given in the Eq.15 (section 2.6.4). The photon counting histogram for two species is obtained by the convoluting the probabilities of each species. This can be obtained by the Eq.16 in section 2.6.4.

In some systems, the background signal can be treated as a species with low brightness and high number and de-convolution can separate the particle signal from

background. In addition, for a population of monomers and dimers, it is possible to constrain the brightness of the second species ϵ_2 , to be double the brightness of the first species, ϵ_1 . Both of these effects can be described by a convolution of three species. The Confocor 2 acquisition software samples total photon counts within the confocal volume, and bins the data by aggregating photon counts “every milliseconds”. These data can be aggregated into a histogram. The experimentally determined PCH data are added in to the PCH algorithm by first assuming that all particles are of a single brightness ϵ . Using this assumption as a starting point, the data are re-fitted considering the possibility of particles of brightness 2ϵ (dimers) as well. Due to the close proximity of the glass slides and other background, it is also necessary to include a term for a background species. As a result we will be able to obtain $N_{monomer}$ (average number of monomer), $\epsilon_{monomer}$ (brightness of monomer), N_{dimer} (average number of dimers), and the fraction of dimerization particles ($X_{dimer} = N_{dimer}/(N_{monomer}+N_{dimer})$). This method has been explicitly described previously (3).

3.2.3.2 Protein Sequestration Analysis (E_{raft}) and Protein Migration Analysis ($X_{migrate}$)

The domain-specific distribution of integrins in the presence of l_o and l_d domains was determined as described before (7). In short, raw data of the integrin distribution was obtained from confocal XY scans of the green and red channels. Each raw data set was corrected for NBD-DHPE, DiD channel bleed through, as well as background. To correct for background, control experiments were conducted without integrins, but with dye-labeled anti-integrin MAbs. Integrin sequestration in coexisting l_o - l_d domains can be quantified in terms of a partition coefficient ($K_p(l_o/l_d)$), (3) defined as the corrected ratios

of the intensities of the signal in the ordered and disordered phases, I_{lo}/I_{ld} . The background was subtracted from the intensities obtained from the control experiments with dye-labeled anti-integrin MAbs. A normalized measure of integrin sequestration is provided by the parameter E_{raft} , which is defined as:

$$E_{raft} = \left(\frac{I_{lo} - I_{ld}}{I_{lo} + I_{ld}} \right) \quad \text{Eq. 17}$$

Then changes in membrane protein sequestration (e.g., due to addition of ligands) can be quantified using the parameter $X_{migrate}$ (3)

$$X_{migrate} = \left(\frac{E_{raft(+ligand)} - E_{raft(-ligand)}}{2} \right) \quad \text{Eq. 18}$$

3.2.4 Image Acquisition and Analysis

3.2.4.1 Acquisition and Analysis of EPI-Micrograph Images of LB Monolayers with Different Concentration of Cholesterol with 3 mol% DSPE PEG-5000

Epifluorescence microscopy images were taken on an inverted optical microscope (Axiovert 200M, Zeiss, Oberkochen, Germany). The beam was focused onto the sample by a microscope objective (Zeiss C-Apochromat, water immersion, 40 x NA = 1.2) with optional optovar magnification (1.6x). Phospholipid-lipopolymer mixed monolayers containing dye-labeled lipids were prepared and the buckling structures were analyzed using EPI. The bearing area (i.e., the percentage of buckled regions) for each monolayer was obtained by analyzing the EPI micrographs using Image J software. Specifically, EPI images were opened in Image J and the bearing area was determined by using the area percentage analysis function of the Image J software. In short, for each opened image, the foreground and background colors are set to white and black respectively, by using the

“edit” options and color tool bars. Next, we utilized the “set measurements” option from the analyze tool bar, selected the area of interest, adjusted the threshold, and determined the bearing area on the basis of the brightness of the image.

3.2.4.2 Atomic Fluorescence Microscopy and Image Analysis from Nanoscope 6.1 Software

AFM experiments were conducted using a Digital Instruments Bio-Scope (Digital Instruments / Veeco Metrology group, Plainview, NY). AFM micrographs were analyzed using Nanoscope IV (V6.12) (Digital Instruments / Veeco Metrology group, Plainview, NY) and Origin 8 (Origin lab Corporation, Northampton, MA) analysis software. AFM data were acquired in soft tapping mode using silicon nitride AFM probes (Budget sensors, Innovative solutions Bulgaria Ltd., Sofia, Bulgaria) characterized by a spring constant of ~ 0.27 N/m and a tip radius of < 15 nm. AFM data acquisition was pursued by scanning $10 \times 10 \mu\text{m}^2$ and $5 \times 5 \mu\text{m}^2$ sections, respectively, of the membrane samples using a scan rate of 1 Hz and a resolution of 256×256 pixels. Typically, AFM images were taken within 24 hours of sample preparation. All AFM data were analyzed using the section analysis tool to determine the width and height of buckling structures. The AFM section analysis was pursued at approximately half micron intervals in the 40 mol% CHOL containing monolayers to obtain the buckle height and the buckle width. In monolayers with less than 40 mol% CHOL, the section analysis was done on the buckles, which are above the height of 2 nm. In order to achieve statistical significance, three separate AFM images from each CHOL category were used to get the height and the width of the buckles, and the average and the standard deviation was calculated.

3.2.5 Calculating Different Buckling Parameters with Different Cholesterol Containing LB Monolayers

A lipid monolayer compressed and transferred to a glass slide has certain parameters describing its stiffness. These parameters include area elastic modulus, bendability or bending modulus, critical compressive biaxial stress at the onset of buckling (σ_c), and compressive biaxial stress in the unbuckled state (film stress - σ_0). These properties will vary depending on the composition of the lipid monolayer. For example, as we previously showed, increasing the concentration of DSPE-PEG 5000 does increase the bending modulus of the monolayer (26). Of more biological interest, these properties can also vary for different concentrations of CHOL. The K_A^0 (elastic area-expansion modulus of a single, bare lipid layer without polymer lipid) for each concentration of CHOL was obtained from a previous work (81). The area elastic modulus (K_A) for varying lipopolymer types and concentrations (X_p) can be calculated from Eq. 2 described in section 2.4.4. The K_A^0 (elastic area-expansion modulus of a single, bare lipid layer, without polymer lipid for each CHOL concentration was obtained from Lasic et al (1995) (81). The bending modulus (K_c) of the film was calculated by using Eq.19 with the value obtained from the Eq.2 for K_A and the thickness of the monolayer (h) using calculations of the film thickness for different concentrations of CHOL as described in section 3.2.5.1.

$$K_c \sim K_A h^2 \quad \text{Eq. 19}$$

The equation for the plain strain modulus of the film E_f^* and its relations to the Young's modulus is given by the Eq. 20 and 21 respectively (96),(97). E_f = Young modulus of the film, ν_f = Poisson's ratio of the film.

$$E_f^* = \frac{E_f}{(1-\nu_f)^2} \quad \text{Eq. 20}$$

$$K_c = \frac{E_f h^3}{12(1-\nu_f)^2} \quad \text{Eq. 21}$$

$$E_f^* = \frac{E_f}{(1-\nu_f)^2} = \frac{12K_c}{h^3} \quad \text{Eq. 22}$$

The plain strain modulus of the film was calculated by using the Eq.22, which is formulated from Eq. 20 and 21. The σ_c and σ_0 are calculated using the Eq.3 and 4 described in section 2.5. The graphs of the K_A , K_c , σ_c , and σ_0 with respect to the CHOL concentration were plotted to understand the relation between these parameters to the CHOL concentration.

3.2.5.1 Calculating the Monolayer Film Thickness with Increasing Cholesterol Concentration

Monolayer film thickness was calculated according to Table 1. An average monolayer thickness without CHOL was considered to be 2.5 nm (98). The percent increase in the bilayer thickness with increasing CHOL concentration was used to calculate the thickness of the monolayer for each category (99). Then the total thickness of the monolayer with DSPE-PEG 5000 was obtained by adding the thickness attributed to the lipopolymer. The length of the lipopolymer was taken as 8.8 nm (77).

Table 2: Monolayer film thickness with increasing cholesterol concentration

CHOL mol %	% increase in the bilayer with increasing CHOL concentration	Thickness of the lipid monolayer /nm	Total thickness of the monolayer (lipid+polymer) /nm
0	0	2.50	11.30
5	5	2.62	11.42
10	10	2.75	11.55
20	18	2.95	11.75
30	20	3.00	11.80
40	20	3.00	11.80

3.2.6 Investigating the Distribution of Lipopolymer, Cholesterol and the Lipids in LB Monolayers

Experiments were conducted with CHOL, phospholipids, and dye-labeled lipopolymers to explore the possibility of large scale phase separations in our CHOL lipopolymer systems. Monolayers were prepared with 3% mol DSPE-PEG 5000, 40 mol% CHOL, and 55.8 mol% SOPC (0.6 mol% dye concentration) lipids. EPI fluorescence microscope images were taken with equal exposure time for all the monolayers in order to compare the dye distribution in different lipid composition. Then the intensity analysis was performed in buckled and unbuckled regions for each monolayer investigated. Next, we compared the intensity of the buckle region to that of the unbuckled region. The value is used to compare the distribution of lipid molecules, lipopolymers, and CHOL in the buckled and unbuckled regions.

CHAPTER 4. RESULTS AND DISCUSSION

4.1 Influence of Bilayer Asymmetry on Integrin Sequestration

4.1.1 Symmetric and Asymmetric l_o - l_d phase Separations in Polymer-Tethered Lipid Bilayers

To explore the relationship between bilayer asymmetry and integrin sequestration, we determined the distribution of $\alpha_v\beta_3$ and $\alpha_5\beta_1$ integrins in a polymer-tethered lipid bilayer of asymmetric lipid composition with coexisting l_o - l_d lipid regions and compared these experiments with previous work on symmetric bilayers. Figure 7 shows the difference between symmetric and asymmetric bilayer systems. In an asymmetric bilayer, the l_o - l_d phase separation is only seen in the top leaflet of the bilayer. In this system, the bottom leaflet contains a homogenous l_d phase. In a symmetric bilayer, the l_o - l_d phase separation spans the whole bilayer.

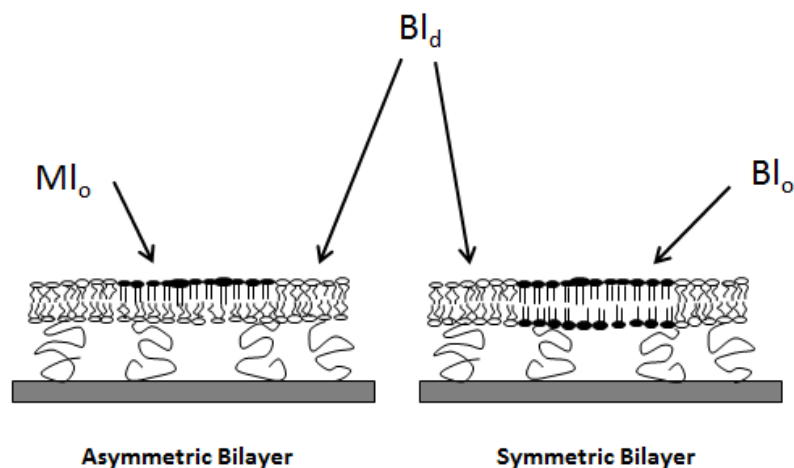


Figure 7: Schematic of l_o - l_d phase separations in polymer-tethered lipid bilayers of asymmetric (left) and symmetric (right) lipid compositions. In the asymmetric bilayer system, l_o - l_d phase separations are exclusively located in the top leaflet (LS monolayer) of the bilayer while the bottom leaflet (LB monolayer) is characterized by a homogeneous l_d phase (coexistence between Ml_o and Bl_d regions). In contrast, the symmetric bilayer exhibits bilayer-spanning l_o and l_d regions (coexistence of Bl_o and Bl_d).

4.1.2 Design and Characterization of Asymmetric Bilayers

Asymmetric bilayers are prepared by using the LB/LS transfer method, which is described in the Materials and Methods section. There are several advantages to use the LB/LS transfer method to make solid supported bilayers over the vesicle fusion method. Dipping in the LB/LS process enables us to form homogenous bilayers with few defects, and fabrication of asymmetric composition is achieved. Figure 8 shows the representative EPI micrograph images of an asymmetric bilayer. The l_o - l_d phase separation in the top leaflet is shown by NBD-DHPE, which is a raftophilic membrane marker (Figure 8 A). The bottom leaflet is labeled with raftophobic membrane marker DiI showing a homogenous l_d phase. This is depicted in Figure 8 B. The lipid composition of the asymmetric bilayer (Figure 8, A and B) is composed of Type I (LS layer) and Type V

(LB layer) lipid composition (Table 1). Figure 8, C and D depicts a representative symmetric bilayer showing the l_o - l_d phase separation in both leaflets through the NBD and DiI channels. Again the top leaflet is labeled with NBD-PE and the bottom leaflet is labeled with DiI. The lipid composition of the symmetric bilayer (Figure 8, C and D) is composed of Type IV (LS layer) and Type II (LB layer) lipid compositions (see Table 1).

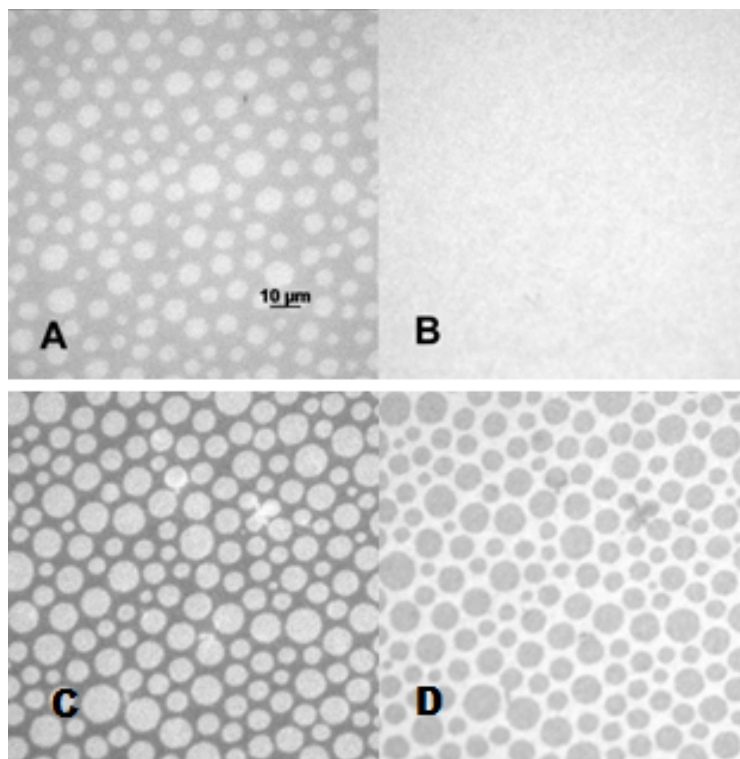


Figure 8: EPI-micrographs showing the asymmetric (A, B) and the symmetric lipid bilayers (C,D) observed through the NBD (A,C) and DiI channels (B,D). (A)-Asymmetric bilayer LS layer (top leaflet) (B)-Asymmetric bilayer LB layer (bottom leaflet) (C)-Symmetric bilayer LS layer (top leaflet) (D)-Symmetric bilayer (LB layer).

DiI is chosen in the bottom leaflet because it is less prone to flip flop across both leaflets (100). This assures that the observation through the DiI channel will only give information about the bottom leaflet. Consequently, the observation through the NBD channel exclusively displays the lipid-lipid phase separation in the top leaflet (l_o) of asymmetric bilayers.

4.1.3 Elucidating the Stability of Bilayer Asymmetry

To confirm the stability of the bilayer, EPI analysis is repeated at different time intervals. Representative EPI micrographs of the asymmetric bilayer after 12 hrs are presented in Figure 9. Again, the EPI micrographs shows phase separation in the top leaflet through the NBD channel (Figure 9 A) and no phase separation in the bottom leaflet through the DiI channel (Figure 9 B). In another control experiment, the asymmetric bilayer was incubated with surfactant in order to confirm the stability of the asymmetric bilayer in the protein reconstitution process. Specifically, the asymmetric bilayer is incubated with 0.55 μM OG for 2 h, rinsed with PBS and incubated for another 10 h. As Figure 9 demonstrates, the corresponding EPI micrographs through the NBD (9 A) and DiI channels (9 B) show no notable differences when compared to the surfactant-free bilayers in Figure 8, A and B.

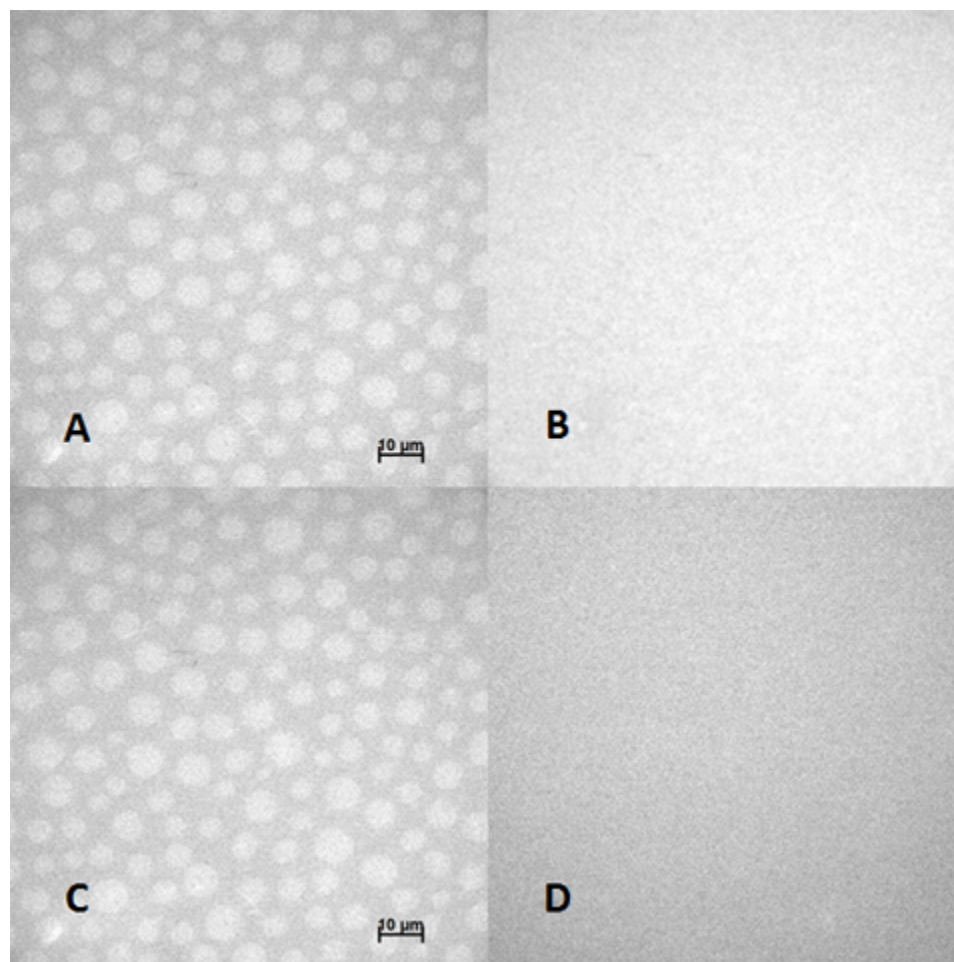


Figure 9: Epi-micrographs showing the stability of the asymmetric bilayer in the presence of surfactants over time. (A) and (B): Images of the asymmetric bilayer after 12 hrs. This bilayer is incubated in an appropriate amount of surfactant for 2 hrs followed by washing with PBS. (A): Top layer-DOPC: DPPC: CHOL- (2.1: 1.2: 1.0) & 0.5% NBD-PE visualized through an NBD-PE filter. (B): Bottom layer - (DOPC: CHOL) -2:1 (5 mol% diC₁₈M₅₀ & 0.1% DiI). (C): Image of the asymmetric bilayers of NBD-DHPE distribution containing *Ml_o* domains [LB composition: (2:1) (DOPC: CHOL); LS composition: (2.1:1.2:1.0) (DOPC: DPPC: CHOL)]. (D): Symmetric bilayer composition [LB and LS lipid composition: (1.5:0.5:1.0) DOPC: DPPC: CHOL]. In both bilayer systems, 5 mol% of diC₁₈M₅₀ is included in the LB composition. The symmetric bilayer composition reflects the condition of disappearing concentration gradients of DOPC and DPPC across asymmetric bilayers

Figure 9, C and D compare the lipid mixing behavior in the top leaflet of an asymmetric bilayer [LS composition: 2.1:1.2:1.0 (DOPC: DPPC: CHOL); LB composition: 2:1 (DOPC: CHOL)] (C) and a symmetric bilayer [LB/LS composition:

1.5:0.5:1.0 (DOPC: DPPC: CHOL)] (D). Here the symmetric bilayer contains the hypothetical equilibrium composition assuming complete loss of bilayer asymmetry via lipid flip flop. Figure 9 D represents the symmetric bilayer obtained from this composition. This figure shows there is no l_o - l_d phase separation in the LS layer. Because lipid-lipid phase separation can be observed in the asymmetric bilayer (C), the control experiment in Fig. 9 D confirms that loss of bilayer asymmetry through flip flop processes appears to be insignificant. In other words, the asymmetric bilayer compositions employed remains remarkably stable. Previous work on asymmetric bilayers has also shown that there is a relatively slow flip flop between the two leaflets (75),(101).

4.1.4 Characterizing l_o and l_d Domains in the Symmetric and Asymmetric Bilayer

Characterization of l_o and l_d domains in the symmetric and asymmetric bilayer is done by analyzing the domain-specific brightness, concentration, and lateral diffusion of lipids. This is accomplished by using confocal fluorescence intensity analysis and FCS analysis of 0.002 mol% TRITC-DHPE in both leaflets of the bilayer. The results of the domain-specific characterization of symmetric and asymmetric bilayers are provided in Table 3. This table also includes the results obtained from control experiments on two binary DOPC-CHOL mixtures (DOPC/CHOL-2:1 and 4:1). The control experiments confirmed that the increase in CHOL in the bilayer is associated with reduced lateral mobility and brightness of TRITC-DHPE. In contrast, there is no difference in lateral mobility and brightness of TRITC-DHPE in l_o and l_d domains of asymmetric and symmetric bilayer systems. The largely indistinguishable lateral mobility in the l_o and the

l_d domains of the symmetric and asymmetric bilayers has also been reported previously (102),(103).

Table 3: Characterization of l_o - l_d phase separations in asymmetric and symmetric bilayers

Bilayer type	Diffusion Time (ms)	Diffusion Coefficient ($\mu\text{m}^2/\text{s}$)	Brightness (PCH analysis)	Normalized Fluorescence Intensity (CS-XY Analysis)
DOPC only	3.16±0.34	1.68±0.20	6.25±0.71	
DOPC :CHOL (4:1)	5.89±0.99	0.89±0.15	4.57±0.79	
DOPC :CHOL (2:1)	8.69±1.50	0.61±0.13	3.45±0.36	
Asymmetric - l_d (Bl_d)	5.87±1.65	0.90±0.21	3.97±0.57	0.60±0.03
Asymmetric - l_o (Ml_o)	6.19±1.17	0.86±0.15	3.77±0.73	0.40±0.02
Symmetric - l_d (Bl_d)	6.21±1.17	0.90±0.14	4.10±0.40	0.70±0.03
Symmetric - l_o (Bl_o)	6.34±1.34	0.83±0.15	3.57±0.44	0.30±0.02

In addition to TRITC-DHPE labeled diffusion and brightness characterization, l_o and l_d domains in asymmetric and symmetric bilayers are also analyzed in terms of normalized fluorescence intensity ($I=I_{i(l_o,l_d)}/I_{l_o+I_{l_d}}$) of TRITC-DHPE using confocal spectroscopy (CS-XY) scans. Again the normalized fluorescence intensity data show comparable values for l_o and l_d regions in asymmetric and symmetric bilayers. Together the PCH brightness and normalized fluorescence intensity data suggest that there is not much difference in lipid packing density between l_o and l_d regions of symmetric and asymmetric bilayers.

4.1.5 Comparison of Integrins ($\alpha_v\beta_3$ and $\alpha_5\beta_1$) Sequestration in Asymmetric and Symmetric Bilayers (in the presence and absence of ECM ligands)

Study of protein sequestration in rafts is challenging, due to the small size and transient nature of raft domains (104). Current methods of raft analysis include detergent extraction assay, crosslinking assay and CHOL depletion assay (49, 50). These methods

are often indirect and have drawbacks. The ideal solution to these problems would be to utilize raft-mimicking model membranes. Model membranes have been used to study the sequestration of membrane receptors and their responses to crosslinking agents (105, 106). However, model membrane systems are well suited to study the protein sequestration without using any artificial cross linking agents. Previously, our group applied this concept and explored the sequestration of integrins in polymer-tethered lipid bilayers of symmetric composition with coexisting Bl_o - Bl_d domains using sensitive fluorescence fluctuation spectroscopy (3). Integrins are used for these experiments because of their involvement in many raft associated activities, such as cell adhesion, morphology, motility, and angiogenesis. They can also be functionally regulated by different factors, such as ligand binding, divalent cations, and micro clustering (107). In the current Ph.D. thesis work, the role of bilayer asymmetry in integrin sequestration is explored using a comparable imaging strategy. In this case, integrins are added to symmetric and asymmetric bilayers according to the description given in section 3.2.2. Integrin sequestration studies in Ml_o and Bl_o domains are characterized using confocal CS-XY scans. . Figure 10, A-J shows representative CS-XY scans of the $\alpha_v\beta_3$ integrin distribution in symmetric and asymmetric bilayers. Here, the top row represents the integrin distribution before addition of ECM ligands and the bottom row exhibits corresponding data after addition of ECM ligands. In the asymmetric bilayer system, Ml_o domains are characterized through DiD (Figure 10, A and F) and NBD (Figure 10, B and G) channels, whereas the corresponding integrin distribution is determined by the Alexa Fluor-555 channel (Figure 10, C and H). In symmetric bilayers, Bl_o domain phase

separation and corresponding integrin distribution are characterized through NBD (Figure 10, D and I) and Alexa Fluor-555 channels (Figure 10, E and J), respectively.

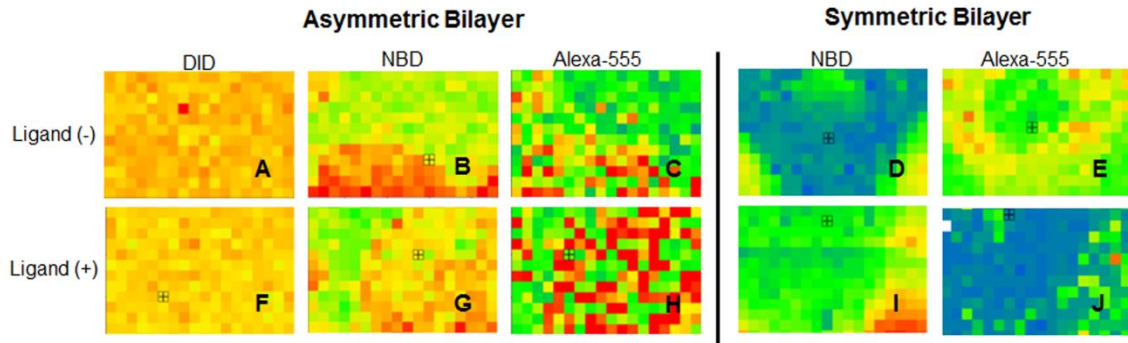


Figure 10: CS - XY scans of $\alpha_v\beta_3$ integrin distribution in the presence of monolayer spanning (asymmetric bilayer) and bilayer-spanning (symmetric bilayer) l_o - l_d phase separations before (top row) and after addition of VN (bottom row). Box = $6 \times 9 \mu\text{m}^2$.

According to Figure 10, D and E the opposite preference in the NBD and Alexa-555 channels suggests that $\alpha_v\beta_3$ integrin prefers the l_d regions in the symmetric bilayer. This work has been published before (3). In contrast, Figure 10, B and C demonstrates that $\alpha_v\beta_3$ prefers the l_o phase in asymmetric bilayers. Addition of ECM ligands also showed a different impact on $\alpha_v\beta_3$ in symmetric and asymmetric bilayers. In symmetric bilayers (Figure 10, I and J), $\alpha_v\beta_3$ prefers l_o phase. As reported previously, ligand binding causes the translocation of integrins from the l_d to the l_o phase (3). In contrast, no comparable $\alpha_v\beta_3$ translocation is observed in asymmetric bilayers (Figure 10, G and H). The sequestration of $\alpha_5\beta_1$ integrin in asymmetric bilayers is also investigated using the same method. Comparable qualitative results are obtained. Next, a more quantitative analysis of integrin distribution is performed in terms of the E_{raft} parameter, which has been introduced in section 3.2.3.2. The results obtained for $\alpha_v\beta_3$ and $\alpha_5\beta_1$ in the

asymmetric bilayer, along with the results from the symmetric bilayer, are given in Figure 11.

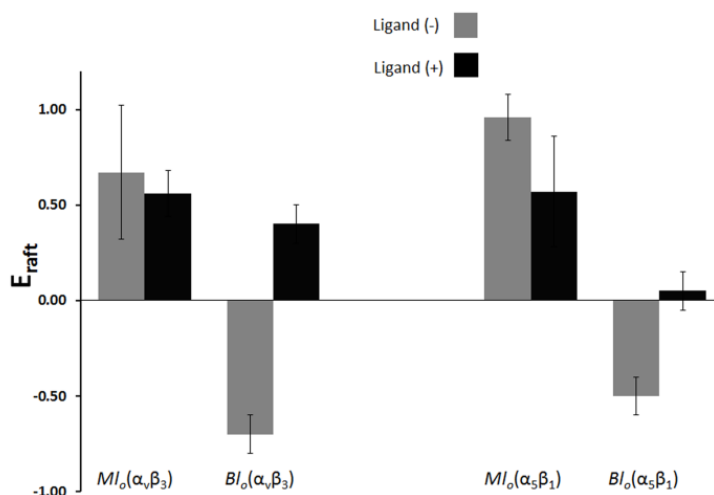


Figure 11: Comparison of E_{raft} values for symmetric (Bl_o domains) and asymmetric (Ml_o domains) bilayers for $\alpha_v\beta_3$ and $\alpha_5\beta_1$ integrins

The E_{raft} values for $\alpha_v\beta_3$ and $\alpha_5\beta_1$ are positive in the asymmetric bilayers but negative in its symmetric counterpart. According to the E_{raft} values, $\alpha_v\beta_3$ and $\alpha_5\beta_1$ prefer the l_o phase (Ml_o) in asymmetric bilayers. In contrast, $\alpha_v\beta_3$ and $\alpha_5\beta_1$ prefer the l_d phase in symmetric bilayers (3). The quantitative E_{raft} data in Figure 11 provide an opportunity to compare the integrin affinity for each phase. The most preferred state for both integrins is the Ml_o domain, followed by the Bl_d and Bl_o phases. There are several partially competing factors that contribute to the specific domain affinity of integrins (108). The most important factors are compressibility of the bilayer, width of the bilayer, and interaction between extracellular integrin head groups and bilayer. These factors and possible mechanisms will be discussed in section 4.1.7.

4.1.6 Influence of Ligand Addition on Dimerization and Brightness of $\alpha_v\beta_3$ and $\alpha_5\beta_1$ Integrins

Because ligands and crosslinking agents are known to change the sequestration of membrane proteins in l_o and l_d phases in the bilayer (10, 109), our next step is to determine the oligomerization status of $\alpha_v\beta_3$ and $\alpha_5\beta_1$ upon addition of extracellular matrix ligands VN ($\alpha_v\beta_3$) and FN ($\alpha_5\beta_1$) (10, 11). We are able to determine the brightness and dimerization values of $\alpha_v\beta_3$ and $\alpha_5\beta_1$ before and after addition of their respective ECM ligands by using the PCH method. This method has been described previously in section 3.2.3.1(3). Representative results of the PCH analysis of the $\alpha_v\beta_3$ and $\alpha_5\beta_1$ in MI_o and BI_d containing bilayers are shown in Figure 12. The PCH data are shown with markers and the best fit model is depicted using in a dotted line (Figure 12, A-D). Molecular brightness and the fraction of dimers for each integrin are given in Figure 12, E and F. According to the PCH data in Figure 12, $\alpha_v\beta_3$ and $\alpha_5\beta_1$ in l_o and l_d phases predominately exist in a monomeric state regardless of the presence of VN and FN. These results are in good agreement with previous work done by our group on integrin in symmetric bilayers (3). These findings are significant because similar results have been obtained previously on integrins without cytosolic linkages in a plasma membrane (110). Here the authors were able to show that addition of ligands does not cause integrin clustering. Figure 12 E depicts the ratio of the brightness of the MAbs in the bilayer over the solution brightness obtained from PCH analysis. According to our results the ratio is around $83\pm 1\%$, which is in good agreement with results obtained from the symmetric bilayer (3). This implies that the brightness of the fluorescence antibody in the l_o and l_d

phase in the asymmetric bilayer is similar to the antibody brightness in the solution. The same results are obtained upon addition of the ligand as well.

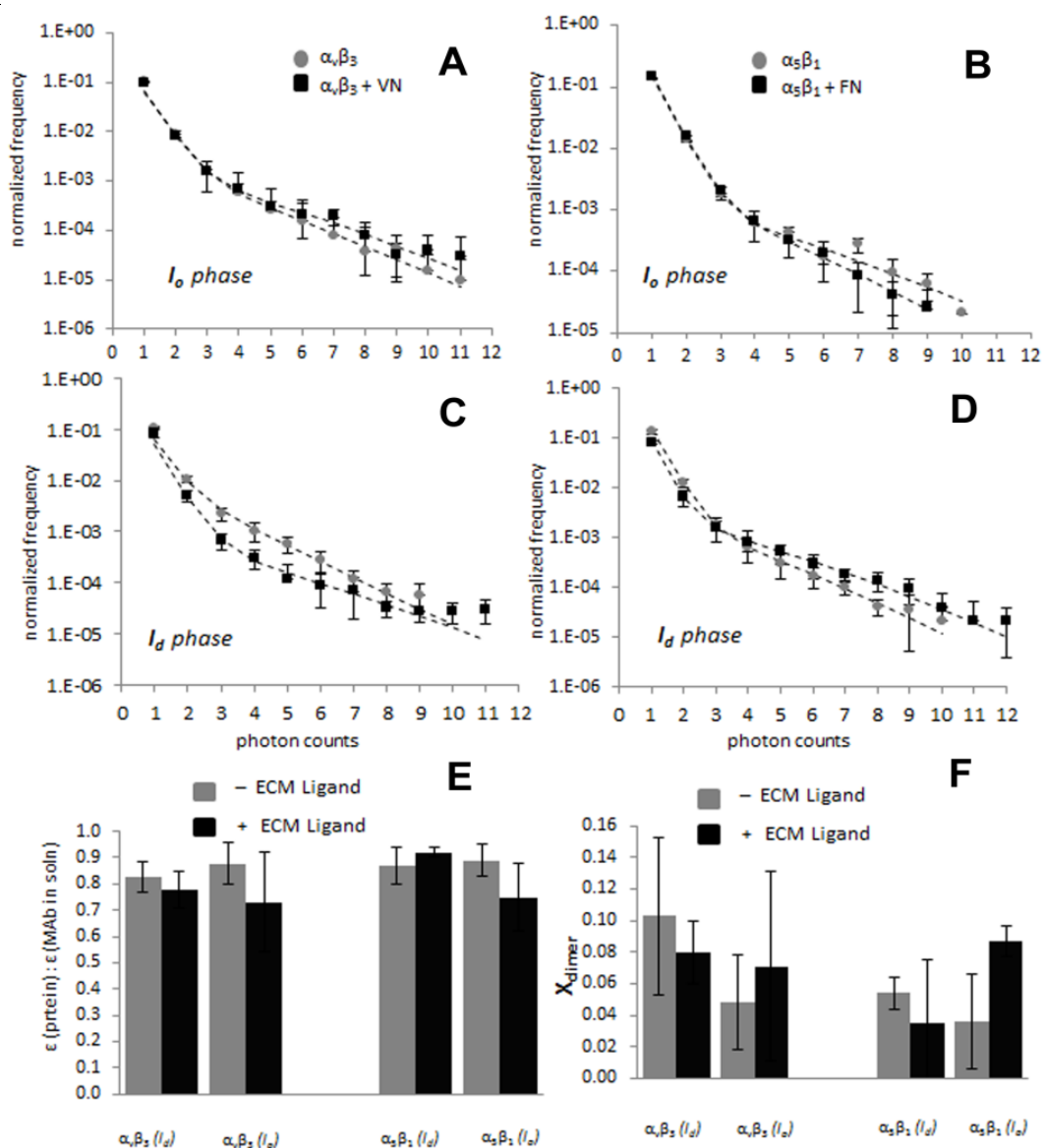


Figure 12: PCH curves for $\alpha_v\beta_3$ (A, C) and $\alpha_5\beta_1$ (B, D) before (*light markers*) and after (*dark markers*) ligand binding in both l_o phase (A, B) and l_d phase (C, D). Dotted lines are best fit curves from the PCH algorithm. (E) Brightness compared to MABs in solution and (F) fraction of dimers found through PCH analysis of $\alpha_v\beta_3$ (*left*) and $\alpha_5\beta_1$ (*right*) integrin proteins before (*light bars*) and after (*dark bars*) ligand binding in l_d and l_o phases

4.1.7 Potential Mechanisms for the Integrin Sequestration in Symmetric and Asymmetric Systems

Several competing factors contribute to the affinity of integrins to specific lipid domains (111). They are compressibility of the bilayer, width of the bilayer, and interaction between the extracellular integrin head groups and lipids of the bilayer. Integrin preference to the l_d phase could be attributed to the lower packing density in this phase (relative to the l_o phase). It has been shown that the α helices of bilayer-spanning peptides strongly associate with the l_d phase (112). Therefore, integrin sequestration properties are associated, at least in part, with differences in the compressibility modulus (lipid packing density) of l_o and l_d phases. In other words, the compressibility modulus of the l_d phase allows integrin incorporation into the bilayer with less energy cost (111).

Characterization of E_{raft} values with dye labeled lipids gives us information on the lipid-packing density in the monolayer and bilayer spanning domains. The E_{raft} values obtained from TRITC-DHPE dye labeled lipids for asymmetric and symmetric bilayers are -0.2 and -0.46 respectively. These E_{raft} values imply that Ml_o domains have a moderately lower packing density and a higher compressibility than Bl_o domains. This criteria energetically favors the incorporation of integrins into Ml_o over Bl_o domains, thus explaining the higher affinity of integrins for the Ml_o over Bl_o domains.

Hydrophobic mismatching between the bilayer and the TM part of the protein may also play an important role in protein sequestration in coexisting l_o and l_d domains. According to X-ray diffraction data of DOPC-CHOL, CHOL-SL, and DOPC lipid mixtures, the hydrophobic thickness values of Bl_d , Ml_o , and Bl_o are 33 ± 1 Å (Bl_d), 35.5 ± 1 Å (Ml_o), and 38 ± 1 Å (Bl_o) respectively (108). These values indicate that the hydrophobic

thickness of the Bl_d closely matches with the thickness of the TM α -helices of α and β units of integrins, which are 31.6 ± 3.4 Å and 30.0 ± 3.6 Å respectively (113, 114). Therefore, the observed Bl_d preference of integrins in symmetric bilayers can be explained on the basis of hydrophobic matching arguments. Interestingly, hydrophobic matching arguments predict no particular preference for Bl_d and Ml_o regions in asymmetric bilayer compositions. Because our results indicate that integrins prefer the Ml_o region over the Bl_d region in such asymmetric bilayer system. We assume that there is another contributing factor regulating integrin's affinity for different lipid domains. This third factor is likely the interaction between lipid bilayer and extracellular head groups of integrins. Such a contribution appears particularly plausible for integrins in the resting state. In this state, the integrins ectodomain is in a bent form and in close vicinity to the lipid bilayer (Figure 13). On the basis of this line of reasoning, we hypothesize that the integrins' higher affinity for the Ml_o domain in the asymmetric bilayer is associated with the preferential interaction between the integrin ectodomain and the lipids in the Ml_o region. Importantly, a higher l_o preference of $\alpha_5\beta_1$ integrins in asymmetric bilayer before ligand addition is also observed.

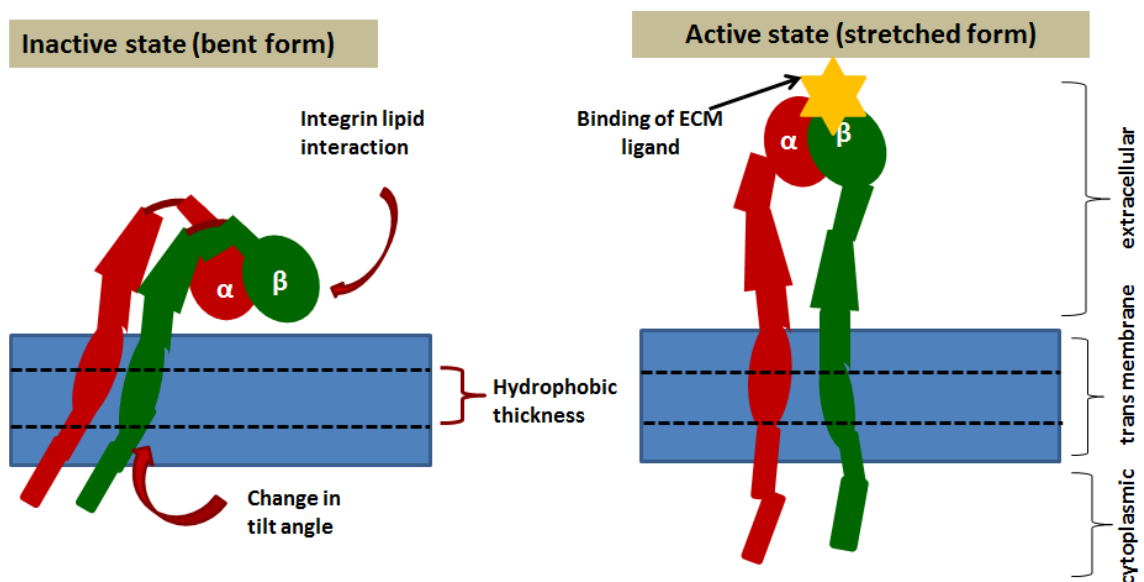


Figure 13: The conformation change of the $\alpha_v\beta_3$ integrin upon addition of the extracellular matrix ligands. (Adapted from (115))

According to Figure 11, in asymmetric bilayers there is no significant change in the E_{raft} value observed upon addition of ligands. This is a significant difference in comparison to the symmetric bilayer, where substantial translocations of integrins are observed from l_d to l_o after addition of ligands (3). In the asymmetric bilayer, the change in raftophilicity of the integrin $\alpha_v\beta_3$ is minute [$X_{migrate}(\alpha_v\beta_3) = -5.5 \pm 6\%$] in comparison to the corresponding value obtained in symmetric bilayers [$X_{migrate}(\alpha_v\beta_3) = 53 \pm 6\%$]. Net translocation between lipid phases are likely caused by ligand-induced allosteric changes of integrins (115, 116). Such allosteric changes may involve all parts of the receptor (i.e., extracellular, TM, and cytosolic domains). In other words, stretching of the integrin ectodomain upon ligand binding is presumably accompanied by a substantial reorganization of TM α -helical structures and integrin cytosolic domains. Importantly, this structural reorganization of integrins will change the tilt angle of the TM helices, thus

affecting the hydrophobic thickness of these receptors (117). Indeed, experiments on integrins have shown that ligand-induced conformational changes in the integrin ectodomain can be propagated through the plasma membrane, thereby separating α and β cytosolic domains (118). At the same time, the ligand-induced stretching of integrin extracellular heads will result in the reduction of interactions between integrin ectodomain and lipid bilayer. Therefore, we hypothesize that integrin's affinity for the l_o phase upon ligand addition in symmetric and asymmetric bilayers is likely due to the rearrangement of the integrin TM region, which affects hydrophobic matching conditions between the bilayer and integrins.

4.2 The Effect of Cholesterol Concentration on Integrin Sequestration in Different Raft Mimicking Lipid Mixtures

Experiments on 1:1:1-DOPC: DPPC: CHOL mixtures suggest that integrin sequestering can be explained, in part, in terms of hydrophobic matching arguments. To test this concept further, we systematically varied CHOL content in DOPC/DPPC/CHOL mixtures. By varying CHOL concentration, it is possible to alter line tension between l_o and l_d phases (line tension reflects differences in hydrophobic thickness between l_o and l_d). It has been shown that line tension decreases if one moves from the center to the boundary of the l_o - l_d coexistence region in the phase diagram (57). According to the phase diagram of the DOPC: DPPC: CHOL mixture (Figure 14), raft forming lipid mixtures for different concentration of CHOL (20 mol%, 28 mol%, 33 mol%, 35 mol% and 37 mol%) are formed. In each case, DOPC and DPPC are kept at an equal molar ratio. The monolayer and bilayer are prepared according to the description in section 3.2.1.5. The presence of l_o - l_d phase separation is confirmed by using 0.2 mol% NBD-DHPE in

both leaflets of the bilayer and by visualizing the bilayer samples using EPI microscopy. Figure 15 depicts representative EPI micrographs of the LS/LB monolayers and their respective bilayers for different CHOL concentrations. The EPI micrographs show that the l_o - l_d domains are significantly smaller in 20 mol% and 35 mol% CHOL than in the 33 mol% and 35 mol% mixtures. This difference in domain size reflects the difference in distances from the phase boundary of the l_o - l_d coexisting phase (57). Next, incorporation of $\alpha_v\beta_3$ into the bilayers is done using a modified Rigaud technique, which has been explained in section 3.2.2.

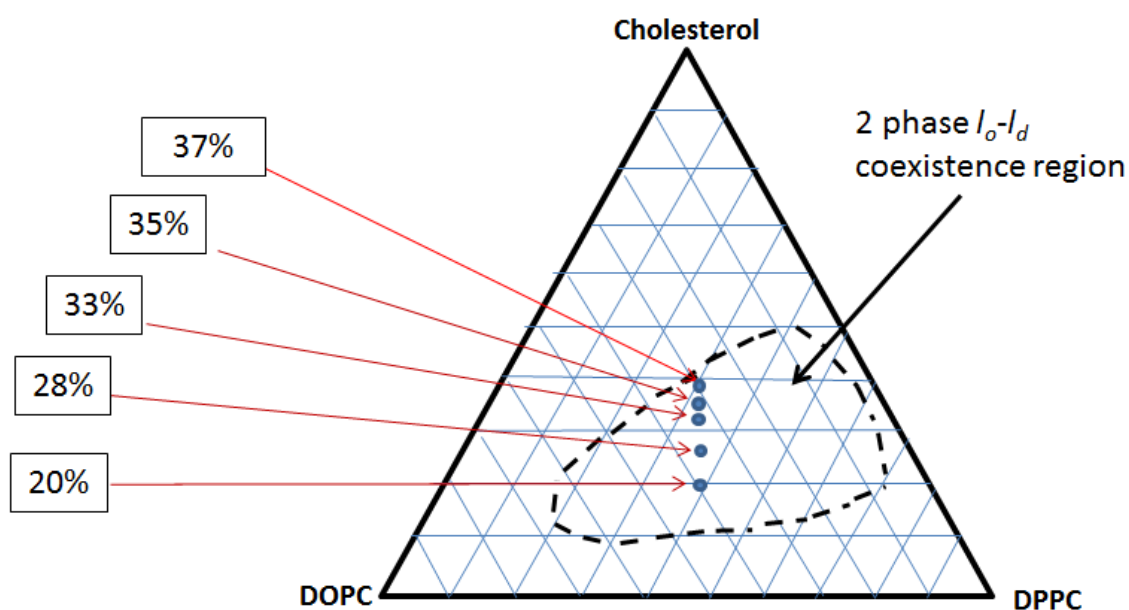


Figure 14: Simplified DOPC: DPPC: CHOL phase diagram showing the phase boundary of the l_o - l_d coexisting phase and the DOPC: DPPC: CHOL mixtures of different CHOL molar concentrations investigated (small circles). As the phase diagram indicates, the DOPC-DPPC molar ratio was kept at an equimolar ratio (59)

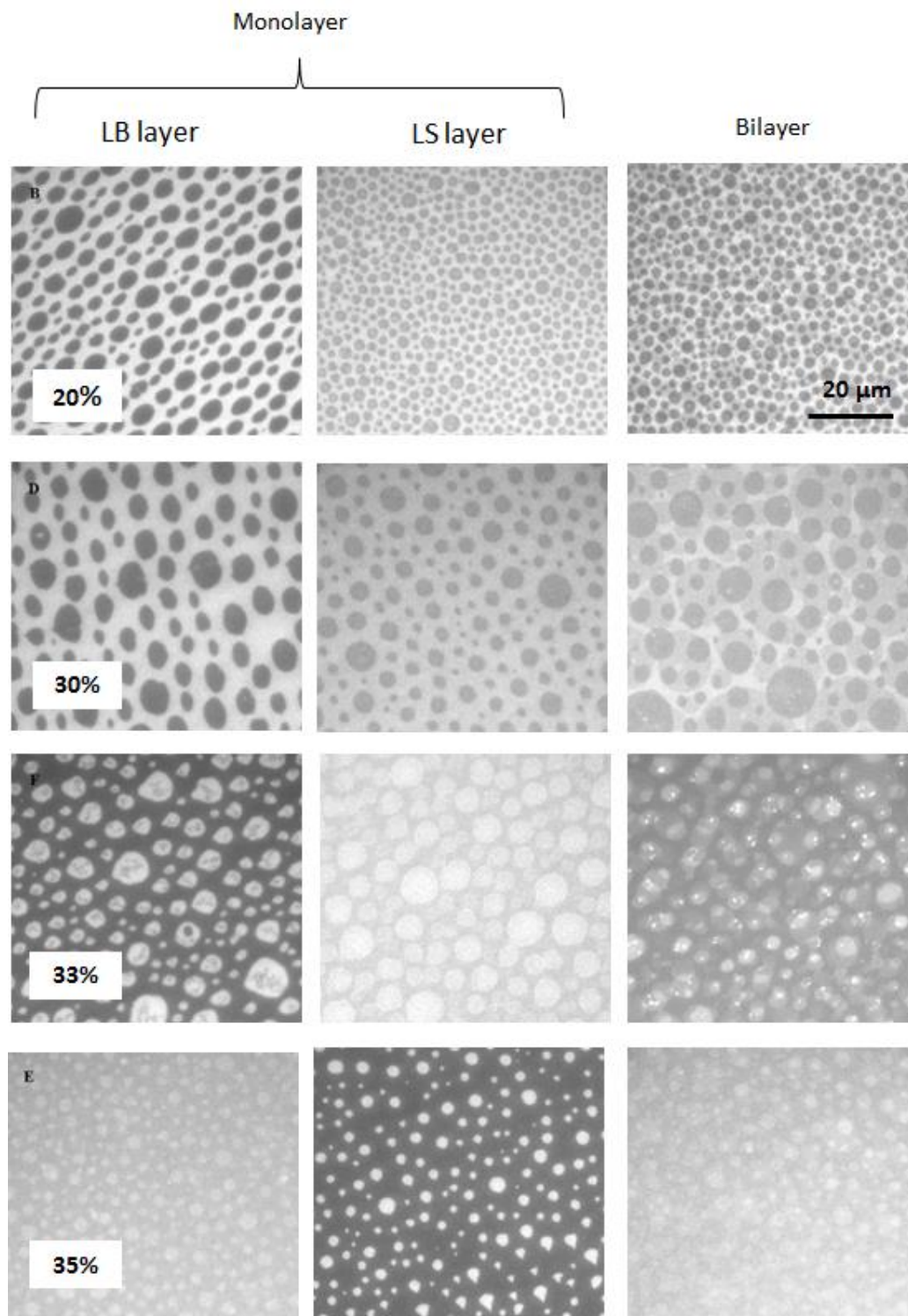


Figure 15: EPI micrographs of LB/LS monolayers and bilayers of raft-mimicking lipid mixtures with different percentage of CHOL (DOPC: DPPC-1:1)

To monitor integrin sequestration, a 543 nm He laser was used to probe the distribution of Alexa 555 labeled proteins. The NBD-DHPE distribution in the bilayer was monitored using a 488 nm Ar laser. Representative CS-XY scans of $\alpha_v\beta_3$ (before and after addition of VN) and NBD-DHPE distributions in bilayers containing 20 and 35 mol% CHOL are presented in Figure 16. Control experiments with NBD-DHPE, but without Alexa-555 labeled anti-integrin MAbs, were done to evaluate the background contribution (data not shown).

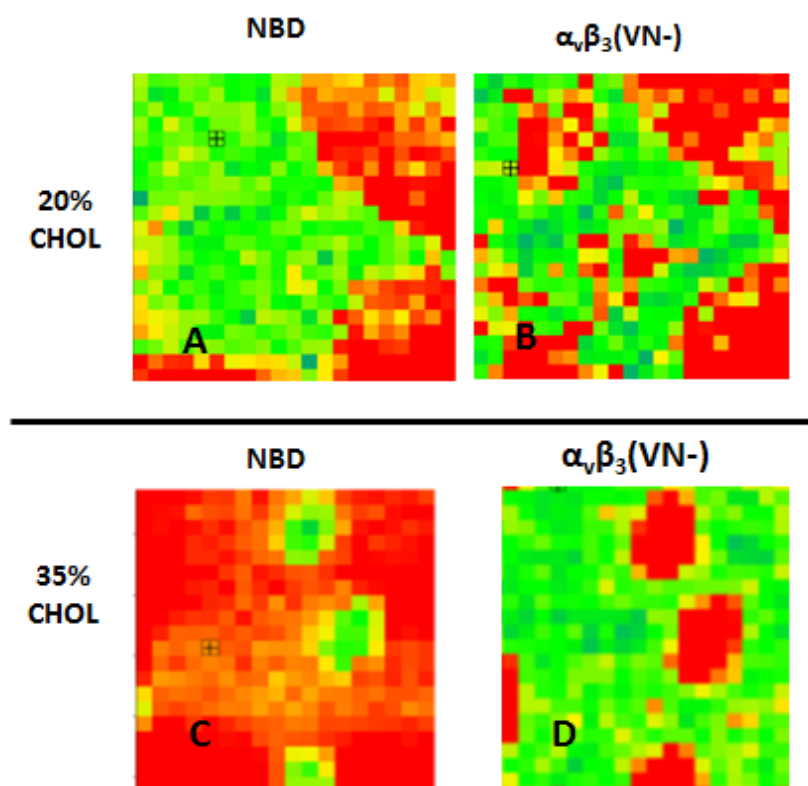


Figure 16: CS-XY scans of $\alpha_v\beta_3$ integrin distribution in DOPC/DPPC/CHOL mixtures with the 20 mol% and 35 mol% CHOL. A, B box = $10.5 \times 10.5 \mu\text{m}^2$. C, D box = $9 \times 10 \mu\text{m}^2$.

The CS-XY scan of the 35 mol% CHOL sample (Figure 16, C and D) indicates that integrin prefers the l_d phase. In contrast, the 20 mol% CHOL sample (Figure 16, A and B) shows no pronounced integrin preference to either phase. E_{raft} and PCH data were

obtained according to the description given in experimental section 3.2.3.2. Figure 17 depicts the E_{raft} values of integrin distribution obtained for different CHOL concentrations. According to the figure, E_{raft} changes substantially between 20 mol% and 35 mol% CHOL.

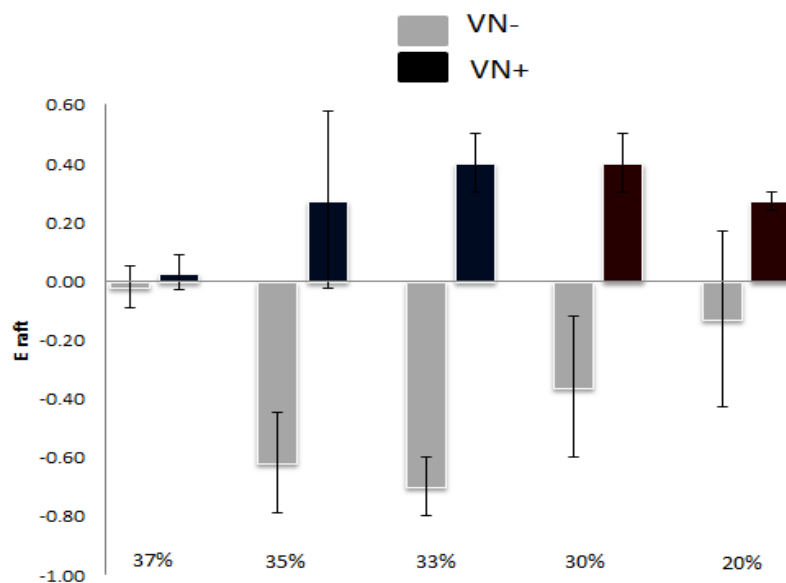


Figure 17: E_{raft} values for different concentrations of cholesterol for DOPC: DPPC-1:1 raft mimicking mixtures

At 20 mol% CHOL, the E_{raft} value before adding the extracellular ligands (VN) is neither positive nor negative. This implies that the integrins equally prefer the l_o and l_d phase at this CHOL concentration. On the other hand, between 28 and 35 mol% CHOL, integrins prefer to go to the l_d phase. Interestingly, the E_{raft} values for 35 mol% and 37 mol% are less negative than those for 33% CHOL. Notably, a similar trend can be observed after addition of VN, albeit E_{raft} values are now positive. Here the integrins have been trans-locating from the l_d to the l_o phases upon addition of VN, presumably due to ligand-induced allosteric changes of the receptors affecting hydrophobic matching of

the TM protein region and the lipid bilayer (30, 119). Again, larger E_{raft} values are found in the center of the l_o - l_d coexistence region (28 mol% and 33 mol% CHOL), whereas the lower values are obtained at the “edges”, i.e. at 20 mol% and 35 mol% CHOL, respectively. Representative CS-XY data of $\alpha_v\beta_3$ integrin sequestration after addition of VN is depicted in Figure 18. According to Figure 18, integrins sequester into the l_o phase for 20 mol% and 35 mol% CHOL respectively.

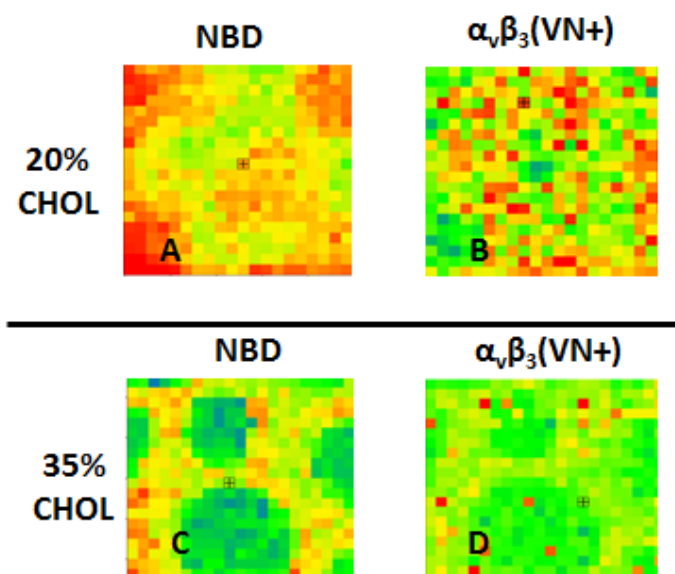


Figure 18: XY scans of the $\alpha_v\beta_3$ integrin distribution in the 20 mol% and 35 mol% CHOL. A, B, C, D box = $10.5 \times 10 \mu\text{m}^2$

Results from Figures 16-18 indicate that the amount of CHOL in the l_o - l_d coexisting phase region has a substantial influence on integrin distribution in the bilayer. This can be attributed to several factors. In the presence of CHOL, lipids become more ordered and tightly packed and the permeability of the membrane is reduced (45). This will facilitate the lipid packing density of the membrane. Lipid packing density is a key factor governing the incorporation of TM proteins, such as integrins, into the bilayers (111). Addition of CHOL also alters the thickness of the bilayer (19, 45, 46). Such CHOL-induced changes in bilayer thickness may influence membrane protein sequestering via changing hydrophobic matching conditions. This is because the hydrophobic thickness of the lipid bilayer is a crucial factor for the energy landscape of TM proteins. It is widely accepted that hydrophobic thickness influences the spontaneous incorporation of proteins into bilayers (19). According to the “mattress model”, lipids adjust locally to mismatch the hydrophobicity of lipids and membrane proteins (19, 46). This will result in lengthening or strengthening the lipids or tilting the proteins. CHOL likely influences membrane protein sequestration behavior because it is expected to suppress membrane adaptation processes in response to hydrophobic mismatch.

Consequently, in the presence of coexisting l_o - l_d domains of different CHOL content, variations in CHOL concentration may result in changes in membrane protein sequestration, as observed in Figure 17. On the basis of the above arguments, the most pronounced integrin segregation is at the center of the l_o - l_d coexisting region. Less significant integrin segregation near the “edges” can be understood in terms of smaller line tensions (i.e., reduced hydrophobic thickness differences between l_o and l_d domains). It has also been shown that CHOL can alter the tilting angle of TM peptide according to

hydrophobic mismatch (19). Such a process may trigger the rearrangement of lipids of different acyl chain lengths needed for TM mismatch. For example, TM proteins with different TM thickness are located in the CHOL poor endoplasmic reticulum (ER) membrane. This shows the adaptability of the membrane to incorporate different lengths of proteins. Intriguingly, Nilson and coworkers have shown that the translocation of proteins in the ER membrane can be reversibly inhibited by CHOL levels (48).

The dimerization of the integrins is obtained using the PCH method, which has been described in section 3.2.3.1. Dimerization values for different CHOL concentration systems are given in Figure 19. These results indicate that no significant change in the dimerization values is observed for different CHOL concentrations. Addition of VN did not influence the dimerization of integrins.

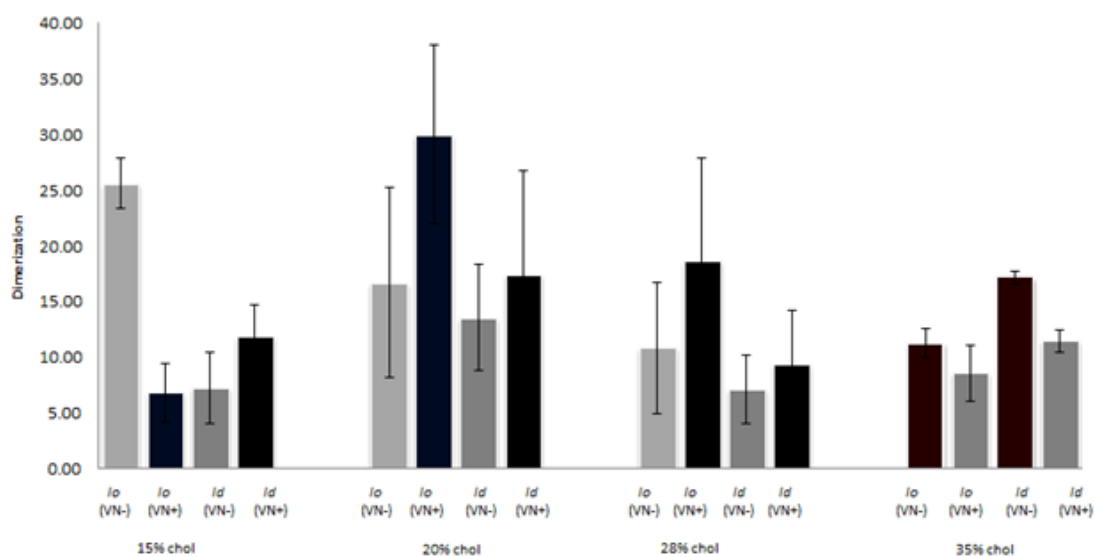


Figure 19: Dimerization values of integrins for different CHOL concentration in raft-mimicking lipid domains.

4.3 Effect of Lipopolymer and Cholesterol Concentration on the Buckling Process in Phospholipid Monolayers

4.3.1 Buckling Phenomena in SOPC: DSPE PEG-5000 Monolayers

The above discussion illustrates that an understanding of important membrane processes, such as membrane protein sequestration in raft-mimicking lipid mixtures, requires a thorough understanding of membrane physical properties. Therefore, my next project focused on the characterization of crucial materials properties of polymer-tethered membranes. In particular, our interest was on the investigation of mechanical properties and stress relaxation phenomena in such membranes. It is well documented that cellular membranes may show membrane buckling phenomena in response to applied stress. . The most common example is the lung, which is covered by a monolayer of lipids (phospholipids and lung proteins). This monolayer undergoes reversible wrinkling and folding during normal breathing (20). Cytoskeleton-facilitated curved structures such as lamellipodia, filopodia, pseudopodia, and phagocytic cups are also seen in biological systems. The mechanisms behind membrane buckling phenomena are complex and remain an open topic of scientific debate. The physisorbed polymer-tethered membrane is an ideal system to contribute to this debate. Recently our group formed buckles in model membrane systems by altering lipopolymer concentration (26) and found that lipopolymers enable tuning of the elastic properties of the lipid bilayers. Interestingly the elasticity of these model membranes could be adjusted by changing the molar concentration of the lipopolymer in the membrane (26). Specifically, elevated lipopolymer concentrations induced substantial stress in the membrane. Polymer-tethered membranes were found to respond to the applied lateral stress by partially delaminating

from the solid substrate, thus forming membrane buckling structures. Fewer buckles were formed at low lipopolymer concentration (low lateral stress), whereas significant amounts of buckling were seen at medium and higher lipopolymer concentrations (high lateral stress). It was also observed that increasing lipopolymer concentration increased the buckling width, and the buckling area (percentage of the buckles) in the membrane. Importantly, a metric relationship between membrane elastic properties and buckling structures formation could be derived for polymer-tethered lipid monolayers (26). This was achieved through the combination of mean-field calculations of polymer-tethered membranes and buckling theory of a straight-sided blister (Euler column).

4.3.2 Cholesterol Induced Buckling in Polymer-Tethered Monolayers with 3 mol% DSPE-PEG 5000

According to the mean-field theory calculations, it has been shown that incorporating lipopolymers into liposomes or planar solid-supported bilayers cause changes in bending modulus and compressibility (77, 78). The change in these properties depends on polymer type, molecular weight, and concentration. It is also known that CHOL plays a major role in the bending elasticity in model and biological membranes. We therefore hypothesized that CHOL could also induce buckles in polymer tethered membranes by influencing stress relaxation processes in the membrane. The goal of these experiments was to investigate the crucial relationship between membrane elastic properties and the buckling structures in physisorbed polymer-tethered monolayers in general, and the role of CHOL content in these systems in particular. The monolayers were characterized through EPI micrographs and AFM images.

4.3.2.1 EPI Micrographs and AFM Images of Polymer-tethered Monolayers with Different CHOL Concentration

First monolayers of SOPC with different concentrations of CHOL in the presence of 3 mol% DSPE-PEG 5000 were constructed using the LB technique. These monolayers were analyzed using EPI. Figure 20 shows representative EPI micrographs from these experiments. As Figure 20 illustrates, there are no large-scale buckling structures in the monolayers between 5 mol% (Figure 20 A) and 30 mol% CHOL (Figure 20 B). In contrast, the EPI micrograph for 40 mol% CHOL (Figure 20 C) suggests the existence of large-scale buckling structures. Interestingly, tiny white dots could be observed at 5 mol% CHOL (Figure 20 A). These white dots became more pronounced with increasing CHOL concentration. At 40 mol% CHOL, ridges were observed in this monolayer (Figure 20 C).

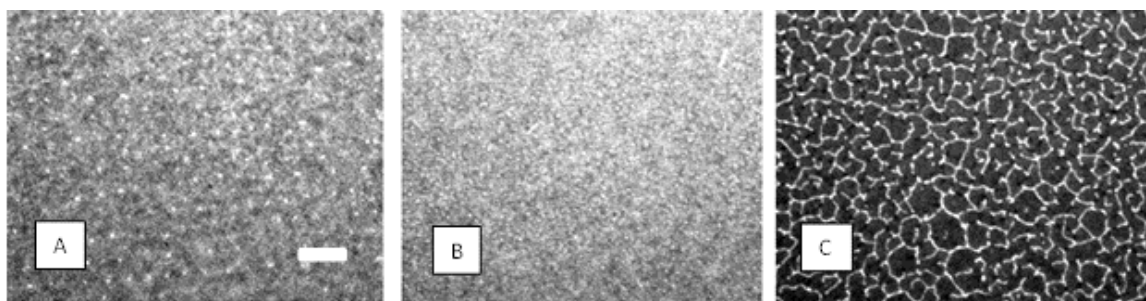


Figure 20: EPI micrographs of physisorbed polymer-tethered lipid monolayers comprised of SOPC: 3 mol% DSPE-PEG5000 with 5 mol% (A), 30 mol% (B), and 40mol% CHOL (C). To conduct EPI experiments, each monolayer contains 0.5% TRITC-DHPE. The white scale bar represents 10 μm in size.

Next we designed a set of control experiments to investigate the mixing behavior of CHOL and lipopolymers in polymer-tethered monolayers. It is well known that CHOL may segregate preferentially in coexisting phases of different membrane curvature (120). Furthermore, according to scaling laws of polymer physics, 3 mol% DSPE-PEG 5000 is close to the mushroom-brush transition. Here, the small lipid

anchor with a bulky polymer moiety interacts primarily through polymer-polymer interactions. At this low lipopolymer concentration, phospholipids are expected to act as template molecules with good mixing properties. Therefore, we assumed that there would be no notable lipopolymer-induced phase separation in our polymer-tethered membranes. In the case of a hypothetical lipopolymer-induced phase separation, energetically unfavorable stretching of the polymer chain will occur in the membrane. On the other hand, partial segregation of CHOL between buckled and non-buckled regions cannot be excluded. In order to confirm these behaviors, we compared the distribution of dye-labeled lipids, CHOL, and lipopolymers in the polymer-tethered monolayer. Figure 21 (A) and (B) illustrates the distribution of dye-labeled lipopolymers (TAMRA-DSPE-PEG 2000) and dye-labeled lipids (NBD-DHPE) in the same monolayer. These figures indicate that the distribution of dye-labeled lipopolymers exactly tracked the distribution of dye-labeled lipids: both are high in buckled region compare to the un-buckled region. This result confirmed that there is no measurable buckling-induced segregation between lipopolymers lipids in polymer-tethered membranes with buckling structures.

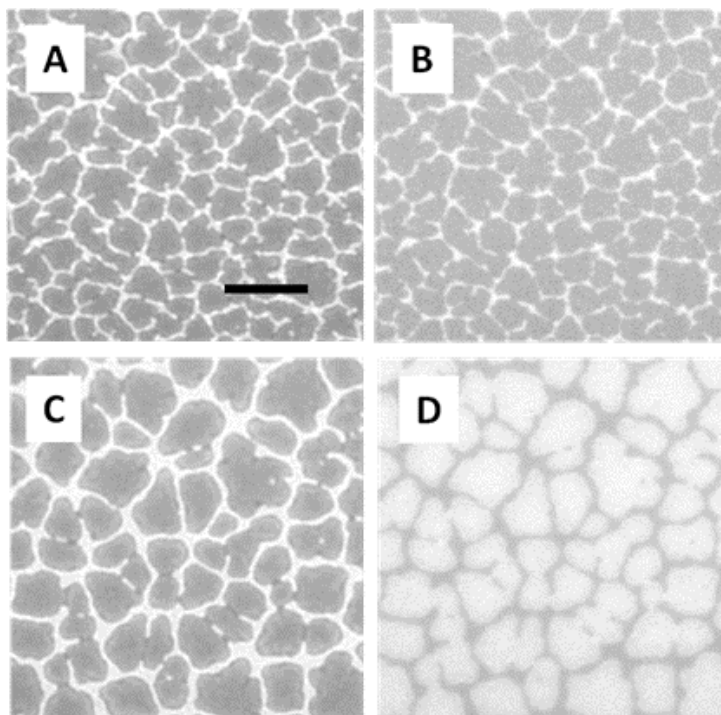


Figure 21: EPI micrographs comparing the distribution of TAMRA-DSPE PEG 2000 (A) and NBD-DHPE (B), as well as TAMRA-DSPE PEG 2000 (C) and NBD-6-cholesterol (D) in a physisorbed polymer-tethered monolayer system consisting of 3 mol% DSPE-PEG 5000, 40 mol% CHOL, and 55.8 mol% SOPC (dye molecule concentration: 0.6 mol%). The size of the scale bar is 10 μm .

The comparison of the distribution of dye-labeled lipids and dye labeled CHOL is provided given in Figure 21(C) and (D) respectively. Analysis of these micrographs suggests that there is a moderate depletion of NBD-6-Cholesterol implying a likely a depletion of CHOL in buckled regions. This result is plausible in light of the well-known preference of CHOL for less curved regions.

Following the described EPI experiments, we investigated the polymer-tethered monolayers using AFM. The AFM micrographs of the monolayers with 5 mol %, 30 mol%, and 40 mol% CHOL are depicted in Figure 22 (A), (B), and (C) respectively. The AFM micrographs showed that the tiny dots detected in the higher magnification EPI micrograph are blisters, a specific form of buckling structures. In good agreement with

EPI results, the number of blisters increases with increasing CHOL concentration until it reached 30 mol% (Figure 22B). Then at 40 mol% CHOL blisters are replaced by ridges (Figure 22 C). Notably, no buckles were observed in a 40 mol% CHOL monolayer without lipopolymer (Figure 22 D). While Figure 22 A-C illustrates the significance of CHOL in the buckling process, Figure 22 D demonstrates the important role of lipopolymer as crowding agents in this process.

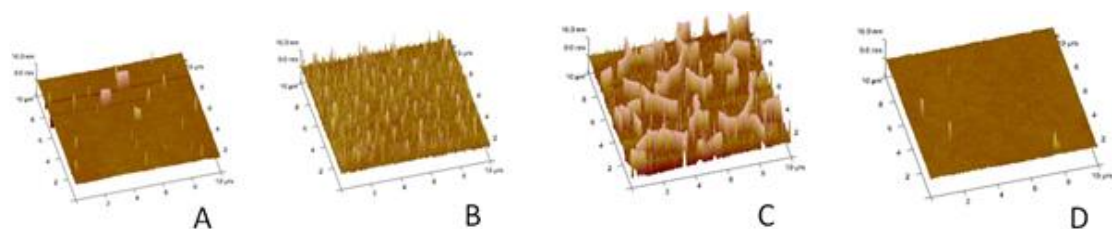


Figure 22: AFM images of the polymer-tethered lipid monolayers containing SOPC: 3mol% DSPE-PEG 5000, and 5mol% (A), 30 mol% (B), and 40 mol% CHOL (C). For comparison, an AFM image from a SOPC monolayer with 40 mol% CHOL, but without DSPE-PEG 5000, is shown as well (D). The image size is 10 μm x 10 μm .

4.3.2.2 Quantitative EPI and AFM Analysis of Monolayers with Different Cholesterol Concentration

AFM section analysis allows a more thorough quantification of buckling structures. Figure 23 and 24 show the section analysis of polymer-tethered monolayers with 0 and 40 mol% CHOL. In each case, AFM micrographs are quantitatively analyzed in terms of height, width, and roughness of buckles. Results of the buckle height analysis in monolayers of varying CHOL concentration are provided in Figure 25. According to Figure 25, buckle height remain constant between 0-20 mol% CHOL, and increases significantly for higher CHOL content.

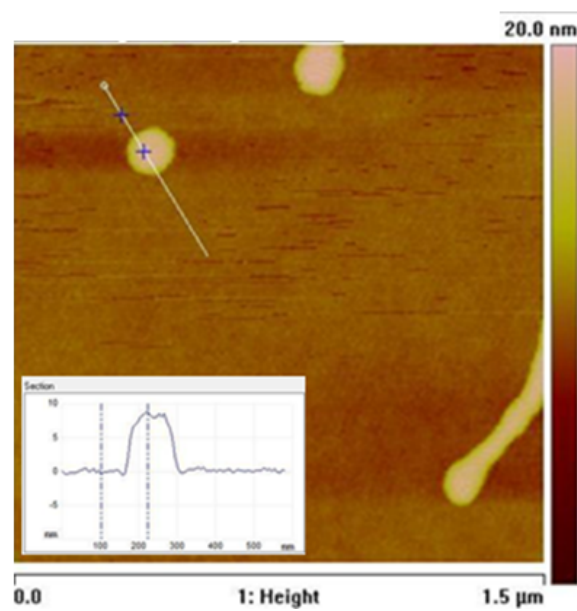


Figure 23: Section analysis for 0 mol% CHOL with 3 mol% DSPE-PEG 5000 in SOPC monolayers

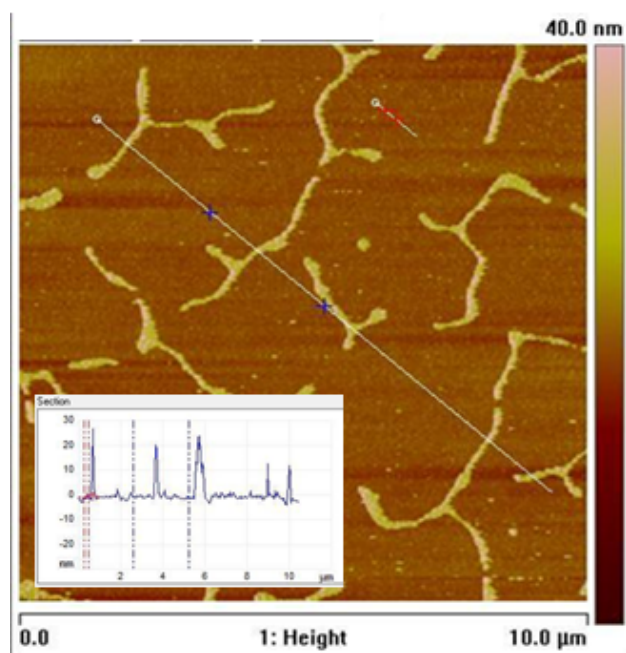


Figure 24: AFM section analysis for the 40 mol% CHOL with 3 mol% DSPE-PEG 5000

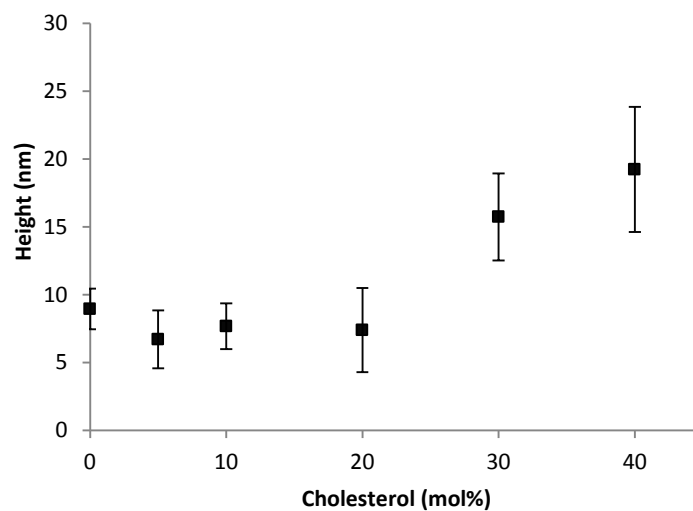


Figure 25: Buckle height vs. CHOL concentration in the monolayers

A similar trend is observed with respect to buckle width (Figure 26) and roughness (Figure 27). Again the width and roughness of the buckles does not change between 0-20 mol% CHOL, but do gradually increase with increasing CHOL content above 20 mol%.

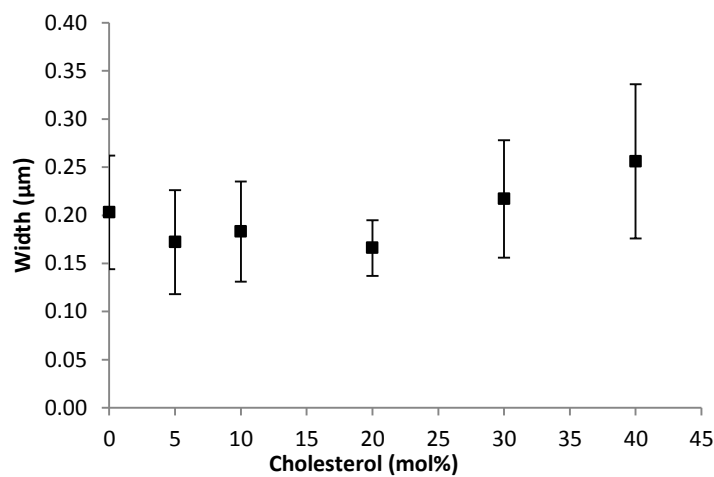


Figure 26: Width of the buckles from the AFM images for different concentration of CHOL

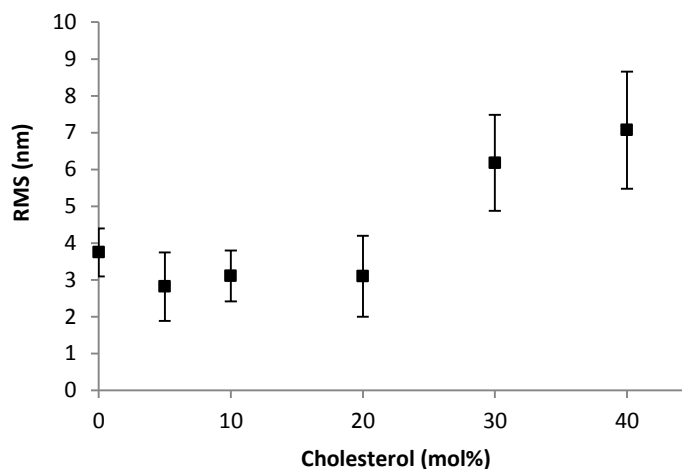


Figure 27: The buckle roughness vs. CHOL concentration in the monolayer

In order to determine the effect of CHOL on membrane thickness, we theoretically calculated the thickness of the film for different concentrations of CHOL (Figure 28). The thickness value is also used in membrane elasticity calculations. The calculation of membrane thickness is done according to the description given in section 3.2.5. Figure 28 shows that the thickness of the film increases from 0-20 mol% CHOL. Then between 20-40 mol% it stays constant. Intriguingly, it has been reported previously that the thickness of the lipid membrane increases by 20% with the increase of CHOL from 0-40 mol% (99).

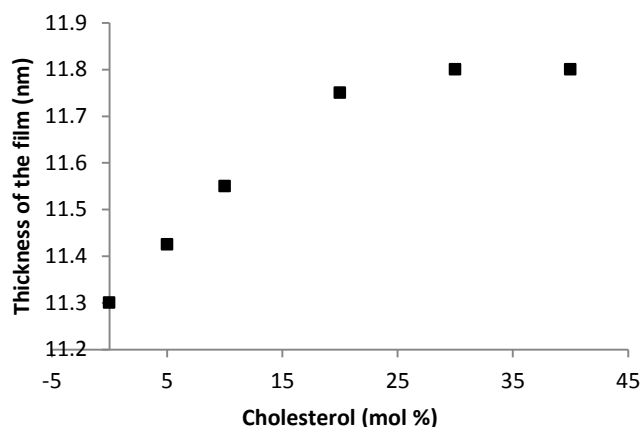


Figure 28: Thickness of the bilayer with increasing CHOL concentration

4.3.2.3 Stress Related Parameters Obtained from EPI-micrograph and AFM Images of the Monolayers with Different Cholesterol Concentration

According to our results (Figure 22, A-C) CHOL influence buckling in polymer-tethered monolayers in the presence of low concentrations of lipopolymers. A quantitative relationship between membrane elastic properties and experimentally accessible buckling structure parameters (buckling amplitude, w_{max} and width, $b/2$) has been developed previously (26). Here, w_{max} and “ b ” were obtained by analyzing AFM micrographs via section analysis. Next we linked the buckling theory of an Euler column to the elastic properties of the membrane. The Euler column is appropriate for our system because the substrate stiffness is much higher than the membrane stiffness and the width of the buckle is substantially larger than the thickness of the buckle (84). The mean-field approach allows the calculation of the film thickness, h , and bending stiffness, K_c , of the membrane (described in more detailed in section 3.2.5). Buckling theory provides the theoretical frame work to link h and K_c to biaxial stress, σ_0 , and critical stress at the onset of buckling, σ_c (Section 3.2.5). According to the mean field calculation approach, K_c of

an SOPC bilayer with 20 mol% DSPE-PEG 5000 was found to be $400 k_B T$. Intriguingly, this K_c value is similar to the bending elasticity found in *Dictyostelium discoideum* (wild type) (121). On the other hand, the K_c of 5 mol% DSPE-PEG 5000 is around $50 k_B T$, which is comparable to K_c values of red blood cells (122). Figure 29 A illustrates the quantitative link between membrane buckling and the CHOL content. Here, we were able to see a linear relationship between the bearing area (BA), and the CHOL molar concentration. Previous work has shown that there is a linear relationship between BA and K_c (26). This result was obtained using SOPC/DSPE-PEG 5000 mixed monolayers with increasing lipopolymer concentrations (0-20 mol% lipopolymer without CHOL). Importantly, a linear relationship between the film stress, σ_o , and CHOL molar concentration was also observed in our experimental system. This result is depicted in Figure 29 B.

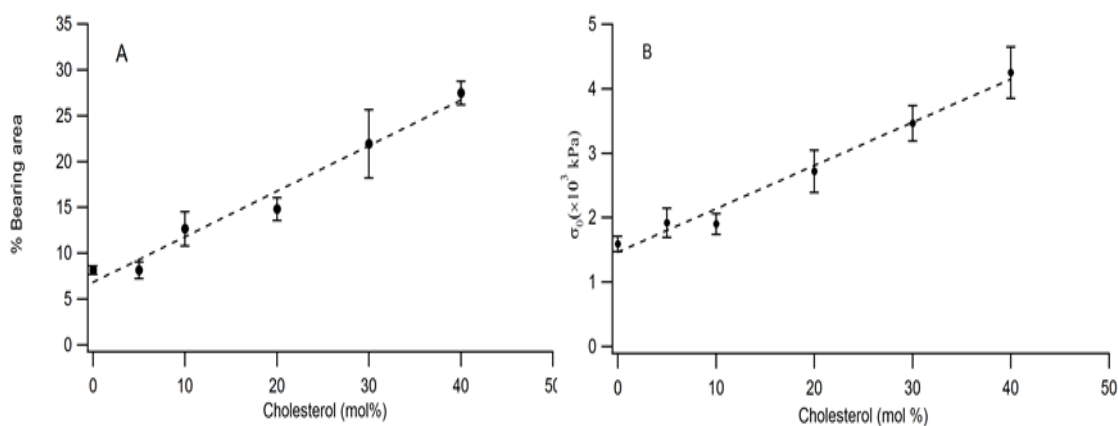


Figure 29: Impact of CHOL molar concentration on bearing area (percentage of buckling regions) (A) and biaxial stress, σ_0 , (B) in a physisorbed polymer-tethered lipid monolayer, as obtained from analysis of EPI and AFM micrographs

The fact that we have demonstrated a linear scaling of BA and σ_o with respect to CHOL concentration, depicted in Figure 29, represents a key result of our work on

membrane buckling. This result is significant because it implies that both bending elasticity and CHOL influence buckling behavior.

According to our results, lipopolymer and CHOL-induced buckling show qualitatively similar behavior (20, 26). CHOL induced buckling can be explained in terms of the combination of stress relaxation phenomena in response to lipopolymers in polymer-tethered membranes and the influence of CHOL on lipid packing and membrane stiffness. Polymer-tethered membranes can reduce the lateral stress through distinct stress relaxation phenomena, such as membrane roughening (outside the buckling region) and/or penetration of polymer chains of lipopolymers into the hydrophobic lipid region (20, 76). The later process was particularly observed in the case of lipopolymers with somewhat amphiphilic polymer chains like PEG. By increasing the lipid packing density and the stiffness of the membrane, CHOL may play an important role in the regulation of these stress relaxation processes. Our findings are also significant because CHOL plays an important functional role in the biological membrane (123, 124). CHOL influences membrane elastic properties, such as bending elasticity and compressibility (124, 125). CHOL also impacts membrane curvature (120). For example, lipid phase separation between CHOL-enriched and CHOL-deficient phases, which are associated with distinct membrane curvature, may induce protein sequestration. Intriguingly, CHOL is enriched in clathrin-coated pits, caveolae and synaptic vesicles (126-128).

Our results are also exciting in light of the previous report that CHOL plays a major role in the normal breathing cycle through the reversible membrane wrinkling and folding in the lung (20). The significance of CHOL in the structure and function of lung surfactant has been reported by Bernardino and coworkers (129). They found that when

CHOL was extracted from the native pulmonary surfactant membrane, a dramatic change in the membrane was observed. They also observed a dramatic change in spreading properties of the native surfactant material at the air-liquid interface.

4.3.2.4 Buckling Regions as Diffusion Barriers

Previously, we have shown that bilayer formation may be suppressed on top of buckling regions in polymer-tethered membranes (20). This buckling-induced “dewetting” has been attributed to the presence of penetrating polymer chains in such substrates. Therefore, our next goal was to investigate the influence of CHOL in membrane organization of polymer-tethered lipid bilayers. In order to achieve this, we prepared polymer-tethered SOPC bilayer samples with 0 and 40 mol% CHOL, respectively (LB monolayer also contains 3 mol% DSPE-PEG5000). Bilayer morphologies were initially analyzed using EPI and spot photo bleaching experiments. As shown in Figure 30, the EPI images show distinct heterogeneities, which largely reflect earlier AFM results obtained using polymer-tethered monolayers of varying CHOL concentrations. At 0 mol% CHOL the bilayer showed small dark spots, whereas at the 40 mol% CHOL, the sample shows dark ridges. We also observed a phase inversion of EPI micrographs from monolayer (Figure 20 C) to corresponding bilayer (Figure 30 D). The ridges in the monolayers became valleys in bilayers and could be seen as dark areas in the EPI microscope in good agreement with findings on CHOL-free polymer-tethered membranes (26). The striking similarity of our data and corresponding CHOL-free data reported recently (26) suggests that the monolayer buckles, and then partially delaminates from the substrate due to the applied lateral stress in the membrane. As a result of monolayer

buckling, bilayer formation on top of the buckled regions is prevented. Here, the bilayer exists only outside of buckled regions. As Figure 31 shows, buckling-induced dewetting regions can act as diffusion barriers, thus compartmentalizing the bilayer. Remarkably, Figure 31 demonstrates that the degree of compartmentalization of the polymer-tethered bilayer can be controlled by adjusting CHOL molar concentration. This result is fascinating in light of the well-documented cytoskeleton-induced membrane compartmentalization in plasma membranes (130).

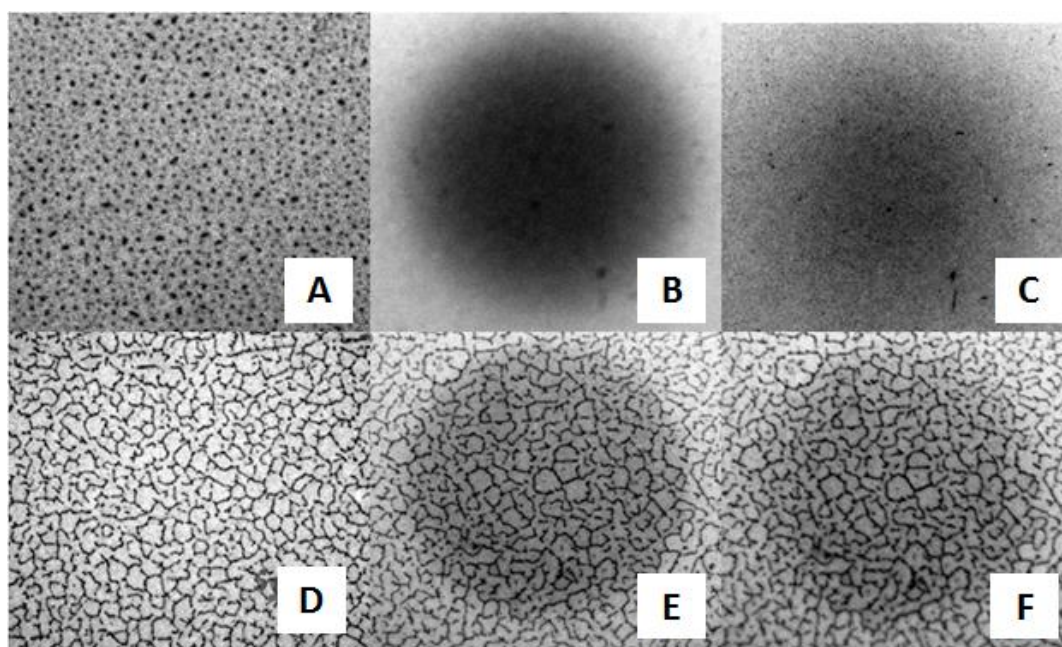


Figure 30: FRAP images of the bilayers for 0% CHOL (A-C) and 40% CHOL (D-F) in SOPC with 3 mol% DSPE-PEG 5000. 0.5 mol% TRITC-DHPE was used as the dye labeled lipid. (A) and (D) - bilayers before bleaching. (B) and (E) bilayers immediately after bleaching. (C) and (F) bilayer 20 s after bleaching, indicating recovery.

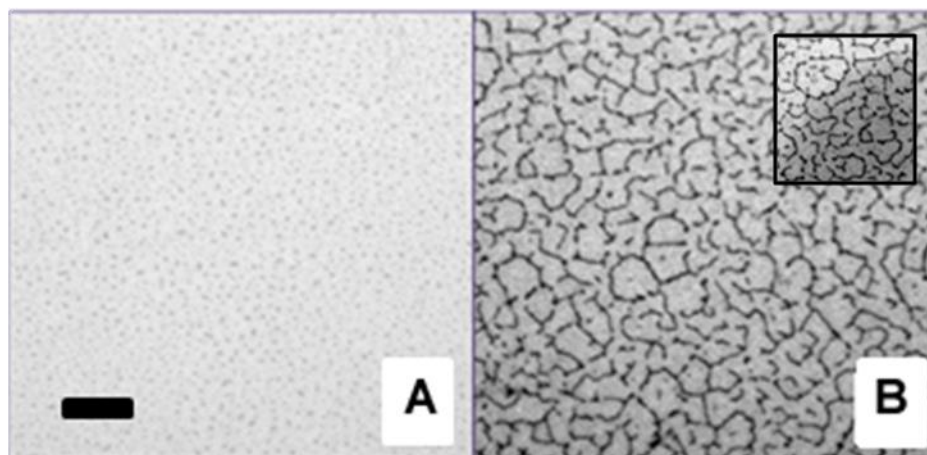


Figure 31: EPI micrographs of physisorbed polymer-tethered lipid bilayer with 0 mol % (A) and 40 mol% CHOL (B) in SOPC with 3 mol% DSPE-PEG 5000 and 0.5 mol% TRITC-DHPE. (The size of the scale bar is 10 μm). The inset (size: 20 μm x 20 μm), which illustrates the boundary region of a bleaching spot, demonstrates that buckling regions act as lipid diffusion barriers, as reported previously.

CHAPTER 5. CONCLUSION

The primary objective of my research was to investigate the influence of distinct lipid environments on $\alpha_v\beta_3$ and $\alpha_5\beta_1$ integrin sequestration in raft-mimicking lipid mixtures. Initially, integrin sequestration was investigated on asymmetric bilayers, where the l_o - l_d phase separation is exclusively present in the top leaflet of the bilayer and the bottom leaflet exhibits homogenous l_d phase. In order to fulfill this objective, we designed and characterized asymmetric bilayers using appropriate lipid compositions with suitable dye-labeled lipids (NBD-DHPE and DiD). The monolayer based l_o - l_d phase separations were analyzed using FCS, EPI, and confocal-XY scans. Next, the sequestration behavior and oligomerization state of integrins in such asymmetric bilayers were determined using CS-XY scan and PCH analyses. These experiments were conducted in the absence and presence of native ECM ligands. Comparison of our data with findings on bilayer-spanning l_o - l_d domains reported recently (3) demonstrated that bilayer asymmetry/symmetry has a profound effect on integrin sequestration. Specifically, these results showed that $\alpha_v\beta_3$ and $\alpha_5\beta_1$ prefer the l_d phase in symmetric bilayers (3) but the l_o phase in its asymmetric counterpart. Ligand addition did not cause any notable change of integrin sequestration in the asymmetric bilayer, but lead to substantial net translocations of $\alpha_v\beta_3$ and $\alpha_5\beta_1$ integrins from the l_d to l_o phases in the symmetric system. The observed differences in integrin sequestration can be explained in terms of distinct

properties of l_o and l_d domains in symmetric and asymmetric bilayers. In particular, differences in bilayer thickness affecting hydrophobic matching condition should be considered. In contrast, differences in lipid packing density appear to be less significant in these model lipid mixtures. Our findings are significant because they highlight the potential importance of bilayer asymmetry on integrin sequestration in real biological membranes. It should be emphasized that our model membrane results are in good agreement with results on cell membranes, which also report l_o phase preference of integrins in the outer leaflet (131). The observed affinity of integrins for l_o domains in asymmetric bilayers represents an interesting result, due to the relationship of integrins with raft domains in several biological functions such as TM signaling, cell adhesion, cell morphology, and angiogenesis (10-12, 132).

The next step was to elucidate the integrin sequestration in raft-mimicking domains of different CHOL concentrations. This enabled us to provide insight into the influence of lipid packing density and hydrophobic thickness on integrin sequestration and oligomerization in biological membrane. Interestingly, our results showed that variations in CHOL concentration are associated with significant change in integrin sequestration. In this case, integrin sequestration appears to be more pronounced at the center of the l_o - l_d coexistence region and less significant near the edges of this region. Interestingly, similar, but qualitatively different, trend was observed on integrins in the presence of native ligands. Overall, these findings coincide nicely with our other integrin sequestration studies in that the observed differences in integrin sequestration can largely be attributed to changes in hydrophobic matching conditions.

My next project was to investigate the impact of CHOL on membrane buckling in polymer-tethered lipid monolayers and bilayers. Buckling structures were determined using EPI and AFM. Quantitative analysis of the AFM data shows that increasing CHOL concentrations were associated with an increasing membrane buckling in the membrane in polymer-tethered membranes of low (3 mol%) lipopolymer concentration.

Interestingly, our data suggest that CHOL partially depletes from buckling regions, while lipopolymers and lipids do not show any measurable phase segregation. CHOL-induced buckling and lipopolymer-induced buckling show qualitatively similar behavior and represent stress-relaxation phenomena in response to applied lateral stress in the membrane. These findings are intriguing in light of the important role of CHOL in biological membranes, especially in the normal breathing cycle process through the reversible wrinkling and folding in the lung. Our results are also interesting because lipopolymers act as crowding agents, thereby mimicking molecular crowding of proteins in cellular membranes.

REFERENCES

REFERENCES

1. Simons, K., and D. Toomre. 2000. Lipid rafts and signal transduction. *Nat. Rev. Mol. Cell Biol.* 1:31-39.
2. Taylor, D. R., and N. M. Hooper. 2007. Role of lipid rafts in the processing of the pathogenic prion and Alzheimer's amyloid- β proteins. *Seminars in Cell & Developmental Biology* 18:638-648.
3. Siegel, Amanda P., A. Kimble-Hill, S. Garg, R. Jordan, and Christoph A. Naumann. 2011. Native ligands change integrin sequestering but not oligomerization in raft-mimicking lipid mixtures. *Biophys. J.* 101:1642-1650.
4. Simons, K., and R. Ehehalt. 2002. Cholesterol, lipid rafts, and disease. *J. Clin. Invest.* 110:597-603.
5. Murase, K., T. Fujiwara, Y. Umemura, K. Suzuki, R. Iino, H. Yamashita, M. Saito, H. Murakoshi, K. Ritchie, and A. Kusumi. 2004. Ultrafine membrane compartments for molecular diffusion as revealed by single molecule techniques. *Biophys. J.* 86:4075-4093.
6. Plowman, S. J., C. Muncke, R. G. Parton, and J. F. Hancock. 2005. H-ras, K-ras, and inner plasma membrane raft proteins operate in nanoclusters with differential dependence on the actin cytoskeleton. *Proc. Natl. Acad. Sci. USA* 102:15500-15505.
7. Sezgin, E., I. Levental, M. Grzybek, G. Schwarzmann, V. Mueller, A. Honigmann, V. N. Belov, C. Eggeling, Ü. Coskun, K. Simons, and P. Schwille. 2012. Partitioning, diffusion, and ligand binding of raft lipid analogs in model and cellular plasma membranes. *Biochim. Biophys. Acta.* 1818:1777-1784.
8. Yoon, T.Y., C. Jeong, S.W. Lee, J. H. Kim, M. C. Choi, S.J. Kim, M. W. Kim, and S.D. lee. 2006. Topographic control of lipid raft reconstitution in model membranes. *Nat. Mater.* 5:281-285.

9. Czolkos, I., A. Jesorka, and O. Orwar. 2011. Molecular phospholipid films on solid supports. *Soft Matter* 7:4562-4576.
10. Wong, S. W., M.J. Kwon, A. M. Choi, H.P. Kim, K. Nakahira, and D. H. Hwang. 2009. Fatty acids modulate toll-like receptor 4 activation through regulation of receptor dimerization and recruitment into lipid rafts in a reactive oxygen species-dependent manner. *J. Biol. Chem.* 284:27384-27392.
11. Cunningham, O., A. Andolfo, M. L. Santovito, L. Iuzzolino, F. Blasi, and N. Sidenius. 2003. Dimerization controls the lipid raft partitioning of uPAR/CD87 and regulates its biological functions. *EMBO J.* 22:5994-6003.
12. Kalvodova, L., N. Kahya, P. Schwille, R. Ehehalt, P. Verkade, D. Drechsel, and K. Simons. 2005. Lipids as modulators of proteolytic activity of BACE. *J. Biol. Chem.* 280:36815-36823.
13. Kiessling, V., C. Wan, and L. K. Tamm. 2009. Domain coupling in asymmetric lipid bilayers. *Biochim. Biophys. Acta* 1788:64-71.
14. Bhide, S. Y., Z. Zhang, and M. L. Berkowitz. 2007. Molecular dynamics simulations of SOPS and sphingomyelin bilayers containing cholesterol. *Biophys. J.* 92:1284-1295.
15. Simons, K., and E. Ikonen. 1997. Functional rafts in cell membrane. *Nature* 387:569-572.
16. Lin, W.C., C. D. Blanchette, T. V. Ratto, and M. L. Longo. 2006. Lipid asymmetry in DLPC/DSPC-supported lipid bilayers: a combined AFM and fluorescence microscopy study. *Biophys. J.* 90:228-237.
17. Harder, T., P. Scheiffele, P. Verkade, and K. Simons. 1998. Lipid domain structure of the plasma membrane revealed by patching of membrane components. *J. Cell. Biol.* 141:929-942.
18. Bastiaanse, E. M. L., K. M. Höld, and A. Van der Laarse. 1997. The effect of membrane cholesterol content on ion transport processes in plasma membranes. *Cardiovasc. Res.* 33:272-283.
19. Kaiser, H.J., A. Orłowski, T. Róg, T. K. Nyholm, W. Chai, T. Feizi, D. Lingwood, I. Vattulainen, and K. Simons. 2011. Lateral sorting in model membranes by cholesterol-mediated hydrophobic matching. *Proc. Natl. Acad. Sci. USA.* 108:16628-33.

20. Siegel, A. P., M. J. Murcia, M. Johnson, M. Reif, R. Jordan, J. Ruhe, and C. A. Naumann. 2010. Compartmentalizing a lipid bilayer by tuning lateral stress in a physisorbed polymer-tethered membrane. *Soft Matter* 6:2723-2732.
21. Paluch, E., and C.P. Heisenberg. 2009. Biology and physics of cell shape changes in development. *Curr. Biol.* 19:R790-R799.
22. McMahon, H. T., and J. L. Gallop. 2005. Membrane curvature and mechanisms of dynamic cell membrane remodelling. *Nature* 438:590-596.
23. Fackler, O. T., and R. Grosse. 2008. Cell motility through plasma membrane blebbing. *J. Cell Biol.* 181:879-884.
24. Takamoto, D. Y., M. M. Lipp, A. von Nahmen, K. Y. C. Lee, A. J. Waring, and J. A. Zasadzinski. 2001. Interaction of lung surfactant proteins with anionic phospholipids. *Biophys. J.* 81:153-169.
25. Häckl, W., M. Bärmann, and E. Sackmann. 1998. Shape changes of self-assembled actin bilayer composite membranes. *Phys. Rev. Lett.* 80:1786-1789.
26. Siegel, A. P., N. F. Hussain, M. Johnson, and C. A. Naumann. 2012. Metric between buckling structures and elastic properties in physisorbed polymer-tethered lipid monolayers. *Soft Matter* 8:5873-5880.
27. Jutila, A. 2001. Lateral heterogeneity in model membranes. In Department of Medical Chemistry. University of Helsinki -Faculty of Medicine, Helsinki. ISBN 952-991-3357-X (nid.) ISBN 3951-3345-9936-3355 (PDF).
28. Schick, M. 2012. Membrane heterogeneity: Manifestation of a curvature-induced microemulsion. *Phys. Rev. E Stat Nonlin Soft Matter Phys.* 85:031902.
29. Mishra, S., and P. G. Joshi. 2007. Lipid raft heterogeneity: an enigma. *J. Neurochem.* 103:135-142.
30. Hussain, Noor F., Amanda P. Siegel, Y. Ge, R. Jordan, and Christoph A. Naumann. 2013. Bilayer asymmetry influences integrin sequestering in raft-mimicking lipid mixtures. *Biophys. J.* 104:2212-2221.
31. Lingwood, D., H.J. Kaiser, I. Levental, and K. Simons. 2009. Lipid Rafts as Functional Heterogeneity in Cell Membranes. *Biochem. Soc. Trans.* 37 (Pt. 5):955-960.
32. Owen, D. M., A. Magenau, D. Williamson, and K. Gaus. 2012. The lipid raft hypothesis revisited – New insights on raft composition and function from super-resolution fluorescence microscopy. *Bioessays* 34:739-747.

33. Edidin, M. 2003. The state of lipid rafts : From model membranes to cells. *Annu. Rev. Biophys. Biomol. Struct.* 32:257-283.
34. Suzuki, K. G. N. 2012. Lipid rafts generate digital-like signal transduction in cell plasma membranes. *Biotechnol. J.* 7:753-761.
35. Rauch, S., and O. T. Fackler. 2007. Viruses, lipid rafts and signal transduction. *Signal Transduction* 7:53-63.
36. Airaksinen, M. S., and M. Saarma. 2002. The GDNF family: signalling, biological functions and therapeutic value. *Nat. Rev. Neurosci.* 3:383-394.
37. Paladina, S., S. Daniela, R. Pillich, S. Tivodar, L. Nitsch, and C. Zurzolo. 2004. Protein oligomerization modulates raft partitioning and apical sorting of GPI-anchored protein. *J. Cell Biol.* 167:699-709.
38. Simons, K., and G. Van Meer. 1988. Lipid sorting in epithelial cells. *Biochemistry* 27:6197-6202.
39. Bastiani, M., and R. G. Parton. 2010. Caveolae at a glance. *J. Cell Sci.* 123:3831-3836.
40. Janes, P. W., S. C. Ley, A. I. Magee, and P. S. Kabouridis. 2000. The role of lipid rafts in T cell antigen receptor (TCR) signalling. *Semin. Immunol.* 12:23-34.
41. Dykstra, M., A. Cherukuri, and S. K. Pierce. 2001. Rafts and synapses in the spatial organization of immune cell signaling receptors. *J. Leukoc. Biol.* 70:699-707.
42. Tansey, M. G., R. H. Baloh, J. Milbrandt, and E. M. Johnson. 2000. GFR \pm -mediated localization of RET to lipid rafts is required for effective downstream signaling, Differentiation, and Neuronal Survival. *Neuron* 25:611-623.
43. Richmond, D. L., E. M. Schmid, S. Martens, J. C. Stachowiak, N. Liska, and D. A. Fletcher. 2011. Forming giant vesicles with controlled membrane composition, asymmetry, and contents. *Proc. Natl. Acad. Sci. USA.* 108:9431-9436.
44. Chiantia, S., P. Schwille, A. S. Klymchenko, and E. London. 2011. Asymmetric GUVs prepared by M²CD-mediated lipid exchange: An FCS Study. *Biophys. J.* 100:L1-L3.
45. Bretscher, M., and S. Munro. 1993. Cholesterol and the Golgi apparatus. *Science* 261:1280-1281.

46. Nezil, F. A., and M. Bloom. 1992. Combined influence of cholesterol and synthetic amphiphilic peptides upon bilayer thickness in model membranes. *Biophys.J.* 61:1176-1183.
47. Kamar, R. I., L. E. Organ-Darling, and R. M. Raphael. 2012. Membrane cholesterol strongly influences confined diffusion of prestin. *Biophys. J.* 103:1627-1636.
48. Nilsson, I., H. Ohvo-Rekilä, J. P. Slotte, A. E. Johnson, and G. von Heijne. 2001. Inhibition of Protein Translocation across the Endoplasmic Reticulum Membrane by Sterols. *J. Biol. Chem.* 276:41748-41754.
49. Lichtenberg, D., F. M. Goñi, and H. Heerklotz. 2005. Detergent-resistant membranes should not be identified with membrane rafts. *Trends Biochem. Sci.* 30:430-436.
50. Ganguly, S., and A. Chattopadhyay. 2010. Cholesterol depletion mimics the effect of cytoskeletal destabilization on membrane dynamics of the Serotonin1A receptor: a zFCS study. *Biophys. J.* 99:1397-1407.
51. Murphy, S. C., B. U. Samuel, T. Harrison, K. D. Speicher, D. W. Speicher, M. E. Reid, R. Prohaska, P. S. Low, M. J. Tanner, N. Mohandas, and K. Haldar. 2004. Erythrocyte detergent-resistant membrane proteins: their characterization and selective uptake during malarial infection. *Blood* 103:1920-1928.
52. Moffett, S., D. A. Brown, and M. E. Linder. 2000. Lipid-dependent Targeting of G Proteins into Rafts. *J. Biol. Chem.* 275:2191-2198.
53. Klotzsch, E., and G. J. Schütz. 2013. A critical survey of methods to detect plasma membrane rafts. *Philos. Trans. R. Soc B: Biol. Sci.* 368:1611.
54. Friedrichson, T., and T. V. Kurzchalia. 1998. Microdomains of GPI-anchored proteins in living cells revealed by crosslinking. *Nature* 394:802-805.
55. Perto, K. A. 2008. Role of lipid rafts in Botulinum neurotoxin serotype A activity and differentiation of Neuroblastoma cells. In Department of Biochemistry and Molecular Biology. The Pennsylvania State University, Pennsylvania.
56. Veatch, S. L., and S. L. Keller. 2003. Separation of Liquid Phases in Giant Vesicles of Ternary Mixtures of Phospholipids and Cholesterol. *Biophys. J.* 85:3074-3083.
57. Veatch, S. L., and S. L. Keller. 2005. Seeing spots: Complex phase behavior in simple membranes. *Biochim. Biophys. Acta* 1746:172-185.

58. Dietrich, C., L. Bagatolli, Z. Volovyk, N. Thompson, K. Levi, K. Jacobson, and E. Gratton. 2001. Lipid rafts reconstituted in model membranes. *Biophys. J.* 80:1417-1428.
59. Veatch, S. L., I. V. Polozov, K. Gawrisch, and S. L. Keller. 2004. Liquid Domains in Vesicles Investigated by NMR and Fluorescence Microscopy. *Biophys. J.* 86:2910-2922.
60. Goñi, F. M., A. Alonso, L. A. Bagatolli, R. E. Brown, D. Marsh, M. Prieto, and J. L. Thewalt. 2008. Phase diagrams of lipid mixtures relevant to the study of membrane rafts. *Biochim. Biophys. Acta (BBA) - Molecular and Cell Biology of Lipids* 1781:665-684.
61. Zhao, J., J. Wu, F. A. Heberle, T. T. Mills, P. Klawitter, G. Huang, G. Costanza, and G. W. Feigenson. 2007. Phase studies of model biomembranes: Complex behavior of DSPC/DOPC/Cholesterol. *Biochim. Biophys. Acta* 1768:2764-2776.
62. Johnston, L. J. 2007. Nanoscale Imaging of Domains in Supported Lipid Membranes. *Langmuir* 23:5886-5895.
63. Samsonov, A. V., I. Mihalyov, and F. S. Cohen. 2001. Characterization of Cholesterol-Sphingomyelin Domains and Their Dynamics in Bilayer Membranes. *Biophys. J.* 81:1486-1500.
64. Koo, L. Y., D. J. Irvine, A. M. Mayes, D. A. Lauffenburger, and L. G. Griffith. 2002. Co-regulation of cell adhesion by nanoscale RGD organization and mechanical stimulus. *J. Cell. Sci.* 115:1423-1433.
65. Pande, G. 2000. The role of membrane lipids in regulation of integrin functions. *Curr. Opin. Cell Biol.* 12:569-574.
66. Du, X., E. F. Plow, A. L. Frelinger, T. E. O'Toole, J. C. Loftus, and M. H. Ginsberg. 1991. Ligands activate integrin α IIb β 3 (platelet GPIIb-IIIa). *Cell* 65:409-416.
67. Banno, A and M. H. Ginsberg. 2008. Integrin activation. *Biochem. Soc. Trans.* 36 (Pt. 2):229-234.
68. Xue, Z.H., C.Q. Zhao, G.L. Chua, S.W. Tan, X.Y. Tang, S.C. Wong, and S.M. Tan. 2010. Integrin α M β 2 Clustering Triggers Phosphorylation and Activation of Protein Kinase C δ that Regulates Transcription Factor Foxp1 Expression in Monocytes. *J. Immunol.* 184:3697-3709.

69. Tiwari, S., J. A. Askari, M. J. Humphries, and N. J. Bulleid. 2011. Divalent cations regulate the folding and activation status of integrins during their intracellular trafficking. *J. Cell Sci.* 124:1672-1680.
70. Subczynski, W. K., and A. Wisniewska. 2000. Physical properties of lipid bilayer membranes: relevance to membrane biological functions. *Acta Biochim. Pol.* 47:613-625.
71. Castellana, E. T., and P. S. Cremer. 2006. Solid supported lipid bilayers: From biophysical studies to sensor design. *Surf. Sci. Rep.* 61:429-444.
72. Kalb, E., and L. K. Tamm. 1992. Incorporation of cytochrome b5 into supported phospholipid bilayers by vesicle fusion to supported monolayers. *Thin Solid Films* 210–211, Part 2:763-765.
73. Deverall, M. A., E. Gindl, E. K. Sinner, H. Besir, J. Ruehe, M. J. Saxton, and C. A. Naumann. 2005. Membrane lateral mobility obstructed by polymer-tethered lipids studied at the single molecule level. *Biophys. J.* 88:1875-1886.
74. Naumann, C. A., O. Prucker, T. Lehmann, J. R uhe, W. Knoll, and C. W. Frank. 2002. The Polymer-Supported Phospholipid Bilayer: Tethering as a New Approach to Substrate–Membrane Stabilization. *Biomacromolecules* 3:27-35.
75. Garg, S., J. R uhe, K. L udtke, R. Jordan, and C. A. Naumann. 2007. Domain registration in raft-mimicking lipid mixtures studied using polymer-tethered lipid bilayers. *Biophys. J.* 92:1263-1270.
76. Deverall, M. A., S. Garg, K. Ludtke, R. Jordan, J. Ruhe, and C. A. Naumann. 2008. Transbilayer coupling of obstructed lipid diffusion in polymer-tethered phospholipid bilayers. *Soft Matter* 4:1899-1908.
77. Marsh, D., R. Bartucci, and L. Sportelli. 2003. Lipid membranes with grafted polymers: physicochemical aspects. *Biochim. Biophys. Acta* 1615:33-59.
78. Rovira-Bru, M., D. H. Thompson, and I. Szleifer. 2002. Size and Structure of Spontaneously Forming Liposomes in Lipid/PEG-Lipid Mixtures. *Biophys. J.* 83:2419-2439.
79. Siegel, A. 2011. Regulating lipid organization and investigating membrane protein properties in physisorbed polymer-tethered membrane. In Chemistry Department. Purdue University, Indianapolis.
80. de Gennes, G. 1990. Introduction to Polymer Dynamics. Cambridge University Press, New York.

81. Lasic, D. D., and D. Needham. 1995. The "Stealth" Liposome: A Prototypical Biomaterial. *Chem. Rev.* 95:2601-2628.
82. Mei, H., R. Huang, J. Y. Chung, C. M. Stafford, and H.-H. Yu. 2007. Buckling modes of elastic thin films on elastic substrates. *Appl. Phys. Lett.* 90:151902-151903. .
83. Moon, M. W., K. R. Lee, K. H. Oh, and J. W. Hutchinson. 2004. Buckle delamination on patterned substrates. *Acta Materialia* 52:3151-3159.
84. Hutchinson, J. W., and Z. Suo. 1992. Mixed mode cracking in layered materials. *Adv. Appl. Mech.* 29:63-191.
85. Schönherr, H., J. M. Johnson, P. Lenz, C. W. Frank, and S. G. Boxer. 2004. Vesicle Adsorption and Lipid Bilayer Formation on Glass Studied by Atomic Force Microscopy. *Langmuir* 20:11600-11606.
86. Kalb, E., S. Frey, and L. K. Tamm. 1992. Formation of supported planar bilayers by fusion of vesicles to supported phospholipid monolayers. *Biochim.t Biophys. Acta* 1103:307-316.
87. Tamm, L. K., and H. M. McConnell. 1985. Supported phospholipid bilayers. *Biophys. J.* 47:105-113.
88. Wagner, M. L., and L. K. Tamm. 2000. Tethered polymer-supported planar lipid bilayers for reconstitution of integral membrane proteins: silane-polyethyleneglycol-lipid as a cushion and covalent linker. *Biophys. J.* 79:1400-1414.
89. Chen, Y., J. D. Müller, P. T. C. So, and E. Gratton. 1999. The Photon Counting Histogram in Fluorescence Fluctuation Spectroscopy. *Biophys. J.* 77:553-567.
90. Schwille, P., U. Haupts, S. Maiti, and W. W. Webb. 1999. Molecular Dynamics in Living Cells Observed by Fluorescence Correlation Spectroscopy with One- and Two-Photon Excitation. *Biophys. J.* 77:2251-2265.
91. Maiti, S., U. Haupts, and W. W. Webb. 1997. Fluorescence correlation spectroscopy: Diagnostics for sparse molecules. *Proc. Natl. Acad. Sci.* 94:11753-11757.
92. Macháň, R., and M. Hof. 2010. Recent Developments in Fluorescence Correlation Spectroscopy for Diffusion Measurements in Planar Lipid Membranes. *Int. J. Mol. Sci.* 11:427-457.

93. Dufrêne, Y. F. 2002. Atomic Force Microscopy, a Powerful Tool in Microbiology. *J. Bacteriol.* 184:5205-5213.
94. Binnig, G., C. F. Quate, and C. Gerber. 1986. Atomic Force Microscope. *Phys. Rev. Lett.* 56:930-933.
95. Sengupta, P., A. Hammond, D. Holowka, and B. Baird. 2008. Structural determinants for partitioning of lipids and proteins between coexisting fluid phases in giant plasma membrane vesicles. *Biochim. Biophys. Acta* 1778:20-32.
96. Liang, X., G. Mao, and K. Y. S. Ng. 2004. Mechanical properties and stability measurement of cholesterol-containing liposome on mica by atomic force microscopy. *J. Colloid Interface Sci.* 278:53-62.
97. Zheng, X.P., Y.P. Cao, B. Li, X.Q. feng, H. Jiang, and Y. Huang. 2009. Determining the elastic modulus of thin films using a buckling-based method:computational study. *J. Phys. D: Appl. Phys.* 42:175506 (175507pp).
98. Lewis, B. A., and D. M. Engelman. 1983. Lipid bilayer thickness varies linearly with acyl chain length in fluid phosphatidylcholine vesicles. *J. Mol Biol.* 166:211-217.
99. de Meyer, F., and B. Smit. 2009. Effect of cholesterol on the structure of a phospholipid bilayer. *Proc. Natl.l Acad. Sci. USA* 106:3654-3658.
100. Wolf, D. E. 1985. Determination of the sidedness of carbocyanine dye labeling of membranes. *Biochemistry* 24:582-586.
101. Crane, J. M., V. Kiessling, and L. K. Tamm. 2005. Measuring lipid asymmetry in planar supported bilayers by fluorescence interference contrast microscopy. *Langmuir* 21:1377-1388.
102. Crane, J. M., and L. K. Tamm. 2004. Role of cholesterol in the formation and nature of lipid rafts in planar and spherical model membranes. *Biophys. J.* 86:2965-2979.
103. Kiessling, V., J. M. Crane, and L. K. Tamm. 2006. Transbilayer effects of raft-like lipid domains in asymmetric planar bilayers measured by single molecule tracking. *Biophys. J.* 91:3313-3326.
104. Stöckl, M. T., and A. Herrmann. 2010. Detection of lipid domains in model and cell membranes by fluorescence lifetime imaging microscopy. *Biochim. Biophys. Acta* 1798:1444-1456.

105. Baumgart, T., A. T. Hammond, P. Sengupta, S. T. Hess, D. A. Holowka, B. A. Baird, and W. W. Webb. 2007. Large-scale fluid/fluid phase separation of proteins and lipids in giant plasma membrane vesicles. *Proc. Natl. Acad. Sci. USA* 104:3165-3170.
106. Kahya, N., D. A. Brown, and P. Schwill. 2005. Raft Partitioning and Dynamic Behavior of Human Placental Alkaline Phosphatase in Giant Unilamellar Vesicles. *Biochemistry* 44:7479-7489.
107. Carman, C. V., and T. A. Springer. 2003. Integrin avidity regulation: are changes in affinity and conformation underemphasized? *Curr. Opin. Cell Biol.* 15:547-556.
108. Gandhavadi, M., D. Allende, A. Vidal, S. A. Simon, and T. J. McIntosh. 2002. Structure, composition, and peptide binding properties of detergent soluble bilayers and detergent resistant rafts. *Biophys. J.* 82:1469-1482.
109. de Almeida, R. F. M., A. Fedorov, and M. Prieto. 2003. Sphingomyelin/phosphatidylcholine/cholesterol phase diagram: boundaries and composition of lipid rafts. *Biophys. J.* 85:2406-2416.
110. Takagi, J., K. Strokovich, T. A. Springer, and T. Walz. 2003. Structure of integrin $\alpha_5\beta_1$ in complex with fibronectin. *EMBO J* 22:4607-4615.
111. McIntosh, T. J., and S. A. Simon. 2006. Roles of bilayer material properties in function and distribution of membrane proteins. *Annu. Rev. Biophys. Biomol. Struct.* 35:177-198.
112. Fastenberg, M. E., H. Shogomori, X. Xu, D. A. Brown, and E. London. 2003. Exclusion of a transmembrane-type peptide from ordered-lipid domains (rafts) detected by fluorescence quenching: extension of quenching analysis to account for the effects of domain size and domain boundaries. *Biochemistry* 42:12376-12390.
113. Lomize, A., M. Iomize, and I. Pogozheva. 2005-2011. Membranome database - human membrane atlas (Integrin alpha-V). College of Pharmacy, University of Michigan, Ann Arbor, MI 48109 USA.
114. Lomize, A., M. Iomize, and I. Pogozheva. 2005-2011. Orientations of proteins in membranes (OPM) database (Integrin beta-3, transmembrane helix). Mosberg lab, College of Pharmacy, University of Michigan, Ann Arbor, MI 48109 USA.
115. Shattil, S. J., C. Kim, and M. H. Ginsberg. 2010. The final steps of integrin activation: the end game. *Nat. Rev. Mol. Cell Bio.* 11:288-300.

116. Du, X., E. F. Plow, A. L. Frelinger, T. E. O'Toole, J. C. Loftus, and M. H. Ginsberg. 1991. Ligands "activate" integrin $\alpha_{IIb}\beta_3$ (platelet GPIIb-IIIa). *Cell* 65:409-416.
117. Lau, T.L., C. Kim, M. H. Ginsberg, and T. S. Ulmer. 2009. The structure of the integrin $\alpha_{IIb}\beta_3$ transmembrane complex explains integrin transmembrane signalling *EMBO J.* 28:1351-1361.
118. Kim, M., C. V. Carman, and T. A. Springer. 2003. Bidirectional transmembrane signaling by cytoplasmic domain separation in integrins. *Science* 301:1720-1725.
119. Kalli, A. C., I. D. Campbell, and M. S. P. Sansom. 2011. Multiscale simulations suggest a mechanism for integrin inside-out activation. *Proc. Natl. Acad. Sci. USA* 108:11890-11895.
120. Yesylevskyy, S. O., A. P. Demchenko, S. Kraszewski, and C. Ramseyer. 2013. Cholesterol induces uneven curvature of asymmetric lipid bilayers. *The Scientific World Journal* 965230.
121. Simson, R., E. Wallraff, J. Faix, J. Niewöhner, G. Gerisch, and E. Sackmann. 1998. Membrane bending modulus and adhesion energy of wild-type and mutant cells of dictyostelium lacking talin or cortexillins. *Biophys.J.* 74:514-522.
122. Hwang, W. C., and R. E. Waugh. 1997. Energy of dissociation of lipid bilayer from the membrane skeleton of red blood cells. *Biophys.J.* 72:2669-2678.
123. Rukmini, R., S. S. Rawat, S. C. Biswas, and A. Chattopadhyay. 2001. Cholesterol organization in membranes at low concentrations: Effects of curvature stress and membrane thickness. *Biophys. J.* 81:2122-2134.
124. Pan, J., T. T. Mills, S. Tristram-Nagle, and J. F. Nagle. 2008. Cholesterol Perturbs Lipid Bilayers Nonuniversally. *Phys. Rev. Lett.* 100:198103.
125. Song, J., and R. E. Waugh. 1993. Bending rigidity of SOPC membranes containing cholesterol. *Biophys. J.* 64:1967-1970.
126. Subtil, A., I. Gaidarov, K. Kobylarz, M. A. Lampson, J. H. Keen, and T. E. McGraw. 1999. Acute cholesterol depletion inhibits clathrin-coated pit budding. *Proc. Natl Acad. Sci. USA* 96:6775-6780.
127. Parton, R. G., and K. Simons. 2007. The Multiple Faces of Caveolae. *Nat. Rev. Mol. Cell Biol.* 8:185-194.

128. Thiele, C., M. J. Hannah, F. Fahrenholz, and W. B. Huttner. 2000. Cholesterol binds to synaptophysin and is required for biogenesis of synaptic vesicles. *Na. Cell Biol.* 2:42-49.
129. Bernardino de la Serna, J., J. Perez-Gil, A. C. Simonsen, and L. A. Bagatolli. 2004. Cholesterol Rules: Direct observation of the coexistence of two fluid phases in native pulmonary surfactant membrane at physiological temperatures. *J. Biol. Chem.* 279:40715-40722.
130. Sako, Y., and A. Kusumi. 1994. Compartmentalized structure of the plasma membrane for receptor movements as revealed by a nanometer-level motion analysis. *J. Cell Bio.* 125:1251-1264.
131. Pankov, R., T. Markovska, R. Hazarosova, P. Antonov, L. Ivanova, and A. Momchilova. 2005. Cholesterol distribution in plasma membranes of $\beta 1$ integrin-expressing and $\beta 1$ integrin-deficient fibroblasts. *Arch. Biochem. Biophys.* 442:160-168.
132. Blystone, S. D., I. L. Graham, F. P. Lindberg, and E. J. Brown. 1994. Integrin alpha v beta 3 differentially regulates adhesive and phagocytic functions of the fibronectin receptor alpha 5 beta 1. *J. Cell. Biol.* 127:1129-1137.

VITA

VITA

Noor Feuza Hussain came from Karlshue place, Colombo, Sri Lanka. She got through her General Certificate of Education Ordinary Level (G.C.E. O/L) exam in 1989 at All Saints Girls College, Colombo. Then she proceeded to Devi Balika, Colombo in order to pursue the General Certificate of Education Advanced Level (G.C. E. A/L) exam. She was fortunate to enter the historical University of Kelaniya in Sri Lanka in 1996 and got her special degree in Chemistry in year 2000 under the supervision of Prof. Priyani Paranagama.

Noor joined East Tennessee State University in Johnson City, Tennessee in 2003 and got her Masters in Chemistry under the supervision of Dr. Mian Jiang. In 2005, she moved to Purdue University in West Lafayette, Indiana and joined Dr. Sulma Mohammed's research group. She completed her Master's degree in Comparative Pathobiology. To pursue doctoral research in Biophysical Chemistry, Noor joined Prof. Christoph Naumann laboratory in Spring 2010. Her dissertation titled "Influence of Cholesterol and Bilayer Asymmetry on Membrane Protein Distribution in Polymer-tethered Raft-mimicking Lipid Membranes" is presented in 2013 in this dissertation.